Charles University in Prague
Faculty of Mathematics and Physics

DIPLOMA THESIS

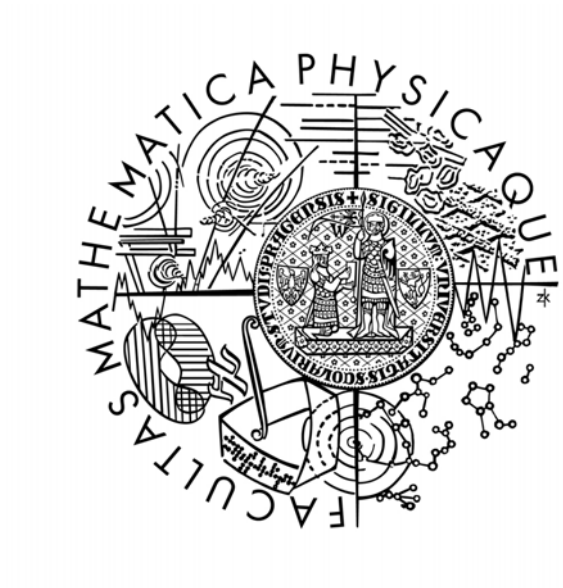

Michaela Blažíková

Cationic porphyrins as transport agents for antisense oligonucleotides

Division of biomolecular physics
Supervisor of the diploma thesis: Doc. RNDr. Peter Mojzeš, CSc.
Study program: Biophysics and chemical physics

In the first place I would like to thank Doc. RNDr. Peter Mojzeš, CSc. for leadership, advices and technical comments to this diploma thesis. I would also like to thank our graduates mainly for friendly advice and help with the programs for treatment of the results. My gratitude also belongs to my parents for their support in my studies and to my friends for help with the language corrections of the text.

I declare that I wrote my diploma thesis independently and entirely with the use of the cited sources. I agree with lending of the work.

Prague, April 21, 2006 Michaela Blažíková

Title: *Cationic porphyrins as transport agents for antisense oligonucleotides*

Author: Michaela Blažíková

Department: Division of Biomolecular Physics, Institute of Physics

Supervisor: Doc. RNDr. Peter Mojzeš, CSc.

Supervisor's e - mail address: mojzes@karlov.mff.cuni.cz

Abstract: Physico-chemical properties of free-base and Cu^{2+} derivatives of H_2TPP-$(Dist)_4$, H_2TPP-p-$(Bru)_4$, H_2TPP-m-$(Bru)_4$, the novel cationic porphyrins of therapeutic importance, have been studied by use of electronic absorption and resonance Raman spectroscopies. Photophysical properties, aggregation in aqueous solutions and binding to single- and double-stranded nucleic acids were studied and compared with properties of structurally relative cationic porphyrins H_2TMPyP_4, H_2TMAP and H_2TPP-$(NMe_3)_4$. Spectrophotometric procedures for determination of extinction coefficients of cationic porphyrins were tested and critically evaluated. Extinction coefficients of several cationic porphyrins have been determined for the first time. Methodology for comprehensive study of porphyrin aggregation was tested. Using absorption and resonance Raman spectroscopies, binding modes of CuTPP-p-$(Bru)_4$ and CuTPP-m-$(Bru)_4$, and their base and sequence specificities were established for the first time, and confronted with $CuTMPyP_4$ and CuTPP-$(NMe_3)_4$. External binding mode and formation of self-associated porphyrin assemblies on the polynucleotide matrices were identified for H_2TPP-$(Dist)_4$ and H_2TPP-p-$(Bru)_4$ with single- and double-stranded nucleic acids. Contrary to CuTPP-p-$(Bru)_4$, CuTPP-m-$(Bru)_4$ was shown to discriminate between divers polynucleotide structures. Structural difference between CuTPP-p-$(Bru)_4$ and CuTPP-m-$(Bru)_4$ have been suggested to have profound consequences for physico-chemical and conformational properties, as well as for interactions with nucleic acids. Experimental results presented here should serve as a starting point for further investigation.

Keywords: porphyrin, nucleic acid, complex, oligonucleotide, antisense, transport

Názov práce: *Kationické porfyríny ako transportný agens pre antisense oligonukleotidy*

Autor: Michaela Blažíková

Katedra (ústav): Oddelenie fyziky biomolekúl, Fyzikálný ústav

Vedúci diplomovej práce: Doc. RNDr. Peter Mojzeš, CSc.

e - mail vedúceho: mojzes@karlov.mff.cuni.cz

Abstrakt: Pomocou elektrónovej a rezonančnej Ramanovej spektroskopie sme študovali fyzikálne-chemické vlastosti nemetalovaný a Cu^{2+} melatoforiem H_2TPP-$(Dist)_4$, H_2TPP-p-$(Bru)_4$, H_2TPP-m-$(Bru)_4$, nových kationických porfyrínov s terapeutickým významom. Určili sme ich základné fotofyzikálné vlastnosti, tvorbu agregátov vo vodnom prostredí a interakcie s jedno- a dvojvláknovými nukleovými kyselinami, a porovnali s vlastnosťami štruktúrne príbuzných kationických porfyrínov H_2TMPyP_4, H_2TMAP and H_2TPP-$(NMe_3)_4$. Kriticky sme testovali vhodnosť viacerých spektrofotometrických postupov pre stanovenie extinkčných koeficientov kationických porfyrinov, a v prípade niektorých porfyrínov sme po prvýkrát stanovili ich extinkčné koeficienty. Ďalej sme overovali metodické postupy pre komplexné študium tvorby porfyrínových agregátov. Za použitia absorpčnej a rezonančnej Ramanovej spekroskopie sme pre CuTPP-p-$(Bru)_4$ a CuTPP-m-$(Bru)_4$ po prvýkrát určili spôsob väzby v závislosti na bázovom zložení a sekvencii nukleovej kyseliny, a porovnali s $CuTMPyP_4$ a CuTPP-$(NMe_3)_4$. Pre H_2TPP-$(Dist)_4$ and H_2TPP-p-$(Bru)_4$ sme zistili, že sa viažu externe na povrch jedno- a dvojvláknových nukleových kyselin, ktorý využívajú ako matricu pre tvorbu samoasociovaných štruktúr. Ďalej sme zistili, že CuTPP-m-$(Bru)_4$ dokáže rozlišiť rôzne polynukleotidové štruktúry, na rozdiel od CuTPP-m-$(Bru)_4$. Zdá sa, že štruktúrny rozdiel medzi CuTPP-p-$(Bru)_4$ a CuTPP-m-$(Bru)_4$ má hlboké dôsledky pre ich fyzikálne-chemické vlastnosti a interakcie s nukleovými kyselinami. Experimentálne výsledky dosiahnuté v tejto práci môžu slúžiť ako východzí bod pre ďaľší výzkum.

Kľúčové slová: porfyrín, nukleová kyselina, komplex, oligonukleotid, antisense, transport

Contents

Abbreviations

DNA	deoxyribonucleic acid
RNA	ribonucleic acid
mRNA	messenger ribonucleic acid
poly(rA)	polyadenylic acid
poly(rC)	polycytidylic acid
poly(rU)	polyuridylic acid
poly(dA)	polydeoxyadenylic acid
poly(dT)	polydeoxythymidylic acid
ssNA	single–stranded nucleic acid
dsNA	double–stranded nucleic acid
RRS	resonance Raman scattering
CCD	charge coupled device
LD	linear dichroism
CD	circular dichroism
NMR	nuclear magnetic resonance
FA	factor analysis
SVD	singular value decomposition
DMSO	dimethylsulfoxide
ST-DNA	salmon testes DNA
zincon	2-carboxy-2'-hydroxy-5'-sulfoformazylbenzene
oligo$(dA)_{15}$	deoxyoligoadenylate with the length of 15 nucleotides

1 Introduction

Water-soluble porphyrins are important because of their ability to cure several diseases, even as serious as cancer. Evidence of their influence on HIV and hepatitis virus exists too. There are several ways how to use porphyrins for disease treatment. The most widespread method is the photodynamic therapy (PDT) of cancer, where the water-soluble porphyrins cumulate freely in malignant cells. There they could be illuminated by intense light of appropriate wavelength, and quenching their excited triplet states through excitation transfer to molecular oxygen dissolved in the cells or tissues they produce singlet oxygen, which causes damage to the cancerous cells. Other therapeutic use of the porphyrins is connected with their role as promising compounds for cellular delivery of short oligonucleotides. Oligonucleotide therapeutic strategies (e.g. antisense and antigene therapies) represent one of the most exciting challenges in the efforts to specifically modulate protein expression inside living cells. Proteins represent the substances responsible for nearly all the processes in living cells. They are located in the plasma membranes, cytoskeleton and in organelles inside the cells and they participate in cell metabolism as enzymes serving as cofactors in many other processes. Consequently, regulation of proteosynthesis seems to be a very powerful instrument for treatment of some serious diseases. By targeted antisense or antigene therapy we are able to suppress the production of various viruses, leukemia cells and other forms of cancer.

Regardless details of particular oligonucleotide strategies, their practical applications have to face with the problem how to transport negatively charged oligonucleotides against potential gradient of the negatively charged inner part of the cells. Negative charge of the oligonucleotides can be lowered, shielded or neutralized by binding of special substances, so-called “carriers”, the purpose of which is to facilitate transport of the oligonucleotides into the cells as well as to protect them from degradation by endonucleases. Several delivery strategies (microinjection, electroporation, nanocapsules, nanospheres) and synthetic systems have been developed (lipid-mediated, cyklodextrin-mediated, dendrimer-mediated, peptide-mediated delivery), each might be useful for a given application, nevertheless each having its own drawbacks and limitations. As demonstrated recently [5-7], non-covalent complexes of water-soluble cationic porphyrins with polyanionic oligonucleotides could help oligonucleotides to penetrate into the cells as well. However, delivery capacity of the porphyrins is dependent on their binding modes and structural properties of the entire complex, that could be rather complex function of properties of

peripheral substituents of the porphyrin, oligonucleotide base-sequence and structure, concentration of the reagents, charge ratio and physico-chemical characteristics of the solvent. Since one of the most important things, that have to be considered for effective oligonucleotide delivery, is the character of interactions between oligonucleotides and delivery agents, it is necessary to start with investigation of the interactions between porphyrins and nucleic acids. As delivery and therapeutic efficiencies of the porphyrins could be negatively influenced by formation of self-aggregated porphyrin structures, other important question concerns behavior of pure porphyrin solutions.

The present work freely relates to the diploma thesis of Mgr. V. Marek, who studied interactions of commercially available and previously well-studied cationic (5,10,15,20-*meso*-tetrakis(4-N-methylpyridyl) porphyrin and its copper(II) derivative with short single-stranded oligonucleotides. The aim of the present work is to investigate some of the newly synthesized porphyrins in their free as well as metallated form with nucleic acids, to specify their basic spectroscopic characteristics, behavior in aqueous solutions and, consequently, their interactions with various nucleic acids.

2 Theoretical part

2.1 Antisense oligonucleotide delivery

All living cells have their genetic information stored in double-stranded deoxyribonucleic (DNA) acids consisting of sugar *deoxyribose*, phosphate and heterocyclic bases adenine (A), thymine (T), guanine (G) and cytosine (C). To express genetic information into building up new proteins, a cell uses transcription of the particular DNA sequence coding a given gene into the single-stranded messenger ribonucleic acids (mRNA) replacing deoxyribose by *ribose* and thymine by uracil (U). In the following translation, mRNA serves as a template for protein synthesis. In eukaryotic cells the transcription takes place inside cell nucleus, while the translation goes on outside the nucleus, in the cytoplasm. Normally, only one of the two DNA strands is transcribed into the mRNA, and it is always the same strand for a given gene. If the opposite DNA strand is transcribed by means of genetic engineering instead, RNA molecule complementary to the normal mRNA will be produced. Resulting mRNA is known as *antisense* RNA and it can hybridize with the normal, i.e."sense" mRNA by forming double-stranded RNA structure. Therefore, if the artificial antisense RNA is delivered into the cell nucleus, it could bind to the complementary mRNA and inhibits the synthesis of the corresponding protein [1]. If a similar strategy is employed to block transcription by forming triple-helix with a double-stranded DNA, it is called *antigene strategy (Figure 1).*

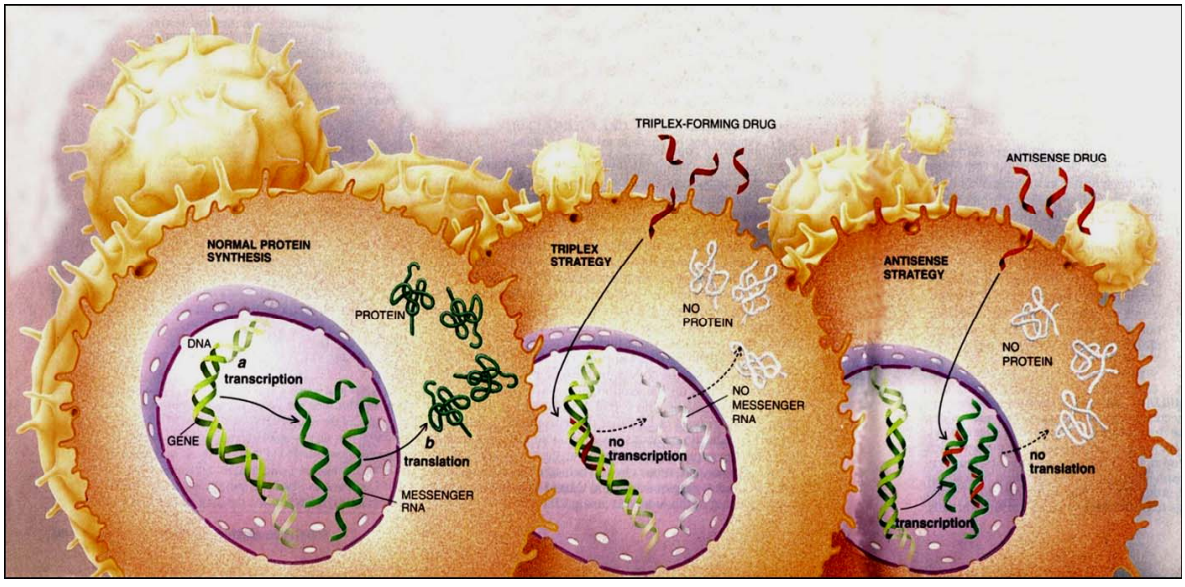

Figure 1. Scheme of antigene and antisense strategy

Both oligonucleotide strategies can be used for silencing expression of undesired genes and, thus, to inhibit propagation of some diseases, e.g. AIDS, leukemia, hepatitis.

Commonly, oligonucleotides with a length of 10 - 30 bases are used for oligonucleotide therapies. Natural oligonucleotides are in general large hydrophilic polyanions that are not able to diffuse alone through the cell membrane. They rest outside of the cells and can form the aggregates at the surface of the cells or could pass into the cells by the endocytosis. However, after endocytosis they frequently stay enclosed in endosomes or lysosomes, and from there they can be released out of the cell by exocytosis or they are often digested by endonucleases. To increase therapeutic effectiveness of the oligonucleotides, some carriers are used to deliver them into the cytoplasm, from where they are more easily transported into the cell nucleus [2]. It was shown that mitosis (process of cell division which results in the production of two daughter cells from a single parent cell) increases the uptake of nucleic acids into cell nuclei. This could be useful for therapy of many types of carcinomas, where the cells undergo rapid proliferation [3]. Compared to the healthy tissue, tumor's vasculature is relatively more permeable, hence it can increase the efficiency of antisense drugs delivery.

At the present, the best known delivery agents are liposomes, which are the complexes of cationic lipids and oligonucleotides. There are several commercially available cationic lipids formed from cationic amphiphiles with hydrophobic aliphatic chains. Liposomes frequently get into the cells via endosomes or lysosomes, not by a direct delivery through the plasma membrane. Further they are released into the cytoplasm and transported into the nucleus. Cationic lipids protect the oligonucleotides from nuclease degradation and they stabilize the final DNA-RNA duplex. Although cationic lipids seem to be the perfect transporters, they have some drawbacks. As the main disadvantages, their toxicity and decreased activity in the presence of serum and antibiotics are to be mentioned. A modification has been made by combining viral vector and liposome, named "virosome", that can deliver oligonucleotides into the cells more efficiently [2].

Another strategy is based on proteins and peptides. When using short peptide vectors, oligonucleotides were protected from the nuclease degradation and they were successfully transported into the cell nuclei [2]. Polyoma virus capsid protein VP1 was used to simulate viral capsids with oligonucleotides inside them. However, only small cellular uptake and high toxicity comparable to cationic lipids [4] does not make this method suitable for mass drug production.

Very interesting is the utilization of cyclodextrines. The main advantage is that they can be taken orally, as they have a high uptake from stomach and small intestine, which avoids the problem of extravasation of oligonucleotides from the bloodstream. Cyclodextrines are very small compared to liposomes, therefore they allow incorporation into pumps thus enhancing membrane penetration. However, some cyclodextrines are strongly cytotoxic. Formation of harmful cholesterol microcrystals in the lysosomes of epithelial kidney cells was observed by long-term taking of the cyclodextrines [3].

Several polymers have also been used as oligonucleotide carriers. PAMAM (polyamidoamine) dendrimers are spherical, highly ordered polymers. These dendrimers have low cellular toxicity and are stable in presence of serum proteins [2]. PEI (polyethyleneimine) polymers can buffer endosomes to prevent potential degradation of nucleic acids. They also cause osmotic swelling and rupture of the endosome, thus allowing the release of nucleic acid into the cytosol. PEI has been used for water purification, mineral extraction, shampoos and according to animal trials it has been found to be safe [3], as its cytotoxicity is very low.

Nanoparticles and microspheres are solid colloidal drug carriers sized from 10 to 990 nm. They consist of macromolecular materials, in which the oligonucleotide is captured or adsorbed onto its surface [2]. They show high cellular uptake, but some of them are very toxic (cyanoacrylate nanoparticles for example [4]).

At last, water-soluble cationic porphyrins have been shown to serve as promising delivery agents for oligonucleotides. They form relatively stable but reversible complexes with nucleic acids; they neutralize negative charge of nucleic acids and protect them from enzymatic degradation [7]. Previously, cationic porphyrins themselves have been used as effective tumor-localizing agents and they have been applied for detection and treatment of some types of carcinomas. When used as transport agents, up to 80 % of the delivered oligonucleotides were found to be localized in the cell nucleus, while for cationic liposomes it was only 30 % [5]. Complexes of porphyrins with oligonucleotides showed generally very low toxicity [4, 5] in comparison with other delivery agents, and provide significant protection from nuclease digestion [6]. Other important advantage of the porphyrins arises from the fact that they have been found to transport oligonucleotides even into leukemic cells where other carriers (e.g. cationic lipids) failed [7].

Several agents (cationic peptides and polypeptides, polycationic dendrimers polyethylenimine, cationic liposomes) studied as potential oligonucleotide cariers are known to promote (under certain conditions) condensation of DNA duplexes into

nanoscale particles. As the condensation, in general, facilitates entry of nucleic acids into the cells and protect them from endosomal degradation, possibility to increase of the oligonucleotide cellular uptake by controlled condensation is studied presently [8]. It was demonstrated that short single-stranded oligonucleotides can be condensed by some agents into very small and homologous non-covalent assemblies in the form of well-defined duplexes with single-stranded nicks and gaps [8]. As some of the cationic porphyrins have been shown to form condensates with single-stranded oligonucleotides [6,7], thus they are interesting also from this point of view.

2.2 Porphyrins

Porphyrins are tetrapyrrolic aromatic macrocycles consisting of four pyrroles linked together through four unsaturated methine junctions *(Figure 2 a)*. Inner 16-membered conjugated ring with 18 π electrons forms central cavity that can host up to four hydrogens attached to pyrrole nitrogens or a metal cation. Porphyrin form with two inner hydrogens is known as neutral *free base* and its macrocycle is planar, in general, with a symmetry D_{2h} By lowering pH, the two remaining pyrrolenine nitrogens can be protonated by forming *monoacidic* and *diacidic* forms, the later with D_{4h}. In the central cavity of the macrocycle a metal atom (preferentially cations of transition metals) can be fixed by coordination bonds to pyrrole nitrogens, and the corresponding *metalloporphyrin* is formed *(Figure 2 b)*. Some physico-chemical and binding properties of metalloporphyrins depend on the nature of the central atom since certain transition metals can form (apart from four coordination bonds with pyrroles) two additional axial bonds perpendicular to the macrocycle ring with other ligands. According to actual electron structure of *d*-orbitals, some transition metals can have various coordination numbers (4, 5, 5-coordinate). When incorporated into the porphyrin macrocycle, they could cause modification of the porphyrin geometry. For instance, Zn^{2+} and Fe^{3+} are 5–coordinating, therefore corresponding porphyrins have deformed square–pyramidal shape (axial ligand is attached to the out-of-plane 5-coordinate bond). Distorted octahedral for 6- coordinating metals like Mn^{3+} (two opposite axial ligands) or even square antiprism for 8-coordinate metals like Sn^{3+}, where the central atom connecting two porphyrins, are also possible. Ni^{2+} forms 4- or 6-coordinate species without axial ligands or with two weakly-bound axial ligands that can be easily released, respectively. On the other hand, porphyrins with Cu^{2+} are known to have no axial ligands in their ground electronic state, however, in some particular excited states (*d-d*) they can

form transient short-living 5-coordinated complexes with proper ligands from their proximity [43-46].

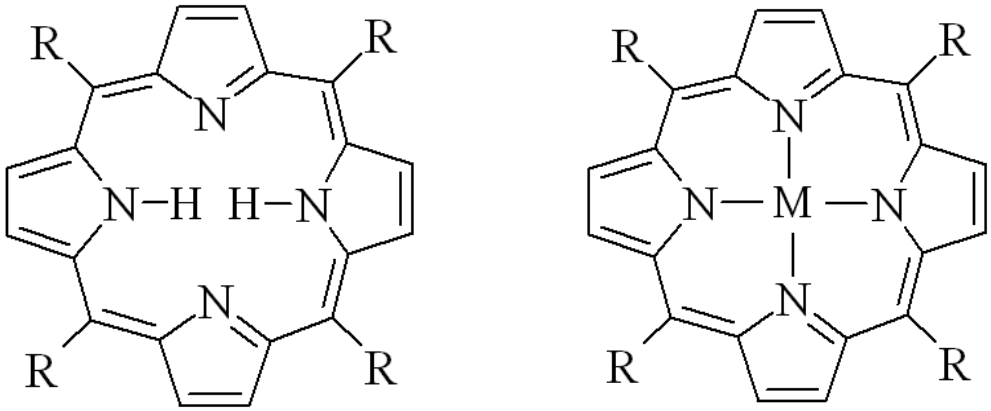

Figure 2 a. Free-base porphyrin *2 b. Metalloporphyrin*

Numerous modifications of porphyrin macrocycle can be achieved by various peripheral chemical groups attached to C_β carbons (farthest from the nitrogen atom) of the pyrrole rings or to C_m carbons of methine bridges, the later constituting plentyful family of *meso*-substituted porphyrins (peripheral substituent marked R in *Figure 2*). These substituents can be of various nature, size and charge, however, from the point of view of interactions with nucleic acids, namely the porphyrins bearing positively charged groups are of prime importance. Cationic porphyrins with *meso*-substituents are usually well soluble in water.

Large aromatic macrocycle of the porphyrins has a relatively small gap between ground and excited electronic states, and all porphyrins and metalloporphyrins absorb light strongly in the visible (VIS) and near-ultraviolet (UV) region of the spectrum. Classical absorption spectrum of the *free-base* porphyrin consists of a very intense band, called the B or Soret, located nearby 400 nm, and of several (usually four) weaker bands, called Q, between 500 – 700 nm. Free base *meso*-substituted porphyrins have usually red color in aqueous solutions due to the strongest Q-band absorption around 500 nm. On the contrary, their diacidic counterparts are usually green due to increased Q-band absorption around 600 nm. Porphyrin protonation has considerable influence also on the position of the Soret band, generally shifting its position to longer wavelengths for about 10 - 20 nm. Metallation of the porphyrin (similarly to diprotonation) results in reduction of number of the Q-bands, whereas position the Soret band could remain virtually unchanged for some

transition metals, e.g Cu^{2+}. Consequently, metallation process can be noticed more reliably in the Q-band region.

Beside the oligonucleotide delivery, cationic porphyrins are frequently used in photodynamic therapy of cancer [11]. Other potential applications include inhibition of the HIV-1 and HSV-1 viruses [12], selective cleavage of DNA and RNA [13], DNA footprinting [14] and telomerase inhibition by stabilization of the guanine quadruplexes [15].

2.3 Nucleotides and nucleic acids

A *nucleotide*, a basic unit of nucleic acids, is composed of pentose sugar (β-D-ribose, β-D-2'-deoxyribose), phosphate residue from phosphoric acid and *planar aromatic* purine or pyrimidine base (A, G, C T, U) *(Figure 3 and 4)*. Complex of the pentose and heterocyclic base only constitutes a *nucleoside*. As the sugar can be either ribose or deoxyribose, the corresponding nucleotides are ribonucleotides or deoxyribonucleotides, the former containing uracil instead of thymine *(Figure 4)*. Nucleic acids exist as long oriented polymers, the oligo- and polynucleotides, consisting of nucleotides connected by 3',5'-phosphodiester bonds between 3' and 5' carbons of two consecutive nucleotides. Individual polynucleotides can form more complex structures due to specific interactions between bases, e.g oriented single-stranded helices, double-helices, or even triple- or quadruple-helices.

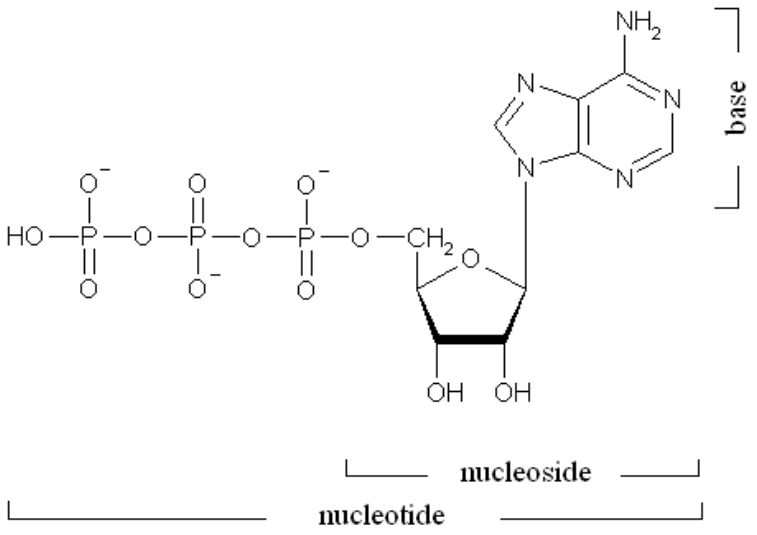

Figure 3. Model of nucleoside and nucleotide (trinucleotide)

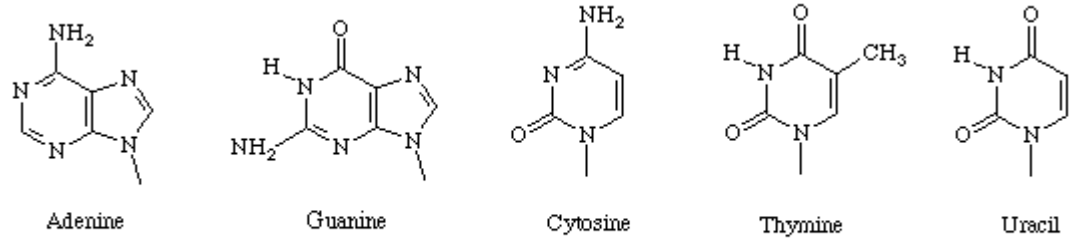

Figure 4. Purine (A, G) and pyrimidine(C, T, U) bases

Forces stabilizing association between bases are of two kinds: in-plane-of-the-bases (thus horizontal) hydrogen bonding between adenine and thymine/uracil (A-T and A-U Watson-Crick base-pairs) and guanine and cytosine (G-C Watson-Crick base-pairs, *Figure 6*), and perpendicular-to-the-base-plane base stacking (mainly London dispersion and hydrophobic forces). Chain direction is oriented from 5'- to 3'- end as shown on *Figure 5*, and forms an oriented helix. The chain orientation and helical structure seem to have important biological consequences since replication, transcription and translation of genetic information from nucleic acids can be accomplished only in a distinct direction, e.g. continuous synthesis of a new chain is possible exclusively from 5'- to 3'-end. Each chain is thus finished at the 5'-end by a phosphate group and on 3'-end by a hydroxyl group. Even slight structural difference between ribose and deoxyribose (OH- and H-groups at the $C_{2'}$ carbon of the respective pentose) seems to have profound structural, conformational and biological consequences. Natural ribonucleic acids (RNA) composed of ribonucleotides form usually single-stranded polynucleotide chains, or they could be partly organized into double-stranded structures (stems) at particular regions with complementary sequences where bases can form Watson-Crick pairs. Unpaired oligonucleotide regions between the complementary sequences form loops (hairpin, bulge or interior). RNA serves as a kind of 'helping' molecule in the cells where it participates in translation (mRNA), transcription (tRNA) or can be part of ribozomes (rRNA) and several enzymes. In bacterial as well as in animal cells the amount of RNA is six times greater the amount of DNA [1]. DNA consisting of deoxyribonucleotides usually forms a double-stranded helix. The strands in the natural double helix are antiparallel (one strand is in opposite direction to the other) and the opposite strands are bound together via Watson-Crick (W-C) hydrogen bonding between bases *(Figure 6)*.

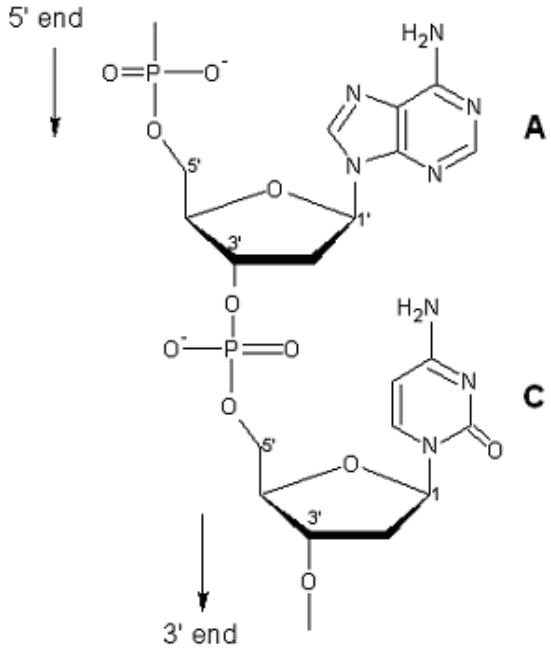

Figure 5. Oriented dinucleotide as basic building block of nucleic acids

In more-stranded structures and in some synthetic polynucleotides other hydrogen bonding can take place, e.g. reversed Watson-Crick, Hoogsteen and reversed Hoogsteen [48]. While A-T Watson-Crick base-pairs are connected only two hydrogen bonds, G-C bases are joined by three bonds and thus are stronger. Since each strand of double-stranded DNA contains a sequence of nucleotides exactly complementary to the nucleotide sequence of the opposite strand, summative contributions of each of the base-pair together with vertical stacking interactions stabilize the helix despite existence of rather strong repulsive forces between identically charged phosphates. Charged phosphates are oriented outside of the helix and are responsible for hydration of the helix surface exposed to exterior, as well as for Coulombic interactions with cations present in the solvent.

Due to flexibility of the polynucleotide helix, nucleic acids can exist in various conformations. The most frequent conformation of DNA is the B-form in which the helix is right-handed and the planes of base-pairs are oriented nearly perpendicular to the helix axis. Each turn of DNA consists of 10 nucleotide base-pairs, vertical distance between two adjacent nucleotides in the same strand is 3.4 Å, and the helical twist between them is 36° [1, 48]. By coiling of the double-helix, two grooves (major and minor) are formed on its surface, separating the sugare-phosphate backbones by two unequally wide surfaces where the base-pairs are somewhat exposed to exterior *(Figure 6)*. For B-DNA, the distance between the opposite sugar-phosphate backbones in the major groove equals to 11.7 Å, while the minor groove is only 5.7 Å wide [9]. Another right–handed form of DNA is the

A-form where has each turn of DNA consists of 11 nucleotide base-pairs and the bases-planes are not perpendicular to the helix axis. The Z-form of DNA, which is left–handed, was observer in oligo- and polynucleotides with alternating G-C sequences in solutions with extremely higher ionic strength [48].

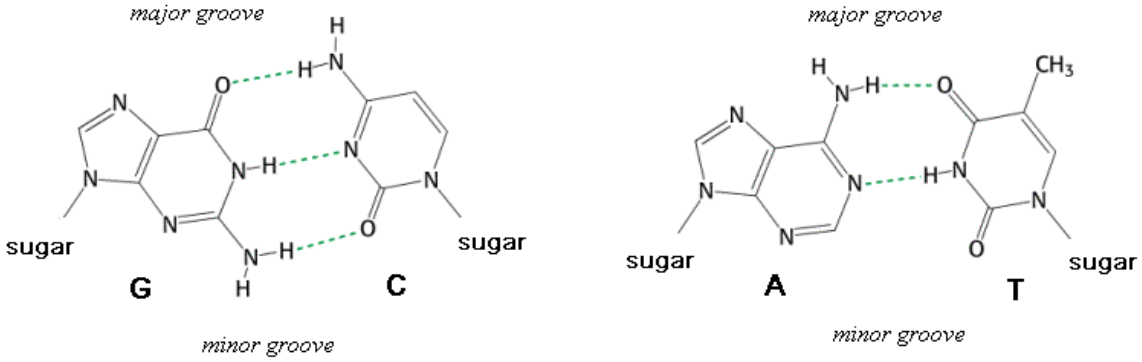

Figure 6. Watson–Crick pairing of G-C and A-T bases

There are considerable differences even between single–stranded structures of the synthetic polynucleotides of DNA and RNA type, and the polymorphism seems to be sequence- as well as structural-dependent. E.g., for a neutral pH value and in the absence of divalent cations, poly(rA), poly(rC) and poly(rU) exist preferentially in the A form single helix while poly(dA) exists as the B form with substantial stacking between adenines, whereas poly(dT) forms only loosely organized (if ever) right–handed structure with non-stacking thymines [9]. The polynucleotide conformation can be strongly affected by physico-chemical conditions (pH, ionic strength, interactions with specific cations or other substances).

2.4 Interactions of porphyrins with double–stranded DNA

The sugar–phosphate backbones of double-stranded nucleic acids are oriented outside the duplex, thus creating two easily accessible negatively charged surfaces allover the helix, separated by more hydrophobic surfaces inside the grooves. The cationic porphyrins are therefore electrostatically attracted to dsDNA or dsRNA, nevertheless hydrophobic and van der Waals interactions with interior of the grooves have to be considered as well. In general, three binding modes have been described: (a) intercalation of the porphyrin macrocycle between base-pairs, (b) outside groove binding and (c) outside binding with self-stacking of the porpyrins [16]. The self-stacking leads to formation of organized

helical structures of the porphyrin molecules on the DNA helix, that serves as a template for organized helical porphyrin structure. Two principal modes of outside grove binding can be suggested. The porphyrins can be attached "face-on" across the groove (probably the major one), being fixed by its charged substituents to opposite sugare-phosphate strands. In that case the plane of porphyrin macrocycle is perpendicular with respect to the base-pair planes. The second possibility is the "edge-on" binding, when the porphyrin macrocycle is partly inserted into the groove of the DNA *(Figure 7)*.

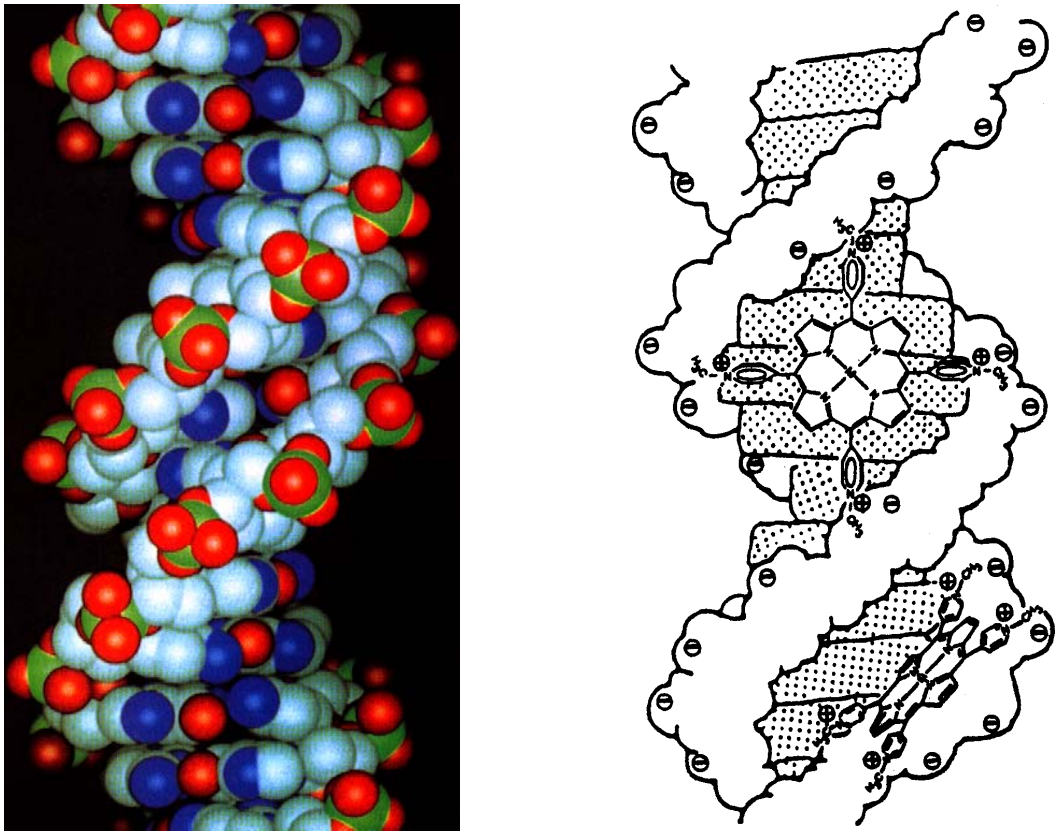

Figure 7. Model of double–stranded DNA with the face-on and edge-on outside groove bound porphyrin in the major and minor grooves, respectively. Charged oxygens of the phosphates on the left figure are depicted in red.

First investigations of the porphyrin interactions with nucleic acids were made by R. J. Fiel *et al.* in 1979 [49]. It was demonstrated that free-base 5,10,15,20-*meso*-tetrakis(4-N-methylpyridyl) porphyrin (H_2TMPyP_4) can intercalate into the calf thymus dsDNA [49, 17]. Apart from typical spectral changes (extensive hypochromicity of the Soret band in absorption spectra), stabilization of the DNA helix against thermal denaturation, increase of relative viscosity of the complex indicating a lengthening of the DNA chain as well as unwinding of covalently closed circular DNA helix upon interaction with H_2TMPyP_4

supported unambiguously identification of the binding mode as intercalation. Great deal of the research was done later by R. F. Pasternack *et al.* [17, 20, 21, 28] with various metal derivatives of H_2TMPyP_4, namely Cu^{II}, Ni^{II}, Zn^{II}, Co^{III}, Fe^{III} and Mn^{III}. They reported first usable methods for preparation and purification of the metallated cationic porphyrins and they contributed enormously to our present understanding of the way how the cationic porphyrins (namely metalloderivatives of H_2TMPyP_4) interact with different binding sites of dsDNA. Pasternack was the first who discovered different binding mode with sequences consisting preferentially from A-T and G-C base-pairs. In the case of H_2TMPyP_4, the most widely studied and the best described cationic porphyrin, preferential intercalation into G-C rich sequences was observed, whereas outside groove binding for A-T rich sequences was confirmed [17].

Apart from the sequence-dependence, the porphyrin binding mode to dsDNA depends also on the porphyrin properties, namely on the size, number, charge and position of its peripheral substituents. Other dependence is given by a dimension and planarity of the porphyrin macrocycle, where supposable axial ligands of the central atom can play important role. For intercalation, small, planar and flexible substituents seem to be favorable, whereas bulky nonplanar substituents dictate other binding modes. Central atoms deforming planarity of the porphyrin macrocycle or having strongly bound axial ligands seem to inhibit intercalation. Outside groove binding seems to be influenced mainly by electrostatic (Coulombic) and H-bonding interactions between porphyrin substituents and DNA backbone, while hydrophobic effects have been considered as less important. On the other hand, in the case of intercalation, hydrophobic effects and van der Waals interactions are as important as electrostatic, dipole–dipole and H-bonding interactions [18].

As mentioned above, binding modes of metalloporphyrins to nucleic acids can also be influenced by the properties of the central atom. Metalloorphyrin species with four–coordinate cations like Cu^{2+} and Ni^{2+} (later with loosely bound axial ligands that can be easily released) having square-planar geometry can intercalate in the same way as their free-base counterparts. Metals with higher coordinate numbers, having one or two tightly-bound axial ligands hindering intercalation, prefer outside binding.

Since there exist several binding modes and each of them requires binding site of different size, interpretation of experimental binding curves could be rather complicated. Pasternack et al. [17] used the McGhee–von Hippel model to analyze data from titration experiments monitored by absorption spectroscopy. This model deals with binding of

drugs to homogenous one-dimensional polynucleotide lattice and includes neighbor exclusion effects. In review made by Chaires [19] it was assumed that neighbor exclusion models count with the DNA lattice consisting of an array of identical and noninteracting potential binding sites, the base pairs. Binding of the ligand (e.g. porphyrin) to one site prevents neighboring sites from interaction with other ligands. Together they form the so-called "neighbor exclusion parameter". As the lattice approaches saturation, the probability of finding a free site on DNA decreases. The binding of the porphyrins to DNA is, thus, predominantly anticooperative. McGhee and von Hippel derived an equation:

$$\frac{r}{C_f} = K(1-nr)\left[\frac{1-nr}{1-(n-1)r}\right]^{n-1} \tag{1}$$

where C_f is the free ligand concentration, r is defined as the ratio between the concentration of bound ligand (porphyrin) and total concentration of the lattice sites (base-pairs), K is an apparent association constant for ligand binding to an isolated lattice site, and n is the neighbor exclusion parameter (number of consecutive lattice residues made innaccessible by binding of a single ligand molecule). For this model, n should be only an integer number. A fractional value makes no physical sense for a lattice composed of identical, noninteracting sites. Therefore this model is not fully appropriate for analyzing the data.

Later it was derived by Friedman and Manning [50] a neighbor exclusion model that involves some aspects of polyelectrolyte theory. Condensation of counterions around DNA is dictated by the spacing of the negatively charged phosphates along the double helix. Specifically, intercalation of a charged ligand between stacked base pairs increases their distance, and consequently, distance between adjacent phosphate charges increases as well. Counterion release induced by charged ligand provides an energetically favourable contribution to the binding free energy. The saturation of intercalators causes decrease in the polyelectrolyte contribution to the binding free energy. A complicated model and equations counting with polyelectrolyte correction was suggested for the B-form DNA [50]. Although this model is more general than the McGhee and von Hippel model, in all examined cases the fits were statistically worse than those obtained by the simpler model. Thus, there is no reason to use this more complicated model.

The neighbor exclusion models count with homogenous lattice sites. On the other hand, chemical and enzymatic footprinting methods have shown that most ligands bind to different DNA sites with different affinities. Preferential binding to AT or GC sites can

occur in several different ways. Molecular dynamics studies concluded that the neighbor exclusion is not a necessary condition for intercalation.

Another possibility besides the neighbor exclusion concept is to count with heterogeneity of DNA and to assume each binding site as a dinucleotide unit [19]. Among 16 possible dinucleotide combinations, there exist only 10 unique: AT, AA (=TT), TA, AC (=GT), CA (=TG), GC, GG (=CC), CG, GA (=TC), AG (=CT) forming intercalation sites composed of two consecutive base-pairs. Supposing that the ligand has different affinities (K_{MN}) to different dinucleotide units (MN), the binding isotherm can be described by [19]:

$$r_D = \sum^{MN} \frac{f_{MN} K_{MN} C_f}{1 + K_{MN} C_f} \tag{2}$$

where r_D is the binding ratio expressed as moles of ligand per mole of dinucleotide, f_{MN} is the dinucleotide frequency (relative occurrence in a given DNA) determined and tabulated for numerous natural DNAs and C_f is the free ligand concentration. Because there are 10 unique dinucleotide steps, the equation has 10 terms and 10 binding constants K_{MN} must be obtained by nonlinear fitting of experimental data. Although such an exercise may seem hopeless, it was shown that it could provide reasonable results [19]. For example, affinities determined for different dinucleotides for ligand daunomycin were in agreement with experimental results [19]. Fractal values of the neighbor exclusion parameter, received from fitting the data obtained from this model to the neighbor exclusion model, were in excellent agreement with fits from the experimental data. It would be interesting to apply similar approach for intercalation of cationic porphyrins to dsDNA.

Some difficulties could appear for oligonucleotides of limited length, because both above presented models expect an infinite lattice. Significant end effects exist for oligonucleotides shorter than 24 base pairs. The data can therefore be analyzed by stochiometric binding models for multiple identical, non-interacting sites:

$$r = \frac{nKC_f}{1 + KC_f} \tag{3}$$

where r represents the moles of ligand bound per mole of oligonucleotides, n is the number of binding sites and K is the association constant.

The most commonly used model for the interpretation of ligand binding to DNA is the McGhee-von Hippel model. Although this model has some imperfections, it is often sufficient for obtaining basic information.

2.5 Interactions of porphyrins with single–stranded DNA and RNA

Interactions between cationic porphyrins and single-stranded nucleic acids have not been investigated in such details as with double-stranded polymers. There are only few publications concerning this problem [20, 21, 50, 51]. The reason for such omission could stem from greater tendency of single-strands to form aggregates and precipitates even with H_2TMPyP_4 and its metalloderivatives. Spectroscopic experiments with single-stranded DNA and RNA are quite complicated due to the presence of various artefacts hindering reproducibility. The results obtained are therefore difficult for unambiguous interpretation. On the other hand, interactions with single-strands represent wide and exciting region of research mainly for oligonucleotide strategies, since porphyrin-assisted oligonucleotide delivery concerns nearly exclusively single-strands.

In a similar way as with double-stranded nucleic acids, three fundamental binding modes could be expected for single-strands: intercalation, outside binding and outside binding with self-stacking of the porphyrins, manifesting similar spectral changes in electronic absorption and CD spectra. Since adjacent bases can interact by vertical stacking even in the single strand, it is possible to suggest partial intercalation, when the porphyrin macrocycle is inserted between two neighboring bases. As there are no grooves in the single-stranded polynucleotides, outside binding signifies attachment of the porphyrin macrocycle to the hydrophobic surface of several vertically stacked bases. In that case the binding site would comprise at least 5 consecutive bases, as shown for H_2TMPyP_4 on *Figure 8*. Interaction with cationic porphyrin can induce formation of more complicated structures consisting of several single-strands folded in different ways and stabilized by hydrogen bonding between bases, as it was demonstrated in the case of guanine quadruplexes [15, 53].

Pasternack *et al.* [20] investigated systematically interactions of free-base and several metallated derivatives (Cu, Ni, Au, Pd) of H_2TMPyP_4 with single-stranded poly(dA) in comparison with calf thymus DNA. As extensive hypochromicity of the Soret band was observed for all porphyrin-poly(dA) complexes suggesting interaction between the π-systems of neighboring porphyrins and/or interaction with the π-system of the adenine bases: it was concluded that pseudointercalation of the porphyrin is a predominant binding mode for poly(dA). However, some spectral differences have been noticed between $CuTMPyP_4$ complexes with dsDNA and ss-poly(dA). Under high porphyrin load and high

ionic strength, poly(dA) complexes with $CuTMPyP_4$ displayed spectral features characteristic of porphyrin-porphyrin interactions on a chiral matrix.

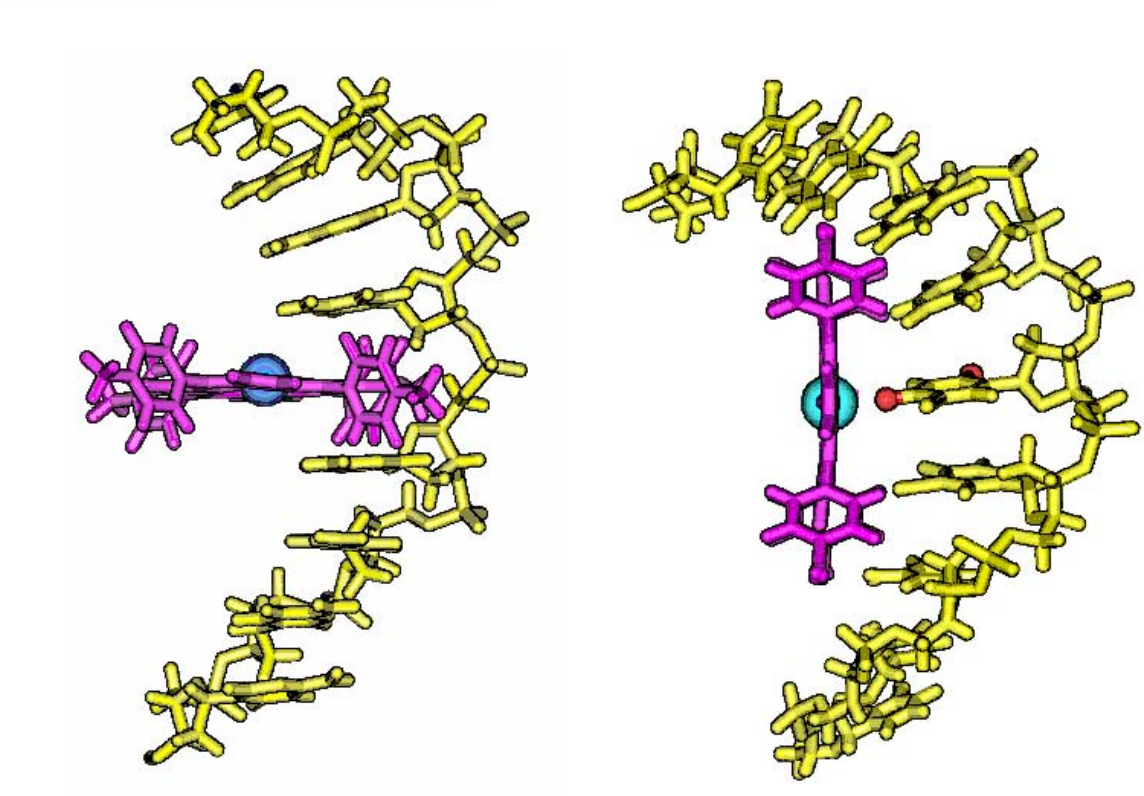

Figure 8. Model of single–stranded NA with intercalated and outside-bound porphyrin

Thus, it is possible that $CuTMPyP_4$ can aggregate on the poly(dA) surface, at least under conditions of high porphyrin load and higher ionic strength. On dsDNA (natural or synthetic) no such aggregation of the $CuTMPyP_4$ was reported yet. The aggregation of porphyrins was shown to be ionic strength dependent.

Later, different binding modes have been observed for synthetic ribonucleic and deoxyribonucleic acids containing the same bases. E.g., based upon absorption and CD spectra, it was reported [21] that H_2TMPyP_4 and $CuTMPyP_4$ are capable to discriminate between poly(rA) and poly(dA), i.e. between interactions with single-stranded helices belonging to A-form in B-form families, respectively. Even thought both polynucleotides poly(rA) and poly(dA) have been shown to promote the self-stacking of H_2TMPyP_4 and $CuTMPyP_4$ on the polynucleotide helices, characteristic differences have found in their absorption and CD spectra. Moreover, recently [46] other evidence for different binding modes was confirmed by resonance Raman spectroscopy and formation of the $CuTMPyP_4$ exciplex.

3 Experimental part

3.1 Spectral measurements

3.1.1 Absorption spectroscopy

Electron absorption spectroscopy is based on the decrease of intensity of optical radiation when going through an absorbing medium [22]. The electron absorption spectra are detected in ultraviolet – visible (UV-vis) region, in the case of chromophores studied in the present work typically 200 – 700 nm. The energy added to molecules from the absorbed radiation is used for the transition of the molecule from the basic to an excited state. Absorption in the near UV – visible region results in the transition of the electrons from π to π^* or n to π^* orbital, therefore the presence of electrons in π or n orbitals of the measured molecules is necessary. The probability of the electron transition and thereby the intensity of absorption depends on the size of the dipole transition moment.

Absorption spectra of the chromophore molecules in aqueous solutions usually do not posses the fine structure of electron transitions due to interactions between the chromophore and solvent molecules that cause a broadening of the spectrum. In absorption spectra we can therefore observe broad bands belonging to electron absorption transitions.

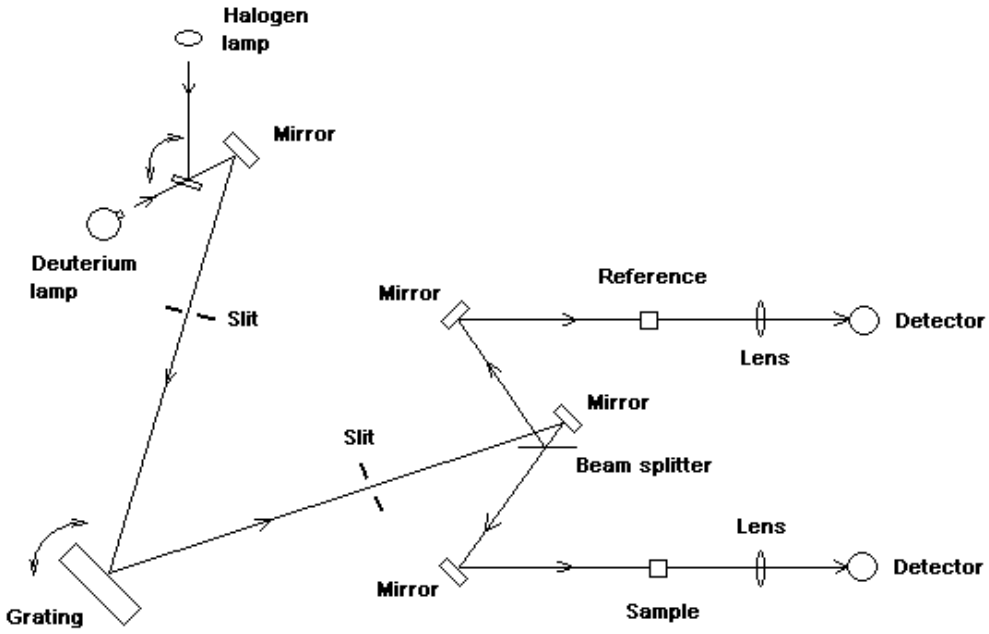

Figure 9. Scheme of the UV-vis absorption spectrometer Perkin-Elmer Lambda 12

Although it is not possible to determine structural properties of the chromophore molecules solely from their electronic transitions, absorption spectroscopy provide simple and practical method for study changes of some basic structural properties caused by intermolecular interactions, and intramolecular structural and conformational transitions. Typical double-beam apparatus used for absorption spectroscopy is depicted in *Figure 9*. The radiation source is a halogen lamp for the visible region of the spectrum and a high pressure deuterium lamp for the near UV region. The original beam is divided into two parts; one beam goes through the reference cell and the other is targeted to the cell with the sample solution. The resulting spectrum is the difference between the values measured for the sample and reference. In our measurements we have used the Perkin–Elmer *Lambda 12* spectrometer with changeable reference and sample holder and with a measuring range of 200 - 1100 nm.

3.1.2 Raman spectroscopy

Raman spectroscopy belongs to the light scattering optical methods. Detail description of the method, experimental tools and application to biochemical and biophysical problems can be found in [56]. In short, Raman spectroscopy is based on inelastic scattering of the photons by molecular vibrations. The vibrating molecule interacts with an incident photon having energy $E = h\omega_i$ and it undergoes transition from its original vibronic state E_i to a virtual state whose energy is, however, lower than the energy of its lowest excited state E_e *(Figure 10)*. This scattering interaction is connected with appearance of the photon whose energy can be higher or lower than that of the incident photon by a difference equal to energy transition between two adjacent vibrational states. If there is no energy exchange between the incident photon and the molecule, the photon is scattered elastically to produce Rayleigh scattering. Thus, in the scattered spectrum around the line of elastic Rayleigh scattering other symmetrically separated lines corresponding to inelastic Raman scattering appear. The region of the lines belonging to lower frequencies is called *Stokes*, the region of higher frequencies is called *anti-Stokes*. Frequencies of the inelastically scattered photons can be expressed as:

$$\omega_S = \omega_i - \omega_M \qquad \omega_{AS} = \omega_i + \omega_M \tag{8}$$

where ω_S belongs to Stokes region, ω_{AS} belongs to anti-Stokes region and ω_M is the frequency of the molecular vibration and is equal to $(E_f - E_i)/h$.

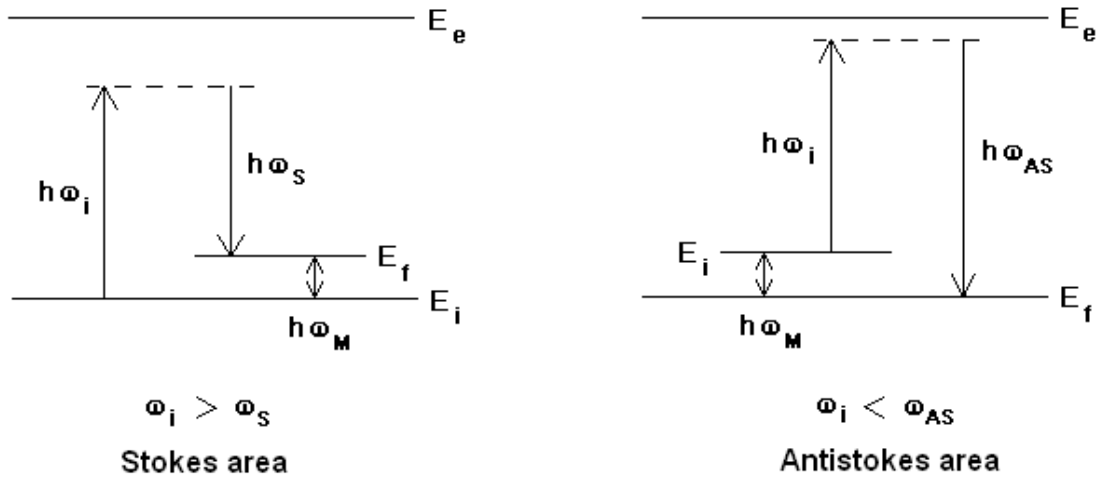

Figure 10. Schematics of Stokes and anti-Stokes Raman scattering

The classical treatment of the Raman effect gives no differences in the expected intensities of Stokes and anti-Stokes transitions, nevertheless the population in both stationary states of the molecule E_i and E_f have to be determined by the Boltzmann distribution, thus the states with lower energy in thermal equilibrium are more populated. As a result of the Boltzmann distribution, the real intensity of the lines in Stokes region is markedly higher than that in the anti-Stokes region. Moreover, intensities of the anti-Stokes lines are quickly decreasing with increase of the energy of vibrational transition. Consequently, at the ambient temperatures only anti-Stokes lines of lower frequencies are observable in the spectra. For practical reasons only more intense Stokes parts of the Raman scattering are usually studied despite the fact that anti-Stokes scattering could also provide some interesting advantages, e.g. possibility to avoid overlap with fluorescence that is always located in the Stokes region.

If the frequency of excitation radiation v_o is sufficiently distant from the frequencies of allowed electron absorption of the molecule, a non-resonance Raman scattering is observed. In this case the intensity of lines in the spectrum is about 6 orders lower than the intensity of the elastic scattering. However, if we choose a frequency of radiation v_0 that is near the frequency of a possible electron transition $(E_h - E_g)/h$, where $g \leftrightarrow h$ is the electron transition we use resonance approximation. If the vibration of the observed line is permitted, a rapid increase of the intensity appears. The intensity increase can be even of several orders. This method is than called the *resonance Raman scattering* (RRS) and causes increase and changes of the whole measured spectrum.

In the present diploma thesis, resonance Raman scattering was used, exiting spectra of the porphyrins in resonance with the Soret absorption band. The apparatus for measuring Raman scattering is represented on *Figure 11*.

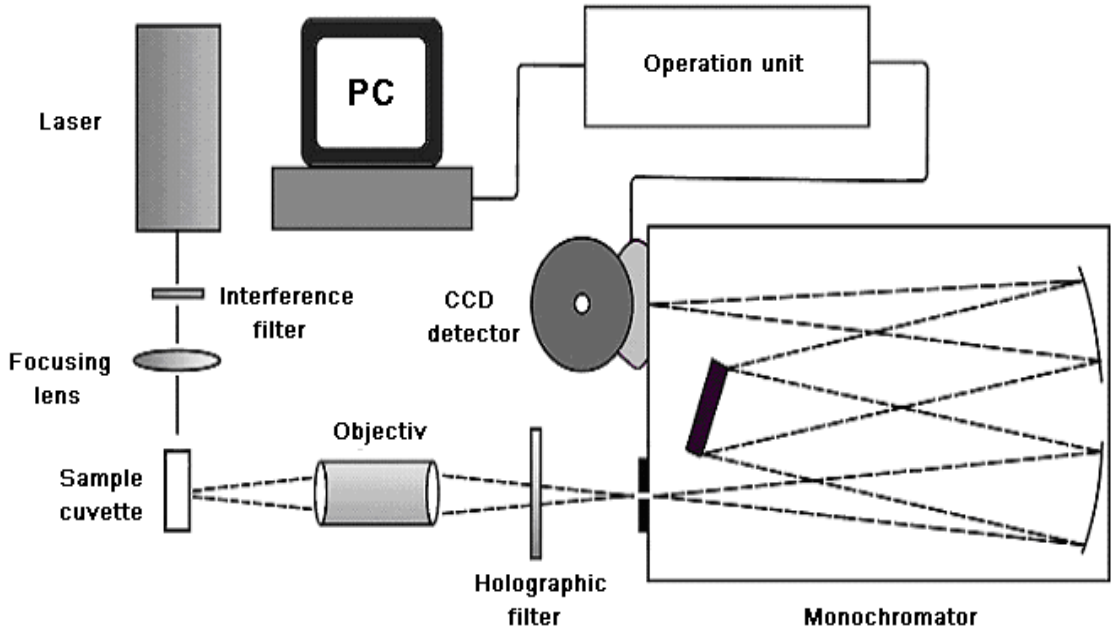

Figure 11. Scheme of the Raman spectrometer with 90° geometry

The modular Raman spectrometer with 90° geometry used in our measurements was rebuilt and upgraded during the course of this diploma work. Participation on the upgrade, adjustment and testing spectral properties was a part of diploma work. For the excitation of the resonance Raman spectra of the porphyrins, we have used a He-Cd laser Liconix with emission wavelength 441.6 nm and typical power at the sample 12-13 mW. For the light dispersion, an imaging monochromator Jobin Yvon-Spex M270 with a focal length of 270 mm was used. Monochomator is equipped with two holographic grating (50 x 50 mm) with 1800 and 1200 grooves/mm. Nevertheless, in all our measurements the grating with 1800 grooves/mm was used. The Princeton Instruments CCD detector, with the chip having 1340 × 100 pixels, was cooled by liquid nitrogen to -110 to -120°C. For rejection of the Rayleigh scattering, a Raman holographic notch filters were used (Kaiser Optical Systems). Due to polarization sensitivity of the holographic grating, a scrambler was placed behind the focusing objective to depolarize the incoming light. As the sample cells we have used standard 1 mm absorption cells with polished bottom. For accurate calibration of the wavenumber scale, a calibration emission spectrum of neon glow lamp or Raman spectrum of toluene, was taken for each measurement. Calibration of the spectra

was performed routinely by special calibration programs *Neokalkspex.exe* and *Tolkal.exe* created by Doc. Jiří Bok form Institute of Physics, Faculty of Mathematics and Physics.

3.2 Studied porphyrins

In the present work, spectroscopic and physico-chemical properties of six cationic porphyrins have been studied by electronic absorption and resonance Raman spectroscopies, along with their interactions with single- and double-stranded polynucleotides. Three novel porphyrins bearing bulky peripheral substituents of biological importance have been recently synthesized by Prof. Vladimír Král from Institute of Chemical Technology in Prague (VŠCHT), and provided to us as a kind gift: (a) 5,10,15,20-tetrakis(α-distamycin ammonio-*p*-tolyl) porphyrin (H_2TPP-(Dist)$_4$, *Figure 20*), (b) 5,10,15,20-tetrakis(α-brucine-*p*-tolyl) porphyrin (H_2TPP-p-(Bru)$_4$, *Figure 22*), (c) 5,10,15,20-tetrakis(α-brucine-*m*-tolyl) porphyrin (H_2TPP-m-(Bru)$_4$, *Figure 24*). Initially, we intended to study only the Cu^{2+} derivatives since they have several spectroscopic advantages from the point of view of Raman spectroscopy: they are photophysically stable and exhibit only weak luminiscence. However, first samples received and declared as Cu^{2+} derivatives were found to be free-bases. Later, truly metallated species have been obtained, but in a meantime we have tried to synthesize the Cu^{2+} derivatives ourselves. As molar extinction coefficients of the novel porphyrins have not been reported yet, we have tried to determine or estimate their values in the framework of this diploma thesis.

Common basic structure of H_2TPP-(Dist)$_4$, H_2TPP-p-(Bru)$_4$ and H_2TPP-m-(Bru)$_4$ is derived from *meso*-tetratolyl porphyrin, similarly to other *meso*-tetratolyl porphyrins synthesized and studied recently [26, 30]. The bulky substituents (distamycin, brucine) are attached to the tolyl methylene group *via* quarternized nitrogens providing to the porphyrin four positive charges. Distamycin is a short naturally occurring peptide antibiotic, which has been shown to bind non-covalently in the minor groove of AT-rich B-DNA tracts. Brucine is a natural alkaloid having certain potential in medical use, structurally related to strychnine but it is not as poisonous. The porphyrins have been received as tetrabromide salts in the form of free-base and/or Cu^{2+} derivatives. Three other cationic porphyrins were used in this study as structurally relative models: 5,10,15,20-tetrakis(1-methyl-4-pyridinio) porphyrin (H_2TMPyP$_4$, *Figure 12*), 5,10,15,20-tetrakis(4-trimethylammoniophenyl) porphyrin (H_2TMAP, *Figure 14*) and 5,10,15,20-tetrakis(α-trimethylammonio-*p*-tolyl) porphyrin (H_2TPP-(NMe$_3$)$_4$, *Figure 16*). Along with the cationic porphyrins, 5,10,15,20-

tetrakis(4-sulfonatophenyl) porphyrin (H_2TPPS_4, *Figure 18*) and its Cu^{2+} derivative were used as representatives of anionic water-soluble porphyrins derived from structurally the most relative *meso*-tetraphenyl porphyrins. Because of four SO_3^- groups bound to each phenyl ring in *para-* position *(Figure 18)* (thus an anionic structural counterpart of H_2TMAP), it could not bind to negatively charged DNA. However, it is known to aggregate spontaneously in water [24]. We have included this porphyrin to see the differences between behavior of cationic and anionic porphyrins sharing identical *meso*-tetraphenyl moiety.

All the studied porphyrins bear four identical substituents symmetrically attached to the C_m carbons, nevertheless symmetry properties of each porphyrin are strongly affected by symmetry properties of its substituents, flexibility of the attachment bonds, planarity of the substituted porphyrin macrocycle and possible substituent rotation around their single-bond attachments.

The most studied cationic porphyrin H_2TMPyP_4 and its metalloderivative $CuTMPyP_4$ *(Figure 12)*, bear four pyridinium groups in a close proximity of the macrocycle. Due to the relatively small charge distance from the macrocycle, they are excellently soluble in water. Both have been reported not to form self-aggregates in water [24] due to considerable electrostatic repulsion between substituents that evidently exceeds attractive hydrophobic forces between macrocycles. Other cationic porphyrins, studied previously by several authors, are H_2TMAP [5, 21, 24] and $H_2TPP\text{-}(NMe_3)_4$ [26]. The charge-bearing nitrogen atoms in these porphyrins are placed further from the porphyrin center than in H_2TMPyP_4 *(Figure 14 and 16)*, and they represent gradual structural transition from H_2TMPyP_4 to $H_2TPP\text{-}(Dist)_4$, $H_2TPP\text{-}p\text{-}(Bru)_4$ and $H_2TPP\text{-}m\text{-}(Bru)_4$.

Free-base porphyrins have typically four Q bands, intensity of which is decreasing with increasing wavelength. Metallation of the porphyrins results in typical changes in their Q bands, reducing their number to one stronger and one weaker Q band. There could be observed some changes also in the Soret band (position, bandwidth, extinction coefficient), however not as noticeable as by Q bands. Absorption spectra of Cu^{2+} derivatives of all the porphyrins studied here are represented in *Figures 13, 15, 17, 19, 21, 23 and 25*.

Except for UV-vis absorption and resonance Raman spectroscopy, other methods can be used for investigation of interactions of porphyrins with nucleic acids. One can use linear dichroism (LD), circular dichroism (CD), time-resolved fluorescence measurements and nuclear magnetic resonance (NMR).

CuTMPyP$_4$

Copper(II) 5,10,15,20-Tetrakis(1-methyl-4-pyridinio) porphyrin, tetrachloride salt
MW: 882.17

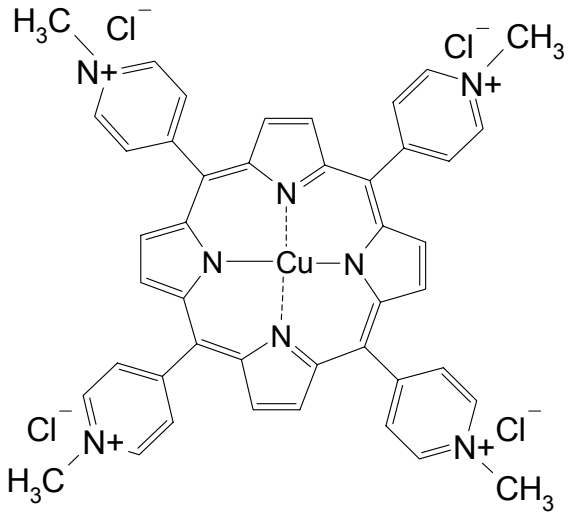

Figure 12. CuTMPyP$_4$ in tetrachloride salt

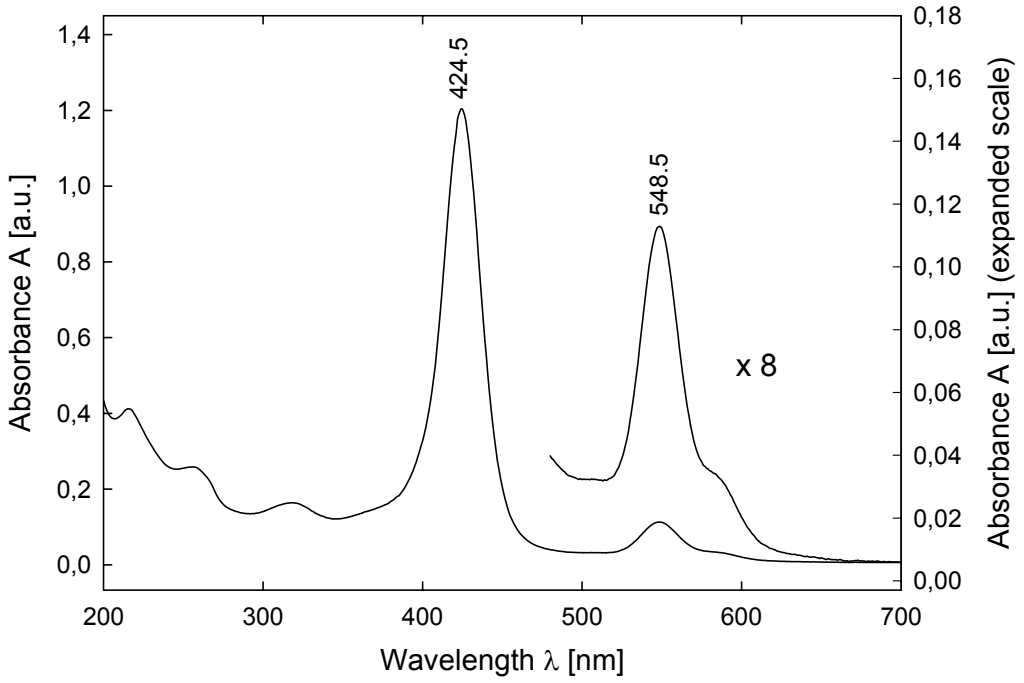

Figure 13. Absorption spectrum of CuTMPyP$_4$

CuTMAP

Copper(II) 5,10,15,20-Tetrakis(4-trimethylammoniophenyl) porphyrin, tetrachloride salt
MW: 1228.29

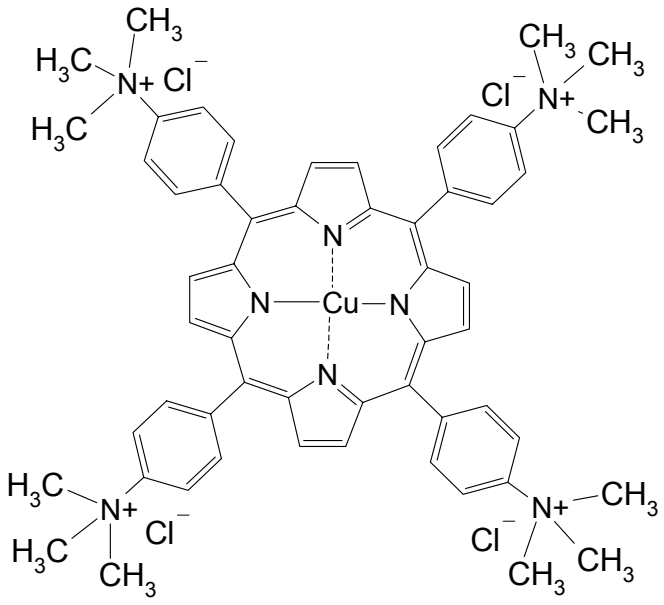

Figure 14. CuTMAP in tetrachloride salt

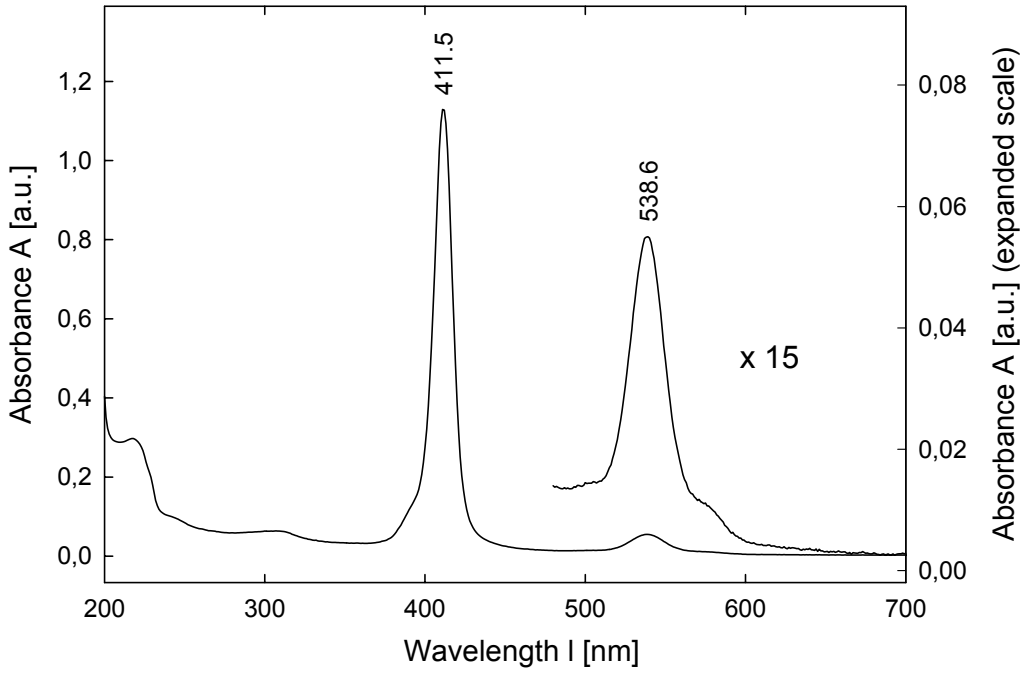

Figure 15. Absorption spectrum of CuTMAP

CuTPP-$(NMe_3)_4$

Copper(II) 5,10,15,20-Tetrakis(α-trimethylammonio-*p*-tolyl) porphyrin, tetrabromide salt
MW: 1284.41

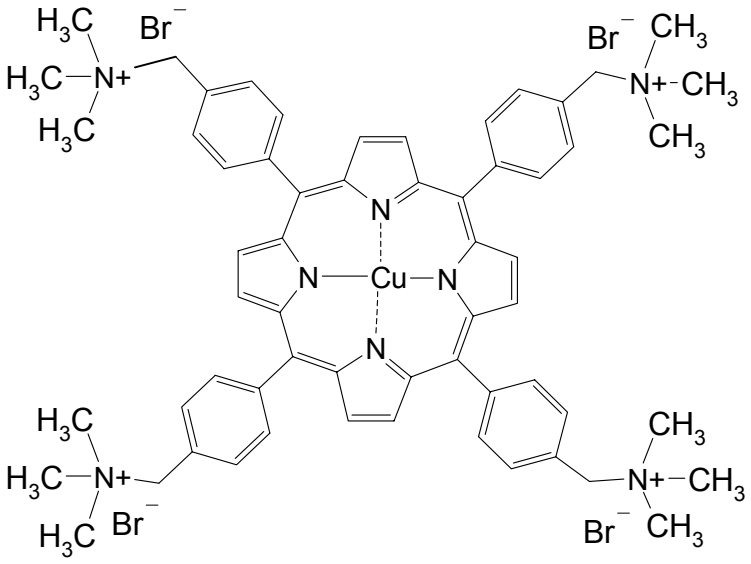

Figure 16. CuTPP-$(NMe_3)_4$ in tetrabromide salt.

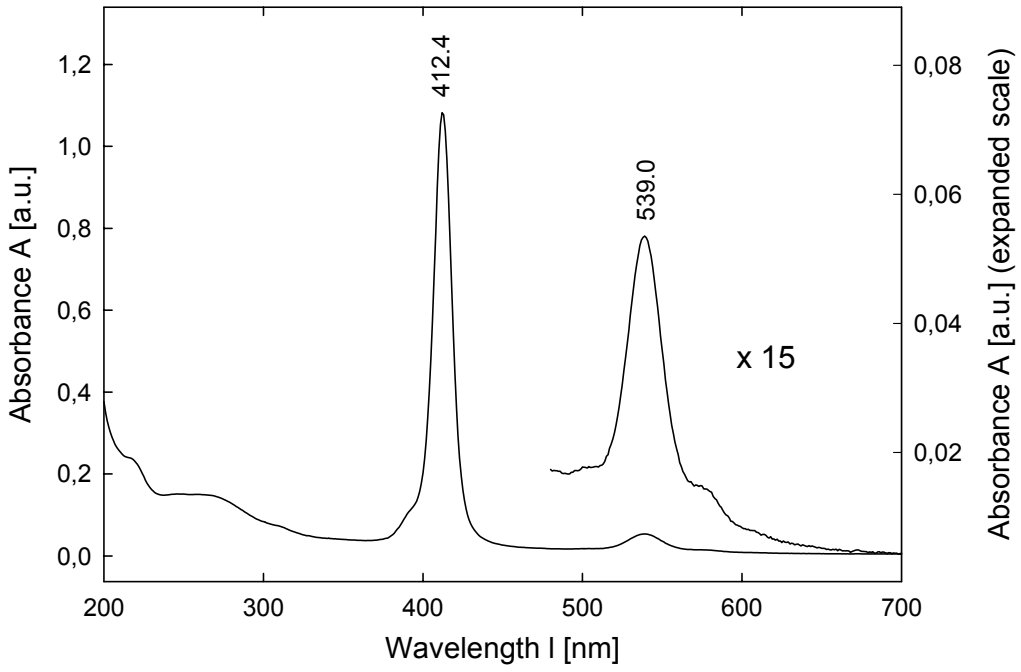

Figure 17. Absorption spectrum of CuTPP-$(NMe_3)_4$

CuTPPS$_4$

Copper(II) 5,10,15,20-Tetrakis(4-sulfonatophenyl) porphyrin, tetrasodium salt

MW: 1084.45

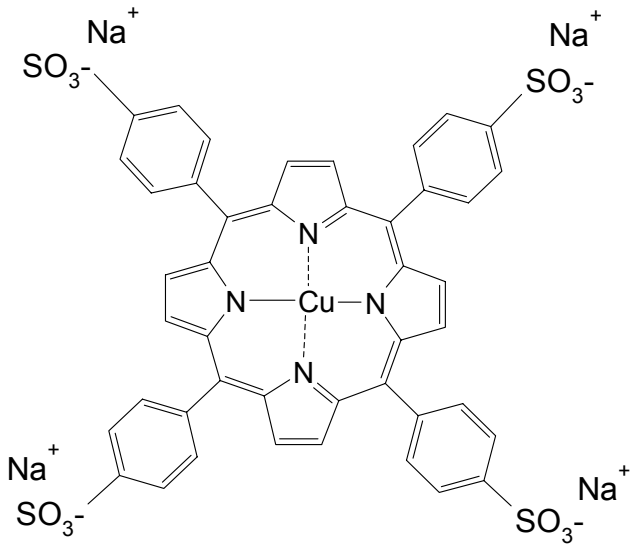

Figure 18. CuTPPS$_4$ in tetrasodium salt

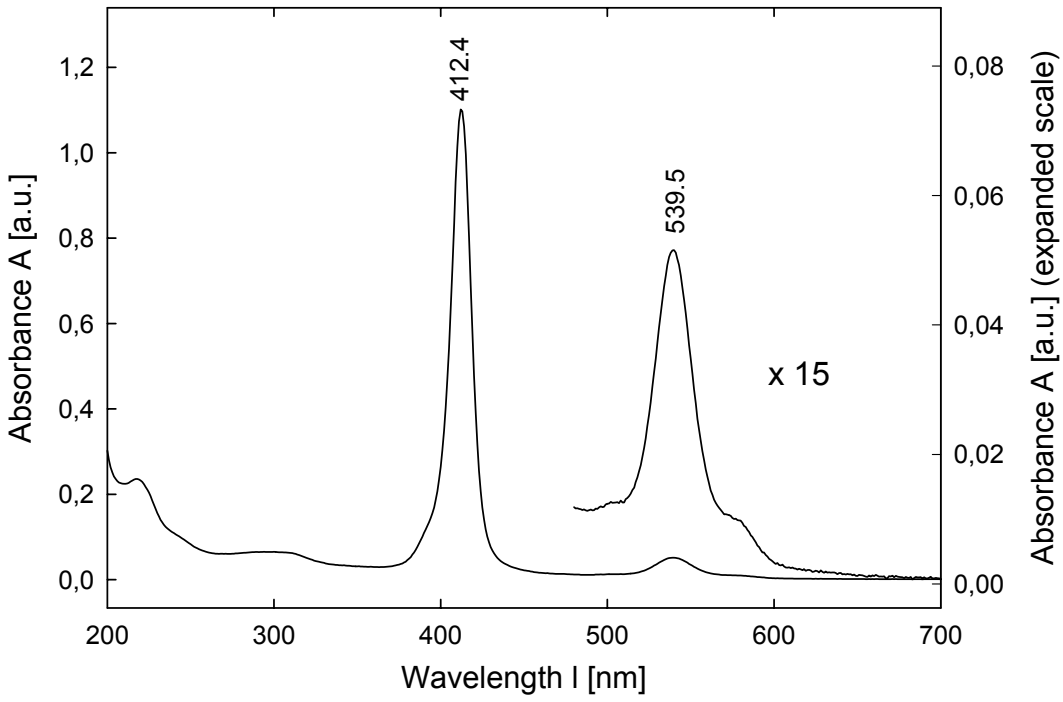

Figure 19. Absorption spectrum of CuTPPS$_4$

CuTPP-(Dist)$_4$

Copper(II) 5,10,15,20-Tetrakis(α-distamycin ammonio-*p*-tolyl) porphyrin, tetrabromide salt

MW: 2065.10

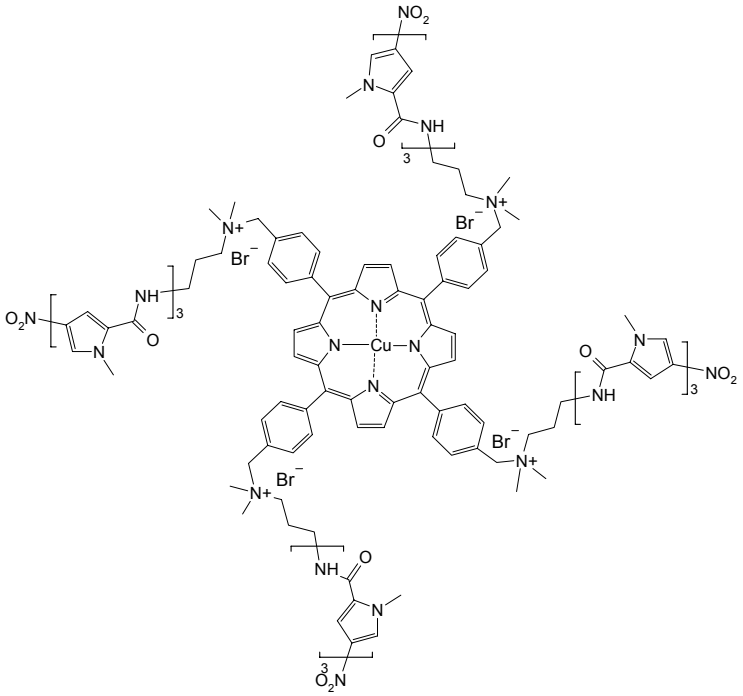

Figure 20. CuTPP-(Dist)$_4$ in tetrabromide salt

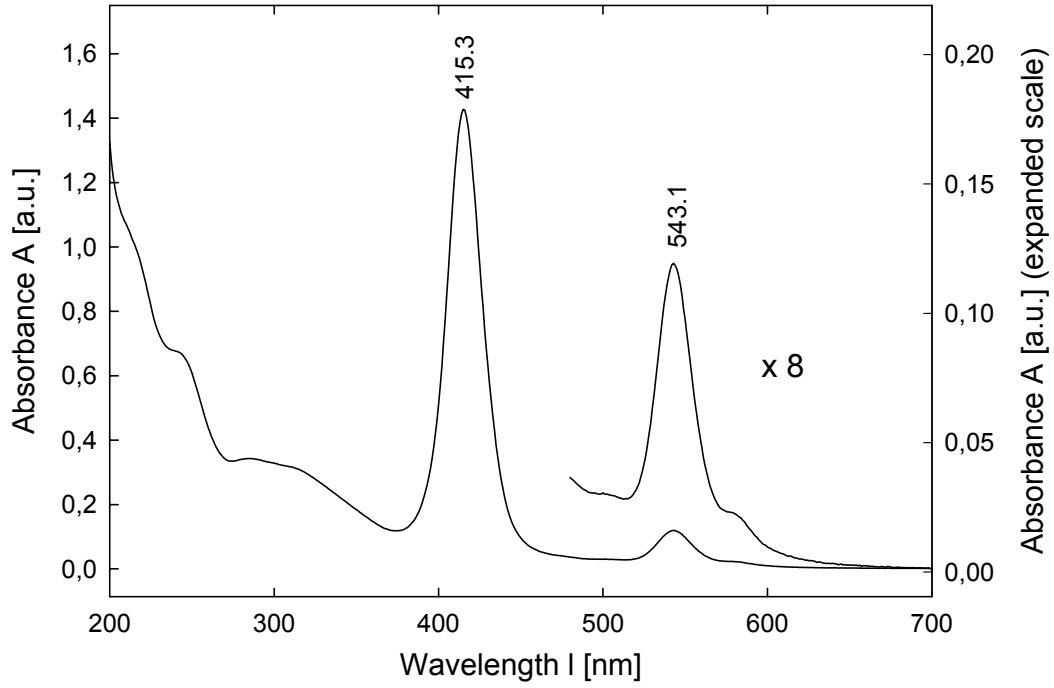

Figure 21. Absorption spectrum of CuTPP-(Dist)$_4$

CuTPP-p-(Bru)$_4$

Copper(II) 5,10,15,20-Tetrakis(α-brucine-*p*-tolyl) porphyrin, tetrabromide salt

MW: 2625.81

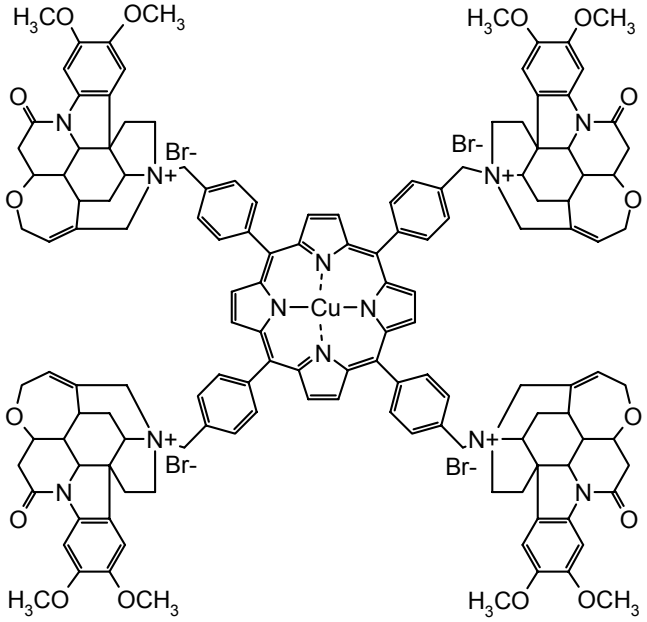

Figure 22. CuTPP-p-(Bru)$_4$ in tetrabromide salt

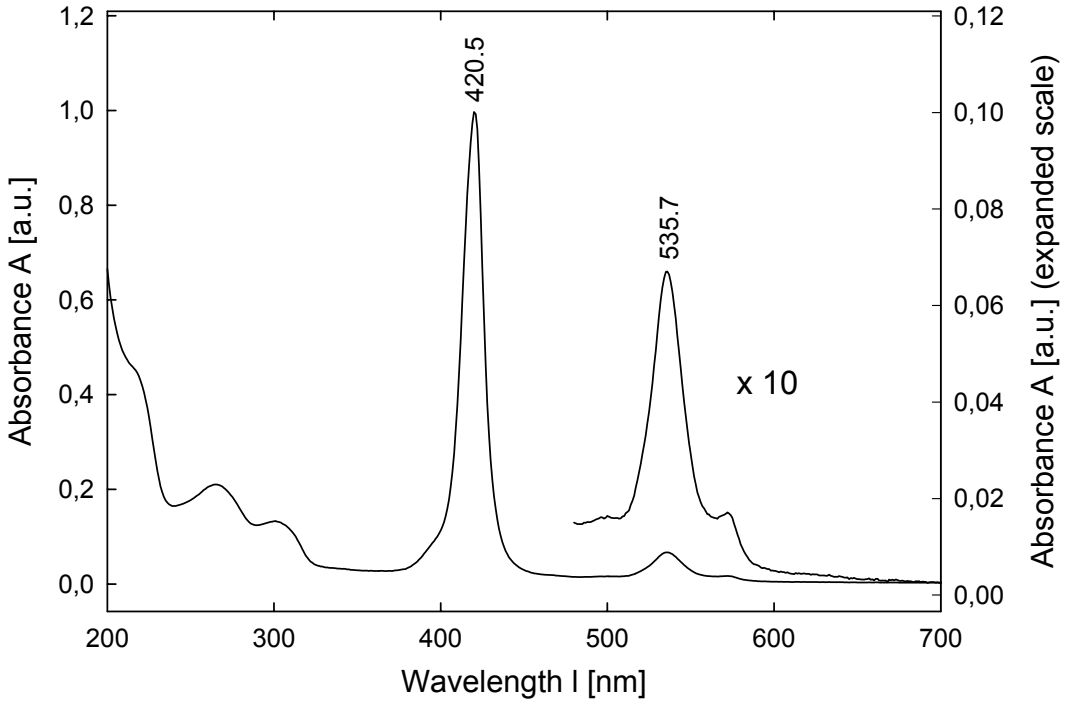

Figure 23. Absorption spectrum of CuTPP-p-(Bru)$_4$

CuTPP-m-(Bru)$_4$

Copper(II) 5,10,15,20-Tetrakis(α-brucine-*m*-tolyl) porphyrin, tetrabromide salt

MW: 2625.81

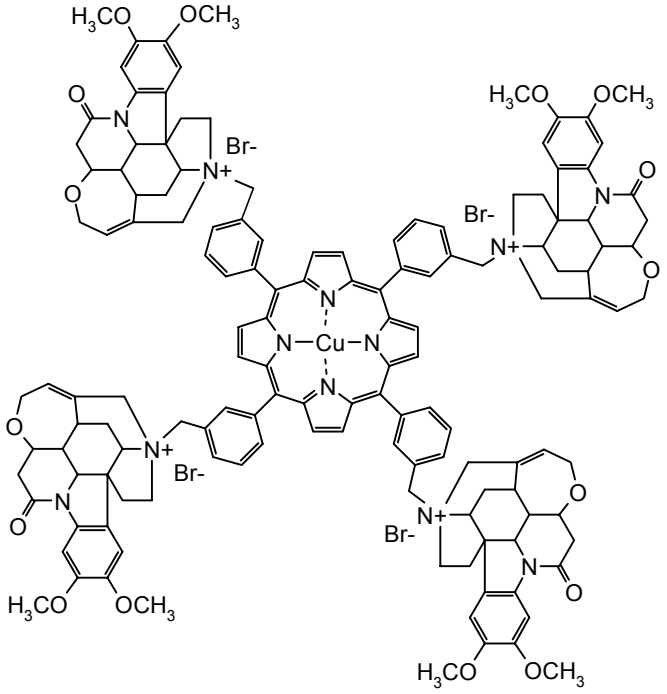

Figure 24. CuTPP-m-(Bru)$_4$ in tetrabromide salt

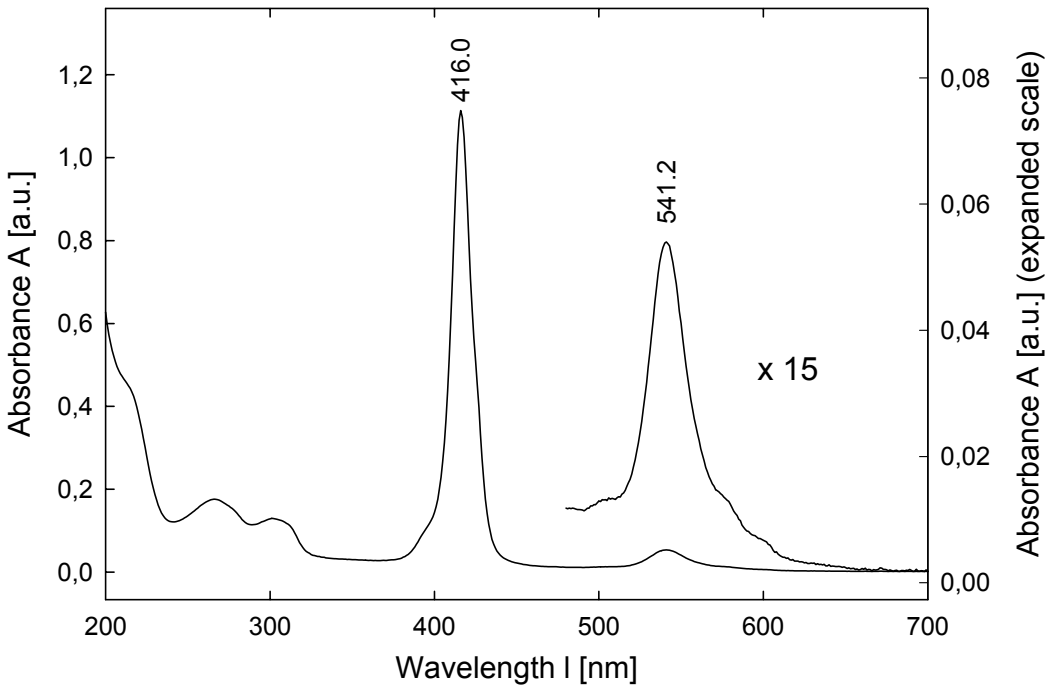

Figure 25. Absorption spectrum of CuTPP-m-(Bru)$_4$

4 Treatment of the results

4.1 Factor analysis

Factor analysis is a multivariate mathematical technique for reducing matrices of data to their lowest dimension using orthogonal factor space [27]. For practical use at *Division of biomolecular physics*, factor analysis was implemented as an EXE program *Fa8m* created by Doc. Jiří Bok (Institute of Physics).

Input data matrix can be constructed from any type of spectroscopic data. For the purpose of the present work, we have treated absorption and Raman spectra. Factor analysis applied to the series of spectra from the system, in which one parameter was systematically changed (concentration, ionic strength, ratio between interacting species) can provide, in principle, valuable information about the system [27], the number of absorbing components (i.e. number of spectroscopically distinguishable species), the concentration of each species in the sample, the spectrum of each component.

Nevertheless, such a task could be difficult, even unfeasible for systems composed from the mixture of more than two distinct species, and sophisticated fitting methods have to be used to convert results of the factor analysis into the terms of real concentrations of the pure species and their spectra. Spectroscopic data treated by factor analysis have to be obtained at identical conditions except of the parameter that is to be changed (e.g. concentration) to avoid interpretation errors issuing from more complex dependencies.

First, we have to prepare the obtained experimental data that are to be analyzed. Our routine FA8m for factor analysis requires a set of spectral data in the format *SpectraCalc*, having identical step (wavenumber, wavelength), hence if data obtained under different conditions, they have to be mathematically modified. Thus, wavenumber scales of the Raman spectra have to be calibrated and expressed with identical wavenumber step (in our case usually 1 cm^{-1}). The procedure is able to tolerate and correct slight differences in the spectral limits resulting from the calibration process. Program FA8m constructs automatically the input data matrix where the columns represents individual spectra, and rows are intensities for increasing values of wavelength or wavenumbers.

Then, the routine is decomposing the input matrix D into three matrices U, S and V (13). This procedure is called *eigenanalysis*, obtaining eigenvalues and eigenvectors. Each eigenvector in the solution represents a factor and each eigenvalue measures the relative importance of the corresponding eigenvector. Generally, a large eigenvalue indicates a major factor, whereas a very small eigenvalue indicates an unimportant factor.

Consequently, only the eigenvector associated with the largest eigenvalue has some physical meaning. The most commonly used method is a singular value decomposition (SVD), due to its numerical stability and wide range of applications. The data matrix **D** is expressed as [27]:

$$\underset{r\times c}{\mathbf{D}} = \underset{r\times s}{\mathbf{U}}\ \underset{s\times s}{\mathbf{S}}\ \underset{s\times c}{\mathbf{V}'} \tag{13}$$

where **S** is a diagonal matrix whose elements are equal to square roots of the eigenvalues and are called *singular values*. **U** is a matrix where each column represents an abstract, orthonormal eigenvector that spans the row space and **V** is a matrix where each column represents an abstract, orthonormal eigenvector that spans the column space. r is a number of data rows, c is a number of data columns and s is equal to either r or c, whichever is smaller. The first pair of eigenvectors represents the first factor and is associated with the largest, most important eigenvalue, while the s^{th} value represents the last factor and is thereby least important. The set of s factors accounts for all the data including the experimental error.

The abstract factors can be divided into two sets: first set of n factors due to real, physical features of data, second set of $s - n$ factors associated with the experimental errors and artefacts. The smallest usable number of factors n, when the reconstructed spectra differ from the measured ones only by a statistical noise, is called the factor dimension, which means the number of independent spectral components disclosed in the measured spectra. In real absorption and Raman spectra there is usually present a background caused by elastic scattering and, in the case of Raman spectra, also by the fluorescence. The component of the background common for all the spectra usually appears in the first subspectrum and can be corrected if the correct shape of the baseline is known. The randomly changing contributions to the background can be included in several subspectra and can thereby increase the factor dimension of the system. Nevertheless, it can be corrected in the subspectra having the greater weights by fitting it with a low-degree polynomic function that can be subtracted from the subspectra using some automatic procedures developed and routinely used at Division of Biomolecular Physics. Consequently, in several steps it is possible to obtain results of the factor analysis from the spectra corrected for unwanted background fluctuations. Such FA results provide first insight into the number of spectroscopically distinguishable species present in the set of studied samples, and information about character of the spectral differences between them.

5 Results and discussion

5.1 Metallation of H_2TPP-(Dist)$_4$

The H_2TPP-(Dist)$_4$ porphyrin, received in amount of few milligrams from Prof. Vladimír Král, was declared as Cu^{2+} derivative. Nevertheless, from absorption spectra (having typical four Q-bands pattern) we have disclosed that great part of the sample (maybe entire) was in a free-base form. To obtain own experiences with a porphyrin metallation of small quantities, we have tried to prepare the Cu^{2+} metallo derivative by adopting (however somewhat modified) procedure described by Pasternack [17]. To the free-base H_2TPP-(Dist)$_4$ dissolved in water (2 mg/10 ml), an appropriate volume of concentrated solution of $CuCl_2.H_2O$ was added. Resulting concentration of the Cu^{2+} was roughly 200-times higher than that of H_2TPP-(Dist)$_4$, the excess sufficient for fast metallation of all of the porphyrin molecules. Cu^{2+} should be incorporated into the porphyrin, by exchanging two hydrogens in the porphyrin macrocycle [17]. Metallation process was monitored by absorption in the Q-band region and it was found to be as fast, that (at the high access of Cu^{2+}), it should be completed after few minutes. Nevertheless, to be sure that all porphyrins were really metallated, the solution was left to stay for about 2 hours. No further changes of the absorption spectra were observed.

Next step was to remove the excess of Cu^{2+}, which did not bind to the porphyrin. For this purpose, solution was gradually titrated by small quantities of 25% NaOH solution. Addition of NaOH induced formation of insoluble $Cu(OH)_2$) precipitates. Titration was finished (final pH = 12) when no further precipitation was observed. Resulting precipitate was segregated by centrifugation and the supernatant was taken away. As a great part of CuTPP-(Dist)$_4$ remained evidently attached to the $Cu(OH)_2$) precipitate, it was eluted by addition of DMSO, because $Cu(OH)_2$ is insoluble in DMSO. By repeated centrifugation and dissolving in DMSO, a great part of CuTPP-(Dist)$_4$ was eluted as DMSO solution. DMSO was removed by evaporation in a vacuum concentrator (Eppendorf Concentrator 5301). Resulting dry powder was redissolved in water (giving pH ~ 10) and its pH was neutralized to ~ 7.0 by addition of 0.1 M HCl. As this solution should contain some amount of NaCl from neutralization, it was therefore lyophilized again, redissolved in pure methanol and filtered to remove crystals of NaCl. Afterwards it was lyophilized again and the resulting powder was used for further measurements. To confirm that CuTPP-(Dist)$_4$ was completely metallated, we have checked its absorption spectrum in water *(Figures 26*

and 27) and compared it with H_2TPP-(Dist)$_4$ dissolved in water as well. Both porphyrins were of the concentration about 3 x 10^{-5} M, and the spectra were measured in 1 mm cell.

For CuTPP-(Dist)$_4$, a 2 nm blue shift of the Soret band and a moderate broadening was observed in comparison with H_2TPP-(Dist)$_4$. Much reliable markers of metallation are the Q-bands. All free-base porphyrin are known to provide four Q-bands, while their metalloderivatives only two. That was observed also for CuTPP-(Dist)$_4$ as seen on *Figure 27*, where first of them, Q_1, is markedly red shifted from the first Q-band of free porphyrin.

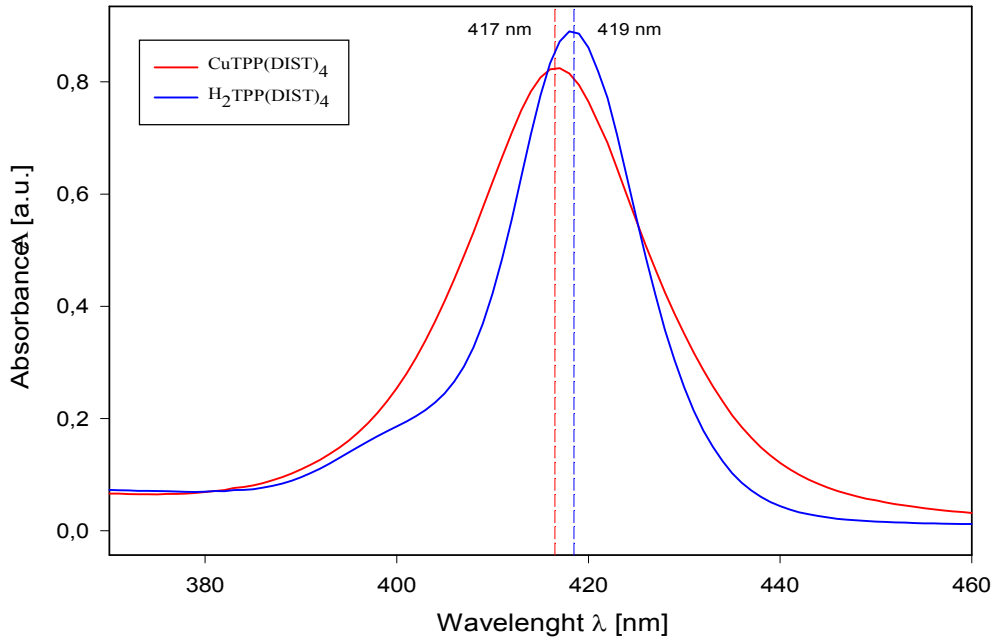

Figure 26. Spectral difference between H_2TPP-(Dist)$_4$ and CuTPP-(Dist)$_4$, Soret band

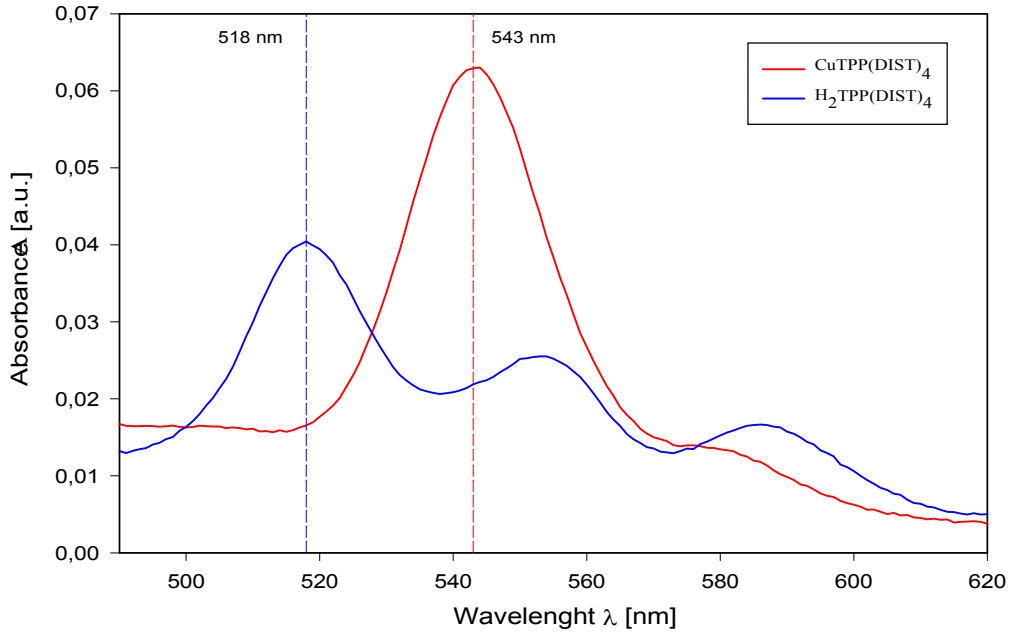

Figure 27. Spectral difference between H_2TPP-(Dist)$_4$ and CuTPP-(Dist)$_4$, Q-bands

5.2 Formation of $H_2TPP\text{-}(Dist)_4$ dimers in water and treatment of results

Most of the water-soluble porphyrins form dimers and higher aggregates in water, especially at higher porphyrin concentrations and under the higher ionic strengths. It is possible to distinguish H-aggregates with blue shifted Soret band and J-aggregates with red shifted Soret band. The monomer transition dipoles in H-aggregates are perpendicular to the line connecting centers of neighboring molecules, while in J-aggregates they are parallel [16]. The structure of aggregates is shown in *(Figure 28)*. The scheme is depicting general features of the aggregates common for all cationic as well as anionic porphyrins, however there can exist some differences in Soret bands positions for various porphyrin.

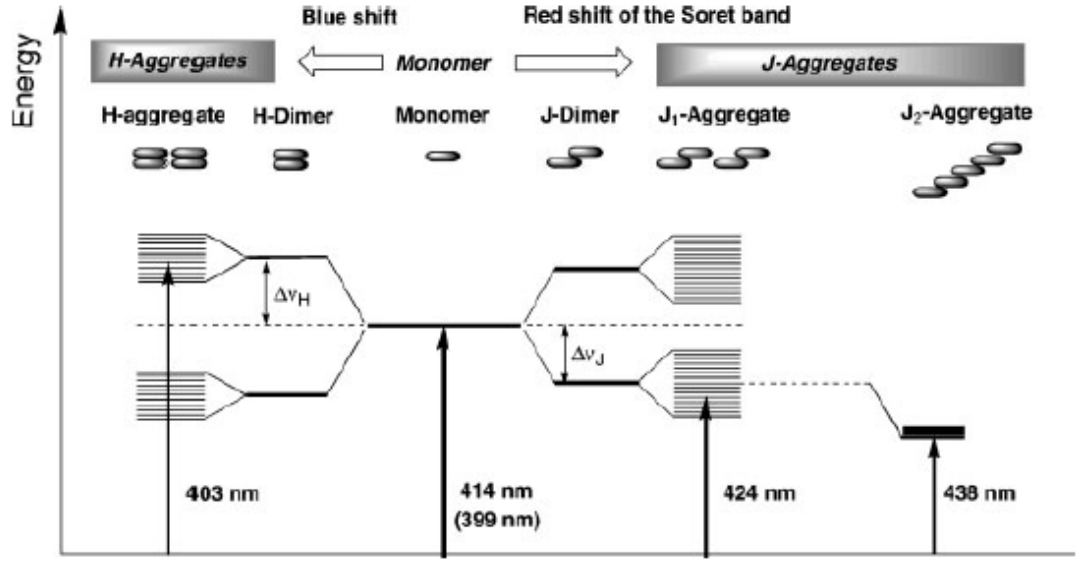

Figure 28. General energy level scheme of Soret bands splitting of meso-tetratolyl porphyrins. Only allowed electronic transitions are shown (taken from [16])

As the aggregation of cationic porphyrins in aqueous solutions without the presence of nucleic acids has deep impact on their spectral characteristics and their interactions with nucleic acids, one of the aims of the present work was to investigate aggregation of the novel porphyrins. Our aspiration was to develop more systematic methodology enabling determination of the dimerisation constant by means of factor analysis.

For that purpose we have studied formation of dimers of the porphyrin $H_2TPP\text{-}(Dist)_4$ in water solution monitored spectrophotometrically in the Soret as well as Q-bans regions. Since we had only very limited amount of the $H_2TPP\text{-}(Dist)_4$, it was necessary to adopt following sample-saving method. Limited volume of aqueous solution of $H_2TPP\text{-}(Dist)_4$ with starting concentration of ~ 1 x 10^{-3} M (determined roughly from the weight and molecular weight) was gradually dissolved by adding appropriate volumes of water.

Corresponding dilution ratio was determined by calculation from the volumes mixed. Since formation of different aggregates was observed especially at higher porphyrin concentrations *(Figure 29a)*, gradual dilution was expected to promote appearance of smaller complexes, and finally the monomers. Spectroscopic cells of different optical path were used, depending on the porphyrin concentration, and the absorption was recalculated (normalized) for identical optical length 10 mm. Concentrations from the range 1.0 x 10^{-3} M – 5.8 x 10^{-5} M were measured in a 0.1 mm cell, 3.9 x 10^{-5} M – 5.1 x 10^{-6} M in a 1 mm cell and 3.4 x 10^{-6} M – 3.0 x 10^{-7} M in a 10 mm cell. Maximum of the Soret band at 418 nm, observed for all concentrations including the most diluted samples *(Figure 29b)*, was preliminary attributed of monomers. As shown on *Figure 29c*, dependence of the Soret absorption on the concentration deviates significantly from Beer's law, nevertheless Q-bands absorption can be approximated well by a linear fit. Species responsible for its broadening at the red-side, appearing at higher concentrations, could not be attributed unambiguously to formation of J-aggregates, since the band is too close to the monomer maximum and has no typical narrow shape [30]. The broad blue-side band at about 400 nm, gradually increasing with porphyrin concentration, seems to belong to H-aggregates.

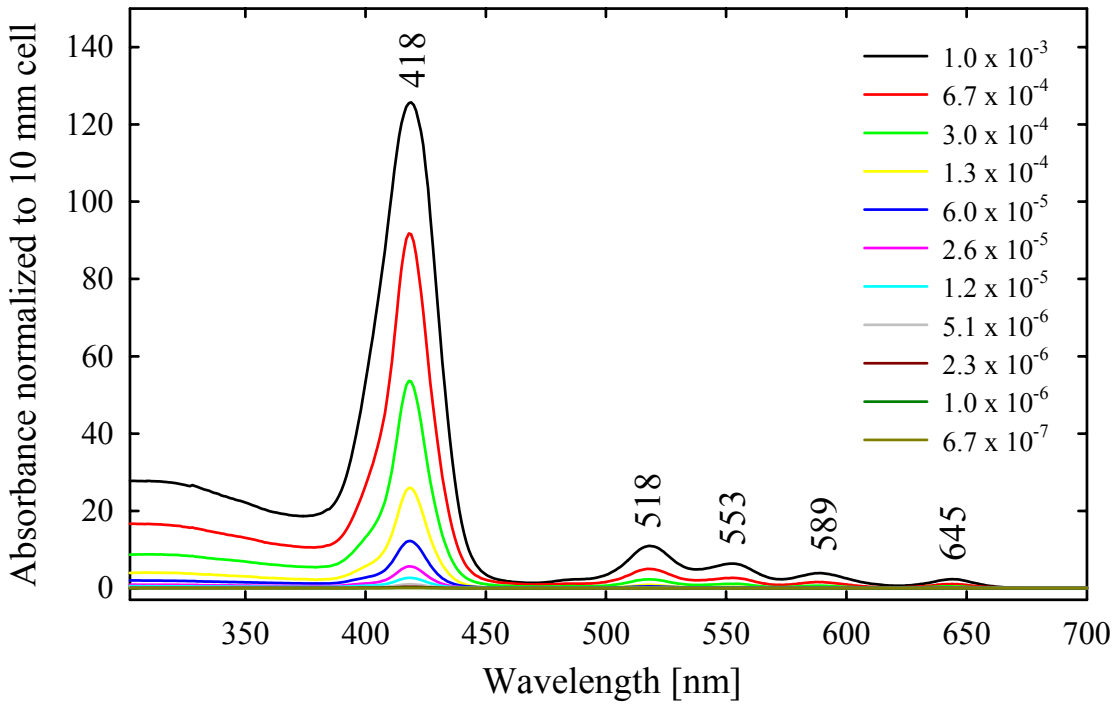

Figure 29a. Concentration dependence of absorption spectra of H_2TPP-(Dist)$_4$ in water

For further treatment of spectra, the factor analysis was used. Experimental spectra were corrected for background differences from analysis of the results coming from factor analysis of the rough data. Afterwards, the background constructed in a form of some simple polynomic functions was subtracted for original spectra and, by applying FA again on the corrected spectra, new subspectra, coefficients, singular values and standard deviation errors were obtained *(Figure 30)*.

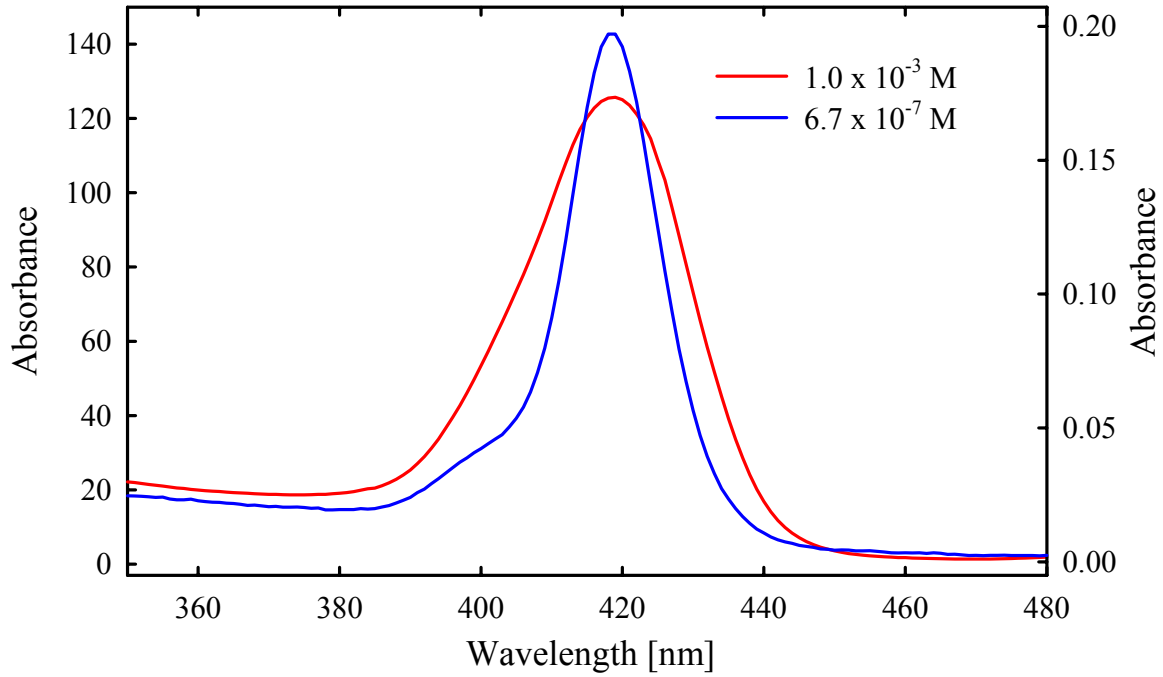

Figure 29b. Concentration dependence of absorption spectra of H_2TPP-(Dist)$_4$ in water. Broadening of the Soret band at high concentrations due to formation of aggregates.

From dependence of singular values as a function of the factor number we have concluded that the factor dimension of the system is 2, thus that only two spectral species can be expected in the solutions. Each experimental spectrum can be, thus, expressed as linear combination of the subspectrum S1 and S2. The subspectrum S1 is, in this case, a mean spectrum, and corresponding coefficient V1 shows how the absolute absorbance is increasing as the concentration increases. The second subspectrum S2 represents spectral changes induced by the concentration differences, and is characteristic for broadening of the Soret band. It is possible to see, that no similar broadening is visible in the Q-band region. It seems that Q-bands are much less affected by the porphyrin aggregation, and thus can be used for approximate determination of the porphyrin also under the conditions

where the Soret band fails. It would be interesting to check systematically applicability of this approach for other porphyrins.

Dependence of the coefficients V2 on concentration demonstrates local minimum for the interval 2 x 10^{-4} - 6 x 10^{-4} M. Starting from the concentration 2 x 10^{-4} M also Soret absorbance starts to deviate from linear dependence (*Figure 29c*). It seems that below 2 x 10^{-4} M, the monomer species prevail in the spectra. Starting from 6 x 10^{-4} M, the dimers or more probably aggregates are formed extensively.

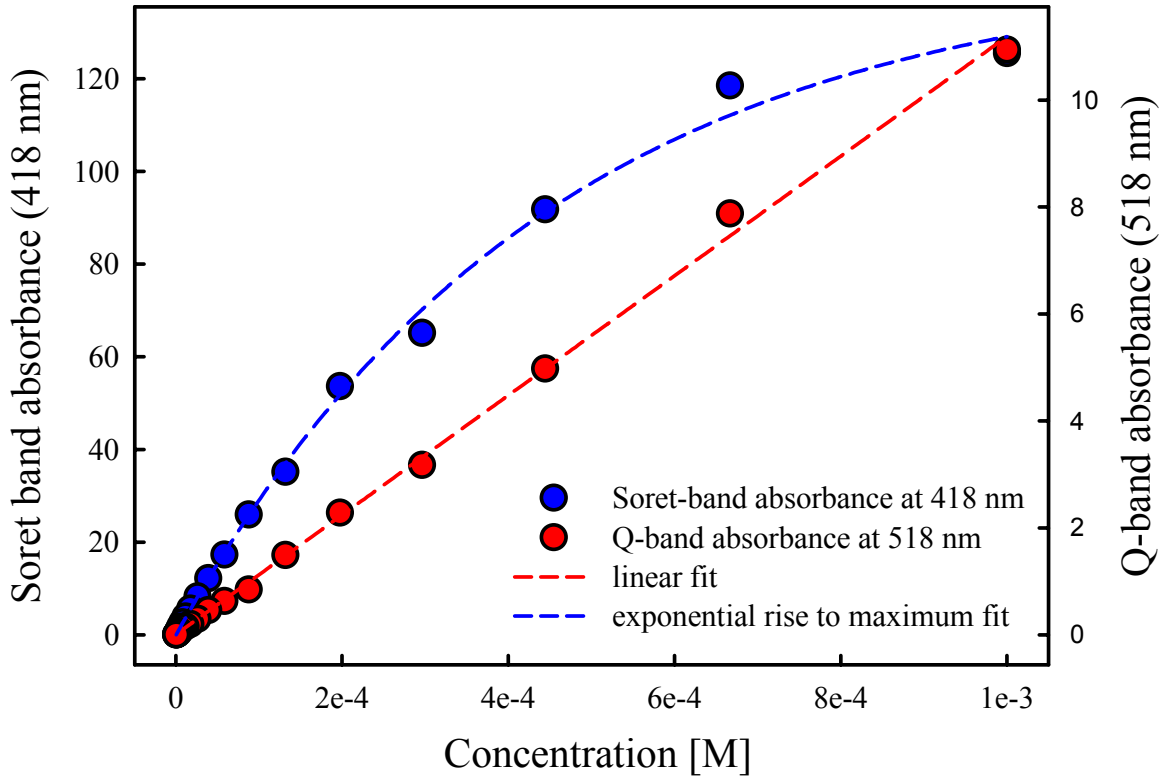

Figure 29c. Concentration dependence of absorption spectra of H_2TPP-$(Dist)_4$ in water

Since we have only two significant spectroscopically discernable forms in FA, we have tried to decompose the FA results into spectra of the pure species and their concentrations. For that purpose, we have supposed simple model counting only with the presence of monomers and dimers, existing in equilibrium with a dimerization constant K and total concentration of porphyrin c_{tot} in solution [29]:

$$M + M \xleftrightarrow{K} D \qquad K = \frac{[D]}{[M]^2} \qquad c_{tot} = M + 2D \qquad (14)$$

where *M* is the concentration of monomers and *D* concentration of dimers. Global fit of the FA results to taking the equation (14) into account was used to obtain concentrations of the monomers and dimers as a function of the total concentration c_{tot}, as well as spectra of the pure species.

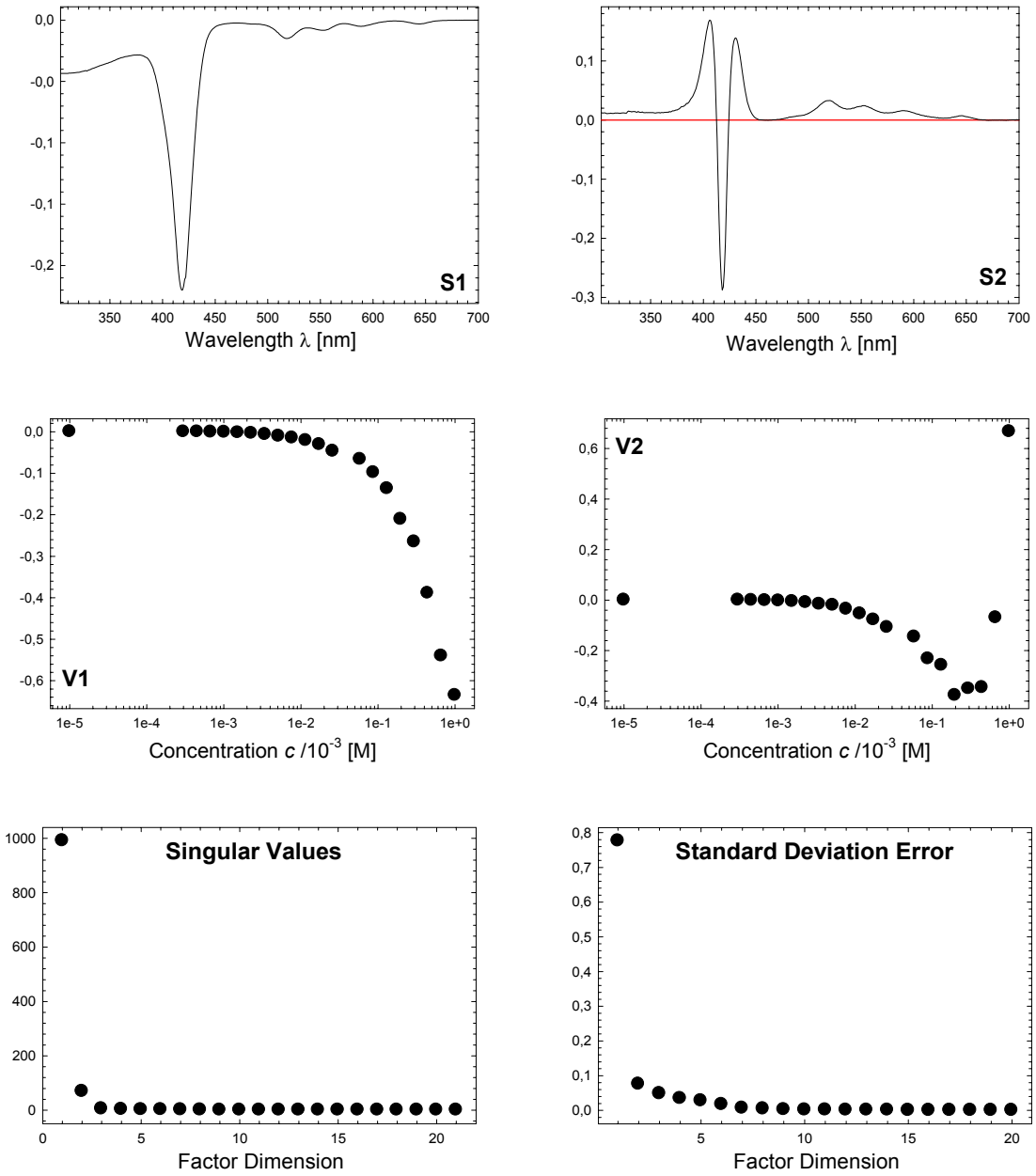

Figure 30. Factor analysis of the entire absorption spectra of H_2TPP-(Dist)$_4$ in water as a function of concentration. S1, S2 represents subspectra, V1, V2 coefficients of linear combination. Contributions of higher factor dimensions were insignificant.

Results of the global fit are shown on *Figure 31*. As evident, two absorption spectra nearly identical in the Q-band region have been obtained. However, negative absorbance in

the Soret region of the dimer spectrum indicates, that the solution has no physical meaning. Several attempts have been done to obtain physically acceptable fit, however without success. It seems that the simple monomer-dimer model is not sufficient to describe adequately the aggregation process. It would be necessary to continue in similar analysis taking into account formation of aggregates, probably of the H-type, consisting of more than two porphyrins.

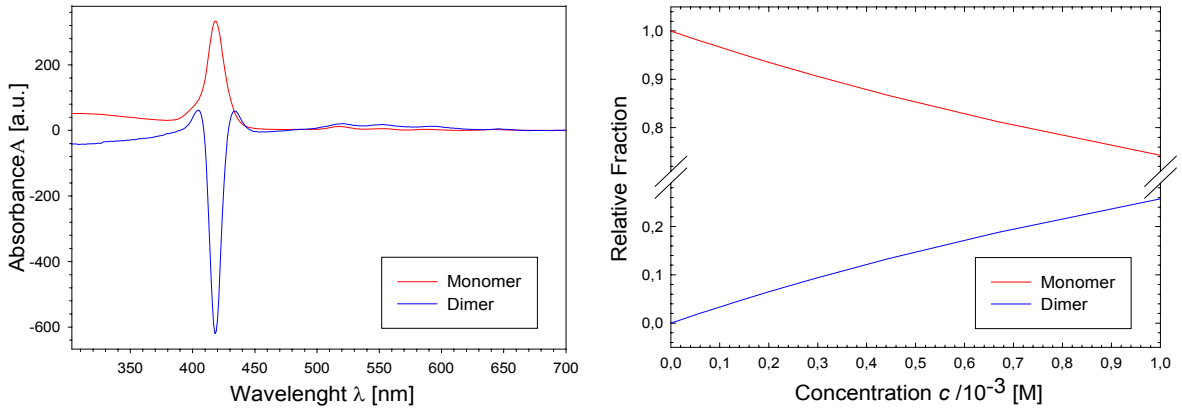

Figure 31. Global fit results (spectra of the pure species and their relative fractions) from the results of factor analysis supposing the simplest model of monomer – dimer equilibrium.

All the cationic porphyrins (free-base and Cu^{2+} derivatives) studied in this diploma thesis form dimers and higher aggregates in aqueous solutions, especially at higher concentrations and increased ionic strength. The only exception seems to be H_2TMPyP_4, which was longtime believed not to form dimers or higher aggregates in water [24, 28, 29, 30] at all. Its aptitude to form self-aggregates was a reason of controversy between Pasternack and Kano [24]. However some authors insist that also H_2TMPyP_4 can exhibit very slight tendency for dimers at extremely high ionic strength [24, 30]. The apparent lack of stacking even at high ionic strengths can be explained by electrostatic repulsive forces [24] between positive charges of H_2TMPyP_4 that can be delocalized over the porphyrin macrocycles, and that can overcome their attractive π–π stacking interactions. In all *meso*-tetratolyl porphyrins, and to some extent in *meso*-tetraphenyl porphyrins, the charged groups are insulated from the macrocycle by a methylene spacer or by a single bond, thus preventing direct coupling with the π-electrons of the macrocycle [16].

5.3 Interaction of H_2TPP-$(Dist)_4$ and H_2TPP-p$(Bru)_4$ with various NA

Complexes of the newly synthesized porphyrins H_2TPP-$(Dist)_4$ and H_2TPP-p-$(Bru)_4$ with double-stranded ST-DNA, and single-stranded poly(rA) and poly(rU) were studied by absorption spectroscopy. The aim was to find whether these new porphyrins with bulky substituents behave in a similar way as other cationic porphyrins, e.g. H_2TMPyP_4, H_2TMAP and $H_2TPP(NMe_3)_4$. H_2TMPyP_4 is known as intercalator into ST-DNA, as identified by methods of absorption spectroscopy [17], as well as by other methods like linear dichroism, circular dichroism and fluorescence energy transfer [31]. Schneider and Wang [32] made first more systematic research on interactions of DNA with the porphyrins bearing bulkier substituents, i.e. ammonium groups spaced at various distances from the macrocycle by an aliphatic chain. Such porphyrins exhibit, in the complexes with double-stranded DNA, small red shift and small/moderate hypochromicity, or the changes typical for porphyrin self-stacking on the DNA template, which indicates some kind of outside binding rather than intercalation into DNA [21, 32]. Moreover, using synthetic double-stranded oligonucleotides, it was shown that binding mode does not depend on the oligonucleotide base composition and sequence [54]. Therefore, it is possible that lack of intercalation could be a common property of the porphyrins with bulky substituents.

There exists sequential- and structural dependence of the porphyrin binding modes to single-stranded polynucleotides. E.g. H_2TMPyP_4 and namely its Cu^{2+} derivative are known as intercalators to poly(rA), while to poly(dA), poly(dT) and poly(rU) outside binding was reported [55]. Thus we wanted to test whether there exists similar discrimination between binding to poly(rA) and poly(rU) for H_2TPP-$(Dist)_4$ and $H_2TPP(pBru)_4$. Poly(rU) unlike other ss-polynucleotides does not form an organized helical structure in water (without presence of Mg^{2+} ions and low temperature) due to weak stacking interactions between bases [33], and it could differ from the stacking poly(rA).

Absorption spectra (Soret region) of the H_2TPP-$(Dist)_4$ complexes with ST-DNA, poly(rA) and poly(rU) are compared on *Figure 32*. Using the porphyrin concentration ~ 3 x 10^{-5} M (approximate ε_{418} ~ 3 x 10^5 $M^{-1}cm^{-1}$) and porphyrin-to-nucleotide ratio 1:50 (in base-pairs for dsDNA, and bases for single-strands), the interaction with any of the nucleic acid induced only a small red shift of Soret band for about 3 nm, however accompanied with rather strong hypochromism of Soret band (~ 40%). Under the same conditions, for poly(rU) the Soret band was somewhat stronger and narrower than for poly(rA) and ST-DNA. Other differences have been observed in the Q-bands. Single-strands exhibited

different red-shifts of the Q-bands than ST-DNA. Small red shift of the Soret band but marked hypochromism indicate, that full intercalation into nucleic acid is impossible and H_2TPP-$(Dist)_4$ is fixed externally, maybe in some self-aggregated manner despite low porphyrin load. Distamycin substituent is definitely hindering regular intercalation (probably because of its own affinity to nucleic acid), and H_2TPP-$(Dist)_4$ is a candidate for typical outside-binder. Slight differences between outside binding to poly(rU), poly(rA) and ST-DNA will be subject of further investigation.

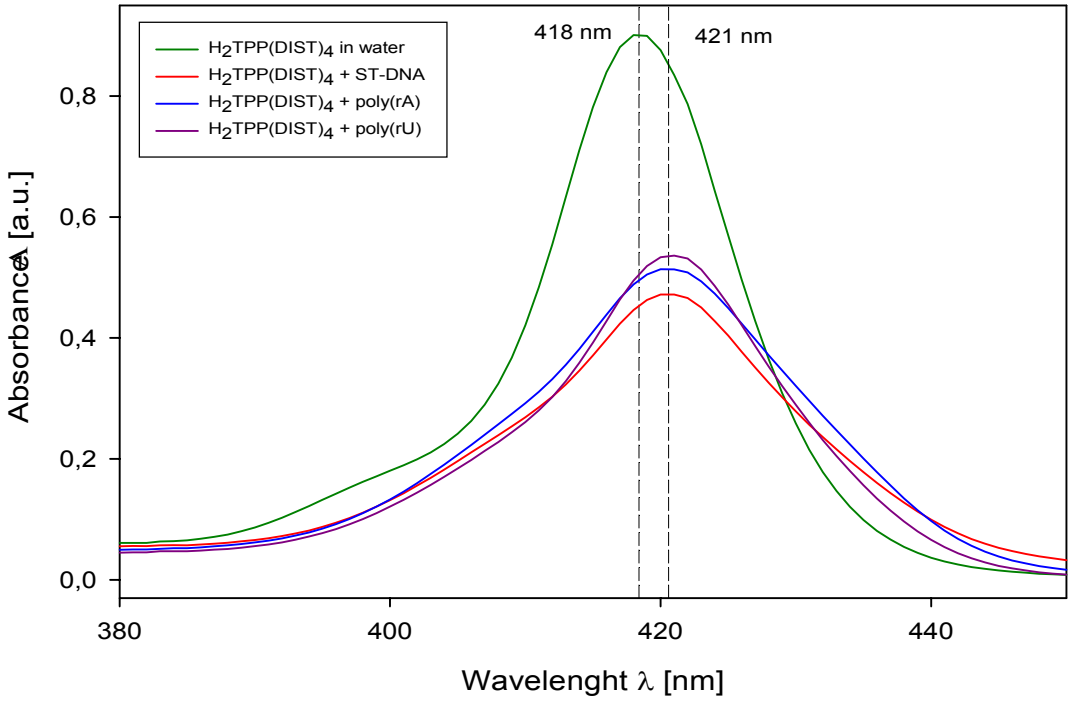

Figure 32. Absorption spectra of H_2TPP-$(Dist)_4$ with ST-DNA, poly(rA) and poly(rU).

Interactions of H_2TPP-p-$(Bru)_4$ with ST-DNA, poly(rA) and poly(rU) are presented in *Figure 33,* using similar porphyrin concentration and the ratio. The red shift of the Soret band with ST-DNA was 2 nm, with poly(rA) and poly(rU) only 1 nm, and hypochromism was somewhat smaller in comparison with $H_2TPP(Dist)_4$ under the same conditions. There was not observed substantial broadening of the Soret band, probably due to broader shape of the non-complexed H_2TPP-p-$(Bru)_4$. There were only small shifts of the Q-bands, approximately the same for all three nucleic acids. We have suggested that H_2TPP-p-$(Bru)_4$ is outside-bound to all three nucleic acids, possibly with somewhat lower extent of self-stacking than for H_2TPP-$(Dist)_4$.

Complexes of both porphyrins with ST-DNA have been found to precipitate when left overnight. It seems that initial structure of the complexes can evolve with time towards more aggregated structures, even at relatively low porphyrin loads.

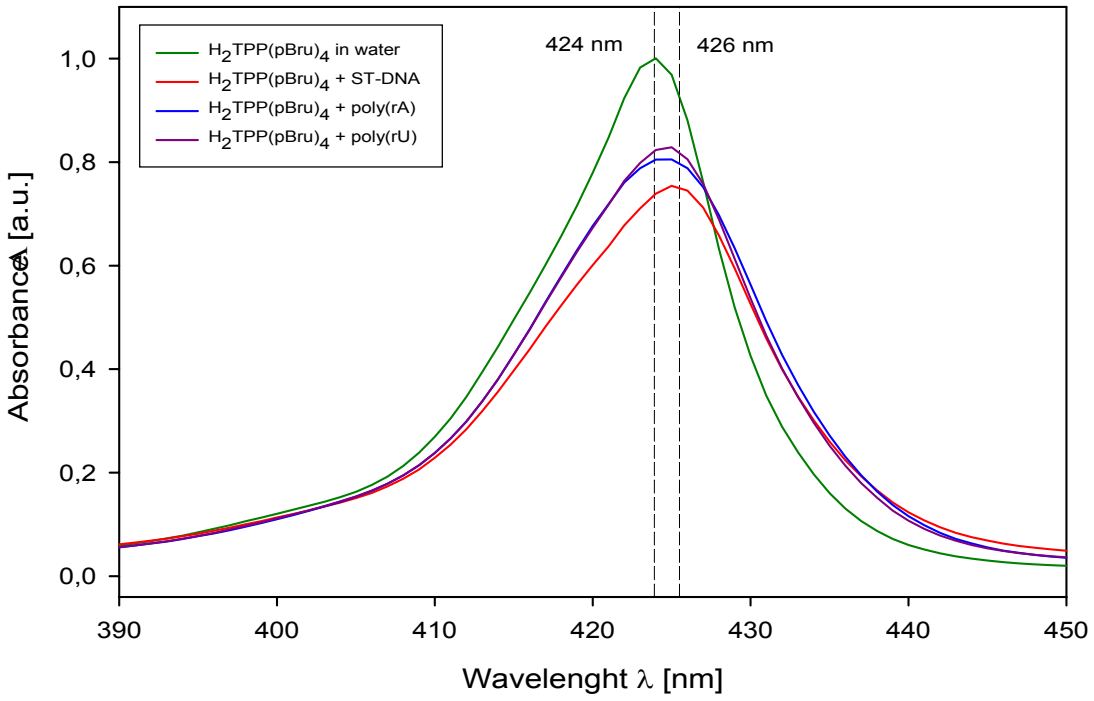

Figure 33. Absorption spectra of H_2TPP-p-(Bru)$_4$ with ST-DNA, poly(rA) and poly(rU).

To better understand the binding modes of H_2TPP-(Dist)$_4$ with ST-DNA as a function of the base pair-to-porphyrin ratio (R = [base pairs]/[H_2TPP-(Dist)$_4$), we have used spectrophotometric titration (*Figure 34a,b*). The titration was started with a porphyrin solution (~ 3 x 10^{-5} M, using approximate ε_{418} ~ 3 x 10^5 $M^{-1}cm^{-1}$) containing multiple excess of DNA (1.56 x 10^{-3} M in base pairs, thus R ~ 50) and appropriate volumes of a porphyrin solution of identical concentration were subsequently added into the cell, thus the R was gradually decreasing at fixed porphyrin concentration. For a great access of the DNA (3 < R < 50) spectra exhibit small red shift and considerable hypochromism (~ 40 %), nevertheless without dramatic changes for a wide ratio interval. However, lowering the number of binding sites (base pairs) below 3 for 1 porphyrin (*Figure 36*), intensity of the Soret band decreased rapidly indicating precipitation of the complex.

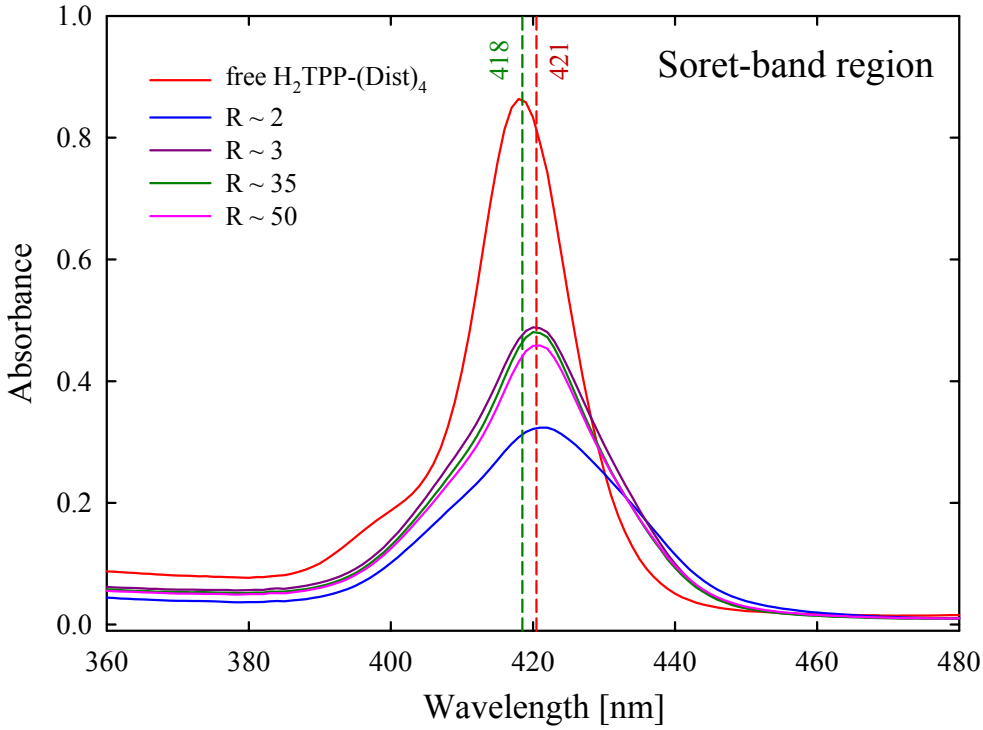

Figure 34a. Titration of H_2TPP-(Dist)$_4$ with ST-DNA in the Q-band region. R = [base pairs]/[porphyrin]

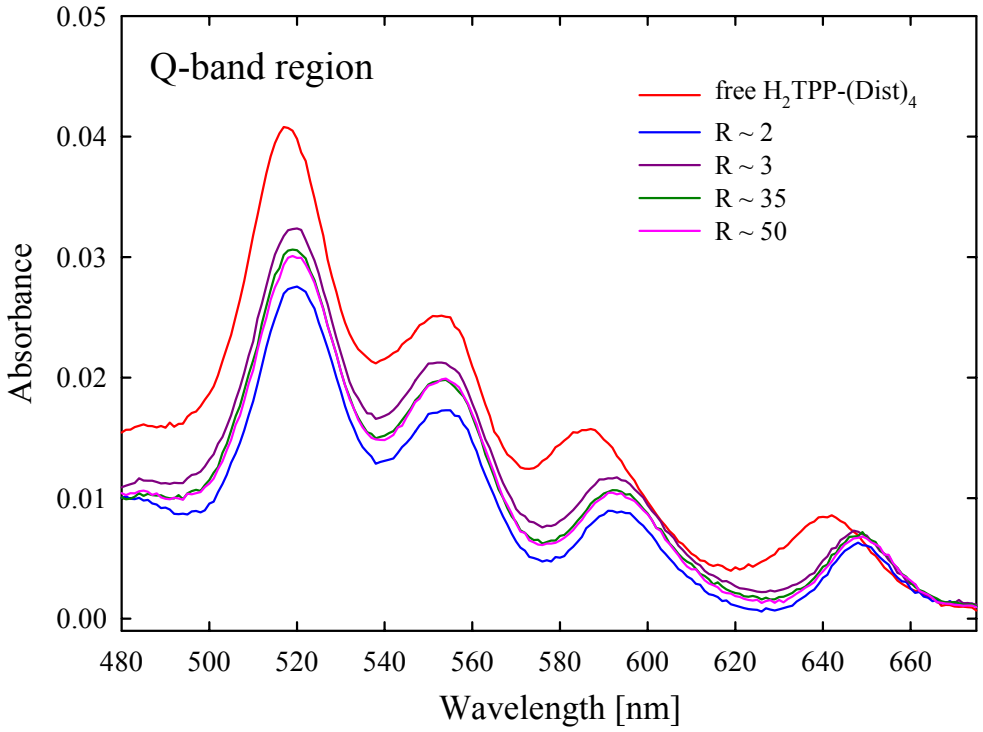

Figure 34b. Titration of H_2TPP-(Dist)$_4$ with ST-DNA in the Q-band region. R = [base pairs]/[porphyrin]

The rapid decrease of the Soret band seems to indicate a sudden saturation of all binding sites on DNA surface, thus neutralization of the DNA charge and formation of

bigger dense particles, as evident also from increase of the background due to elastic scattering. Even if the turning point (2 - 3 base pairs for 1 porphyrin) is only approximate because of uncertainty of the extinction coefficient of $H_2TPP\text{-}(Dist)_4$, it corresponds surprisingly to the exact formal charge neutralization (~ 4 cationic groups of the porphyrin neutralizes ~ 4 negative charges of two base pairs).

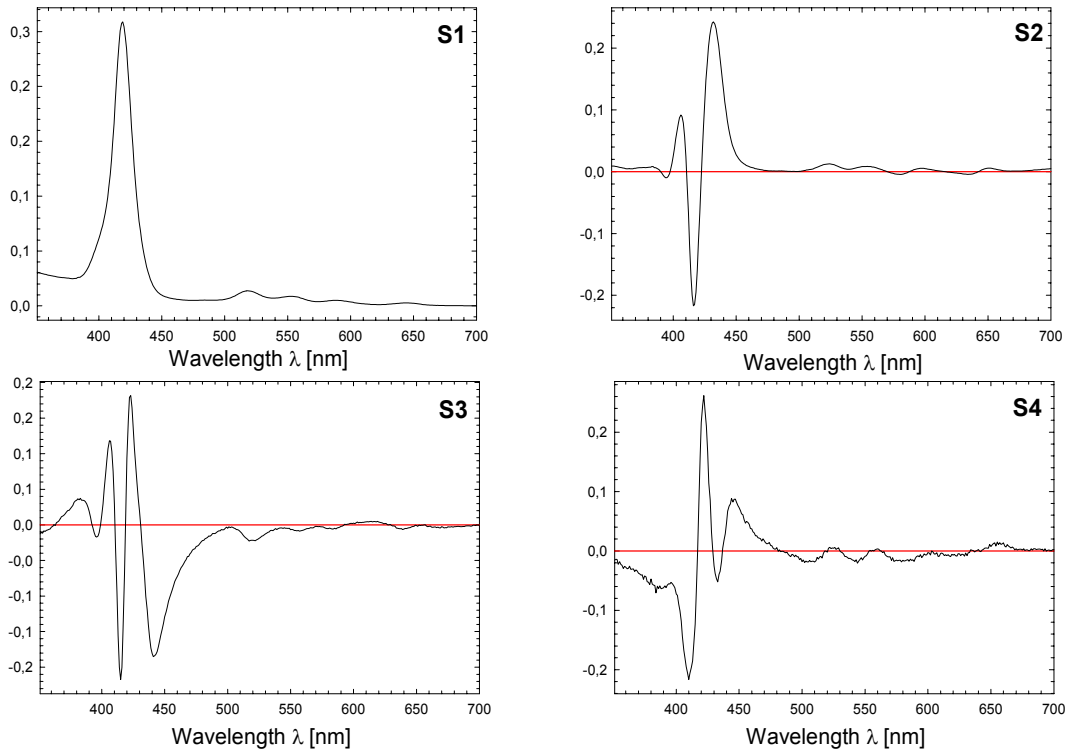

Figure 35. Subspectra from FA of titration of $H_2TPP\text{-}(Dist)_4$ with ST-DNA (spectra corrected for the baseline have been used).

We have used factor analysis also to interpret the titration results *(Figures 35 – 37).* According to singular values and standard deviation error (Figure 37), only two species are present in the spectra. However, regular character of the subspectrum S3 and continuous dependence of the corresponding coefficients V3 on DNA concentration indicate more complicated behavior. It seems that for the base pair-to-porphyrin ratio R greater than 2, two slightly different species can coexist. Evident rupture in the coefficient V1 – V3 dependencies at the ratio 2 indicate sudden collapse of the DNA structure. Dependencies below ratio 2 signify only gradual increase of the free $H_2TPP\text{-}(Dist)_4$ in the solution after condensation of the porphyrin-DNA complex.

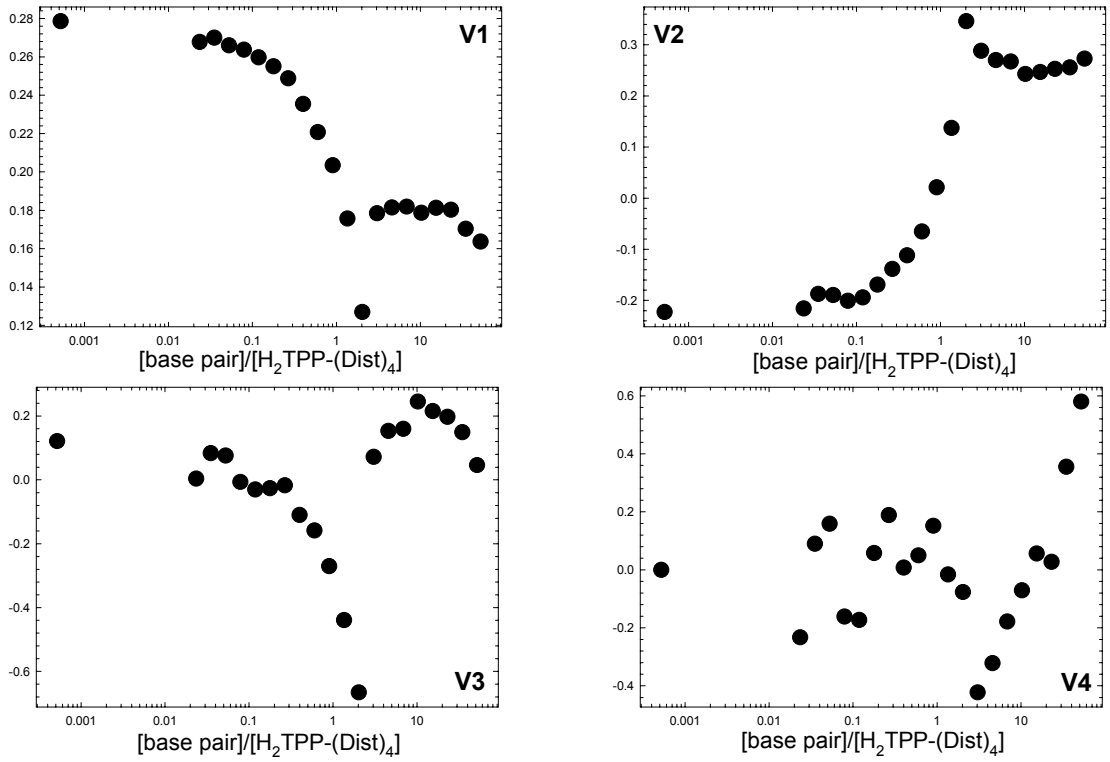

Figure 36. Coefficients from FA of titration of H_2TPP-$(Dist)_4$ with ST-DNA

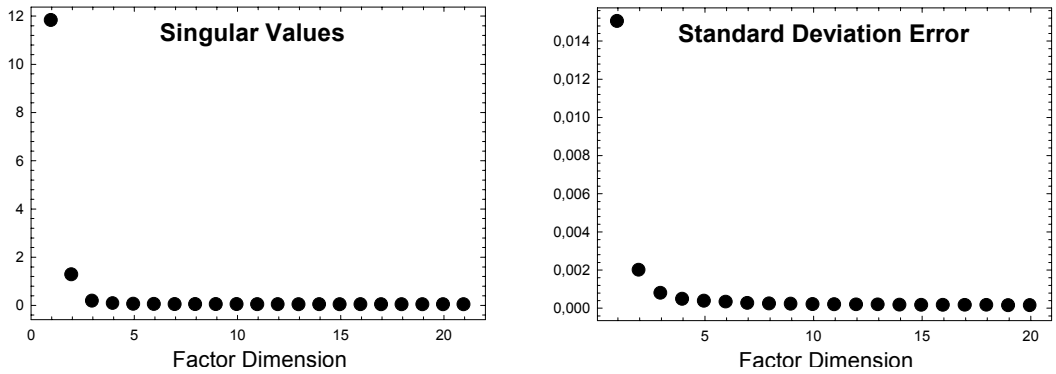

Figure 37. Singular values and standard deviation error from FA of spectrophotometric titration of H_2TPP-$(Dist)_4$ with ST-DNA

5.4 Formation of H_2TMAP dimers in dependence on ionic strength

Formation of porphyrin dimers is strongly ionic strength dependent. With increasing ionic strength, usually by adding solid NaCl or its solution, formation of dimers increases. In all relevant publications [for review see e.g. 29], the ionic strength dependences were studied in the solutions with fixed porphyrin concentration, into which small amounts of salt (usually NaCl) were added. There are no systematic studies counting with dependence of the aggregation as a function of the porphyrin concentration along with dependence on

the ionic strength. In [29] it was noted that there might be such dependency and that it would be worthwhile to measure a reverse titration where the porphyrin is gradually added into solution with fixed NaCl concentration. In the present diploma thesis we would like to test the methodology for such a study. The methodology was tested on the H_2TMAP, since this porphyrin was available in sufficient quantities and it was reported to form H-dimers and aggregates.

To cover up sufficient range of data, six sets of solutions with fixed concentration of NaCl ranging from 0 M to 5 M were used. Concentration of H_2TMAP ranged from 2 x 10^{-6} to 2 x 10^{-5} M (measured in 1 mm cell) and 2 x 10^{-5} – 2 x 10^{-4} M (measured in 0.1 mm cell). In the Soret band region *(Figures 38 – 40)*, two characteristic bands at 412 and 399 nm were observed. Soret band located at 412 nm was decreasing with increasing ionic strength and porphyrin concentration. For the solutions without NaCl *(Figure 38)* formation of dimers with increasing porphyrin concentration was observed as well, recognizable by appearance of a weak band (shoulder) at 390 – 400 nm. With increasing the ionic strength this band became stronger, with the maximum at 399 nm.

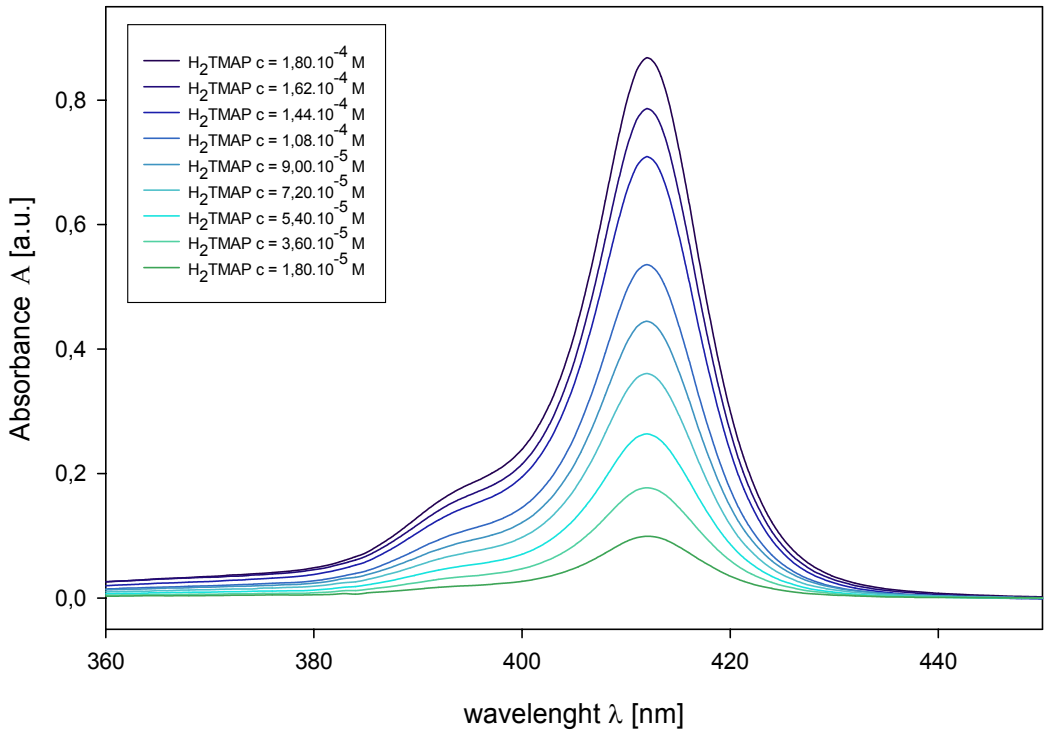

*Figure 38. Concentration dependence of the Soret band of H_2TMAP in **0 M NaCl***

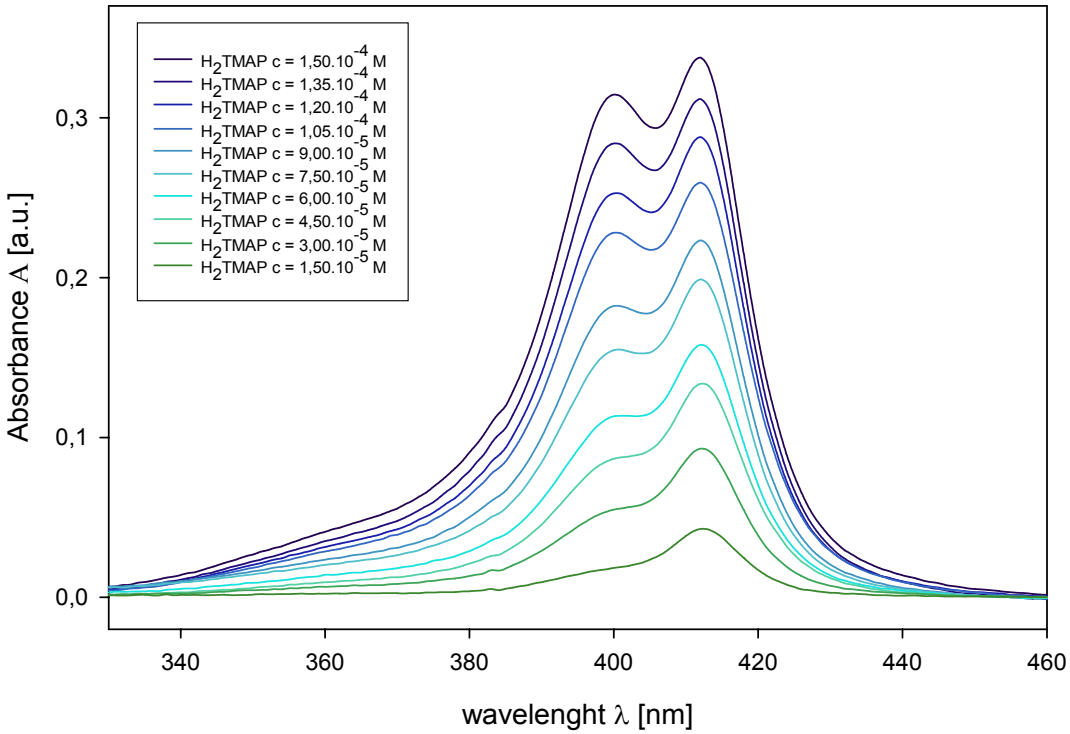

*Figure 39. Concentration dependence of the Soret band of H_2TMAP in **1 M NaCl***

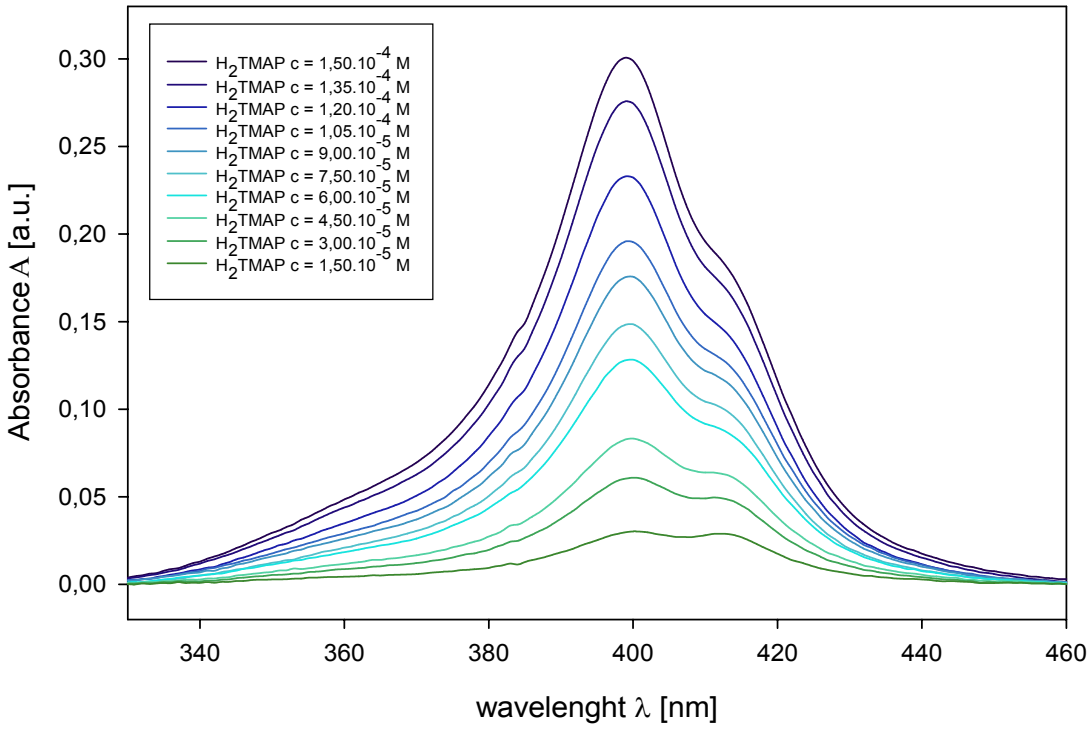

*Figure 40. Concentration dependence of the Soret band of H_2TMAP in **3 M NaCl***

By decomposition of the spectra into separate Gaussian bands, a third peak located at ~ 380 nm was disclosed. It was found to increase with increasing ionic strength, and probably it indicates formation of some higher H-aggregates of H_2TMAP.

For better visualization of the ionic strength effect on dimers and H-aggregates formation, absorbance ratios A_{412nm}/A_{399nm} and A_{412nm}/A_{380nm} obtained from decomposition of the Soret band into 3 components are shown on *Figures 41 and 42*, respectively. There are not remarkable differences between salt-dependences of the formation of the dimers and H-aggregates at very low H_2TMAP concentration (< 2 x 10^{-5} M). On the other hand, for higher H_2TMAP concentrations (2 x 10^{-5} – 6 x 10^{-5} M), the H-aggregates seem to be formed more readily than dimers under the same ionic strength, except for the lowest ionic strengths (0 –1.0 M NaCl). For the porphyrin concentrations higher than 6 x 10^{-5} M it seems that the ratio between dimers and higher aggregates is approximately constant for a given ionic strength NaCl, both increasing gradually with a total porphyrin concentration.

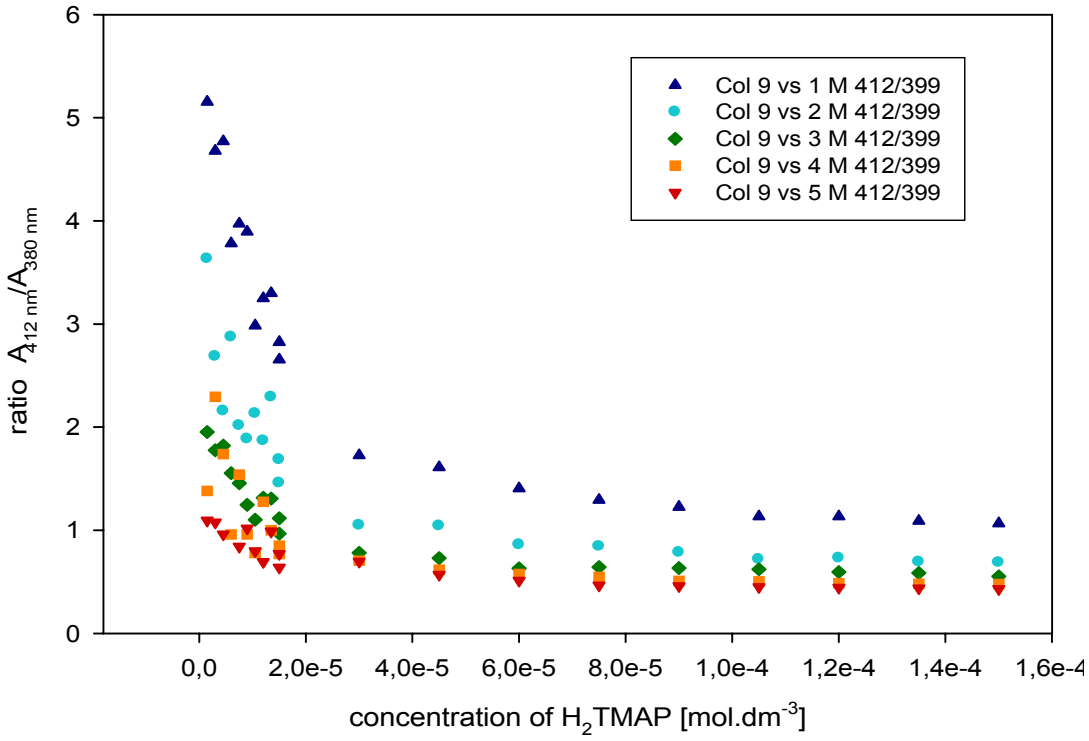

Figure 41. Dependence of absorbance ratio $A_{412\ nm}/A_{399\ nm}$ on H_2TMAP concentration

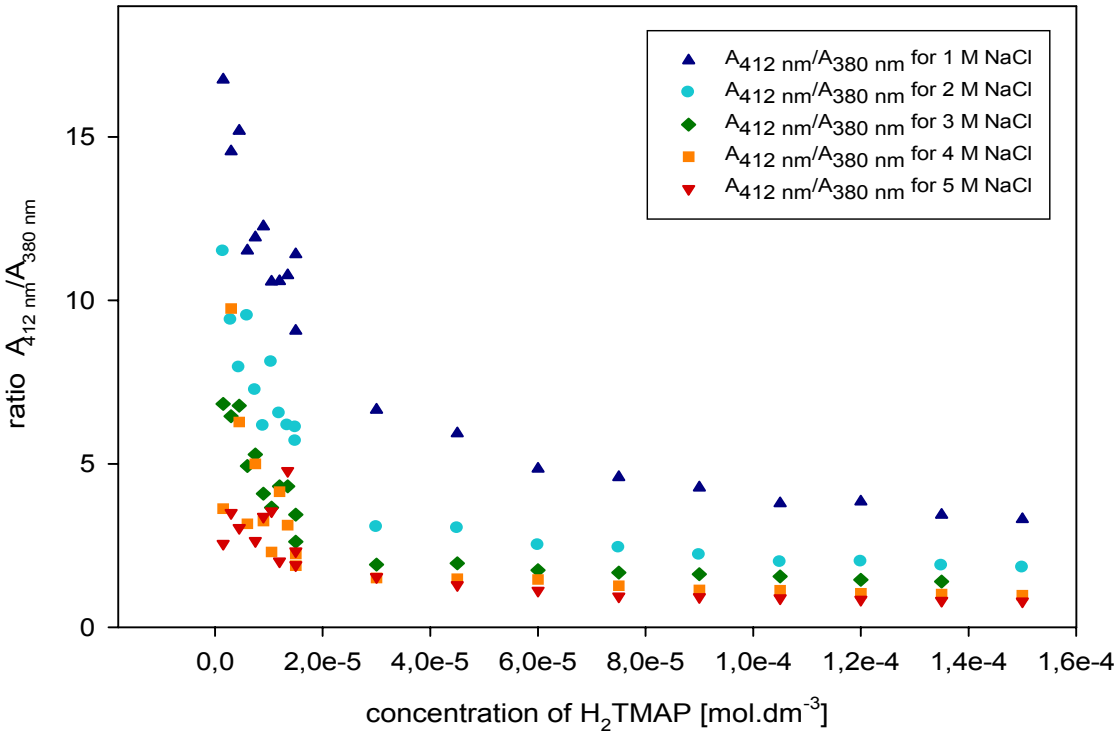

Figure 42. Dependence of absorbance ratio $A_{412\ nm}/A_{380\ nm}$ on H_2TMAP concentration

To understand better the complicated relationship between dimerization and aggregation on ionic strength at various porphyrin concentrations, it would be necessary to use more sophisticated methods of data analysis, e.g. factor analysis and global fits. Experimental data obtained for H_2TMAP can serve as a model system for testing methodology. However, such an analysis represents great deal of work and was going beyond the aims of the present diploma thesis. Results obtained on the aggregation of H_2TPP-$(Dist)_4$ demonstrated difficulty of such a task. Similarly complications can be expected for other cationic porphyrins with bulky substituents, but their aggregation properties have to be studied as well in next future.

5.5 Determination of extinction coefficients of metalloporphyrins

5.5.1 Zincon (2-carboxy-2'-hydroxy-5'-sulfoformazylbenzene)

Extinction coefficients of the porphyrins are of great importance for accurate studies of their properties and interactions, namely in the case of newly synthesized species. Even in the case of well-studied cationic porphyrins one can find considerably different values of extinction coefficients reported by various authors [34]. Because extinction coefficients of the newly synthesized free-base (and at the same time of their Cu^{2+} derivatives) porphyrins have not been reported previously, we have tried to determine according to a differential spectrophotometric method proposed by Pethö and Marzilli [34] using zincon *(Figure 43),* as reagent for colorometric determination of some divalent metals [35].

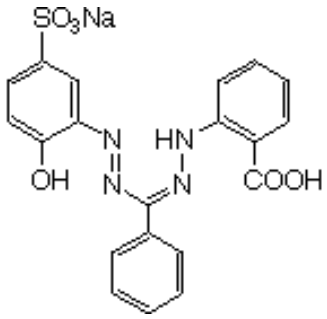

Figure 43. Zincon, 2-[1-(2-Hydroxy-5-sulforphenyl)-3-phenyl-5-formazano]benzoic acid, monosodium salt

The method is based on a metallation of the free-base cationic porphyrin by a slight access of the corresponding metal cation, and on determination of the concentration of remaining unreacted metal ions by means of zincon colorimetric titration. Zincon interacts strongly with Zn^{2+} and Cu^{2+} ions [35] by undergoing characteristic spectral changes in visible region, and is routinely used for selective determination of Zn^{2+} and Cu^{2+} ions, according to pH [34, 35].

The porphyrin (at approximate 2 x 10^{-4} M concentration) was transformed into the Zn^{2+} or Cu^{2+} derivative by addition of solution of $ZnCl_2$ or $CuCl_2$, respectively. Here the concentration of metals was roughly twice the concentration of porphyrin. Reaction should proceeded at pH ~ 12 of pH ~ 7, for Zn^{2+} or Cu^{2+}, respectively, and it takes about 30 minutes. Reference solution for differential measurements contains exactly the same amount of metal but no porphyrin. Remaining metal ions are titrated by addition of the same amount of zincon to both solutions, and the concentration of the porphyrin in the

sample can be determined directly from differential absorption of both solutions (*Equation 15*).

Following in all details procedure of Pethö and Marzilli [34], four solutions were prepared (*Table 1*). *Solution 1* was used as reference and *solution 2* as sample. From a difference spectrum, the absorbance *Abs* (*Equation 15*) at 622 nm was obtained, which corresponds to the maximum absorbance for Zn-zincon complex at pH = 9.0. In the case of Cu^{2+}, *Abs* value at 603 nm, corresponding to absorbance of Cu-zincon complex at pH = 6.5 was acquired. By a similar way, *Abs** was obtained using the solutions A and A*. The final concentration of the porphyrin (c_P) in the cell was calculated as [34]:

$$c_P = \frac{Abs + Abs^*}{\varepsilon} \tag{15}$$

where ε is the extinction coefficient of Zn-zincon complex at 622 nm (2.45 x 10^4 $M^{-1}cm^{-1}$ [34]) or Cu-zincon complex at 603 nm (2.29 x 10^4 $M^{-1}cm^{-1}$ [35]).

Solution 1	**Solution 2**
250 μl porphyrin solution ~ 2.10^{-4} M 250 μl ZnCl2/CuCl2 6.10^{-4} M 100 μl NaOH 0,15 M/ phosphate buffer pH 6,5	250 μl water 250 μl ZnCl2/CuCl2 6.10^{-4} M 100 μl NaOJ 0,15 M/ phosphate buffer pH 6,5
wait 30 minutes	*wait 30 minutes*
500 μl borate buffer pH 9,0/ phosphate buffer pH 6,5 250 μl zincon solution ~ 2 mM 1150 μl water	500 μl borate buffer pH 9,0/ phosphate buffer pH 6,5 250 μl zincon solution ~ 2 mM 1150 μl water
Solution A	**Solution A***
250 μl porphyrin solution ~ 2.10^{-4} M 250 μl ZnCl2/CuCl2 6.10^{-4} M 100 μl NaOH 0,15 M/ phosphate buffer pH 6,5	250 μl water 250 μl ZnCl2/CuCl2 6.10^{-4} M 100 μl NaOH 0,15 M/ phosphate buffer pH 6,5
wait 30 minutes	*wait 30 minutes*
500 μl borate buffer pH 9,0/ phosphate buffer pH 6,5 250 μl water 1150 μl water	500 μl borate buffer pH 9,0/ phosphate buffer pH 6,5 250 μl water 1150 μl water

Table 1. Solutions for determination of the porphyrin extinction coefficients by zincon

However, our own experiments have clearly demonstrated that the method of Pethö and Marzilli provide wrong results due to its inherent drawback. To be sure about our critical disclosure, we have done numerous experiments using cationic porphyrins H_2TMPyP_4 and H_2TMAP having the most certain extinction coefficients. As shown on *Figure 44*, differential absorption spectra H_2TMPyP_4 and H_2TMAP show negative absorbance in the region 700 - 800 nm, where no absorption of zincon (or its metal complex) nor of the porphyrin itself was expected. For cationic porphyrins with larger substituents ($H_2TPP\text{-}(NMe_3)_4$, $H_2TPP\text{-}(Dist)_4$, $H_2TPP\text{-}p\text{-}(Bru)_4$) the negative absorption was even greater. The procedure with use of Cu^{2+} resulted in the same effect, however the negative absorption was somewhat blue-shifted *(Figure 45)*. The effect was most obvious for $H_2TPP\text{-}p\text{-}(Bru)_4$, where also the absorbance values for 622 or 603 nm were negative *(Figure 46)*, giving thus evidently unreasonable porphyrin concentration c_P (15). Resulting extinction coefficients were thus of unrealistic values.

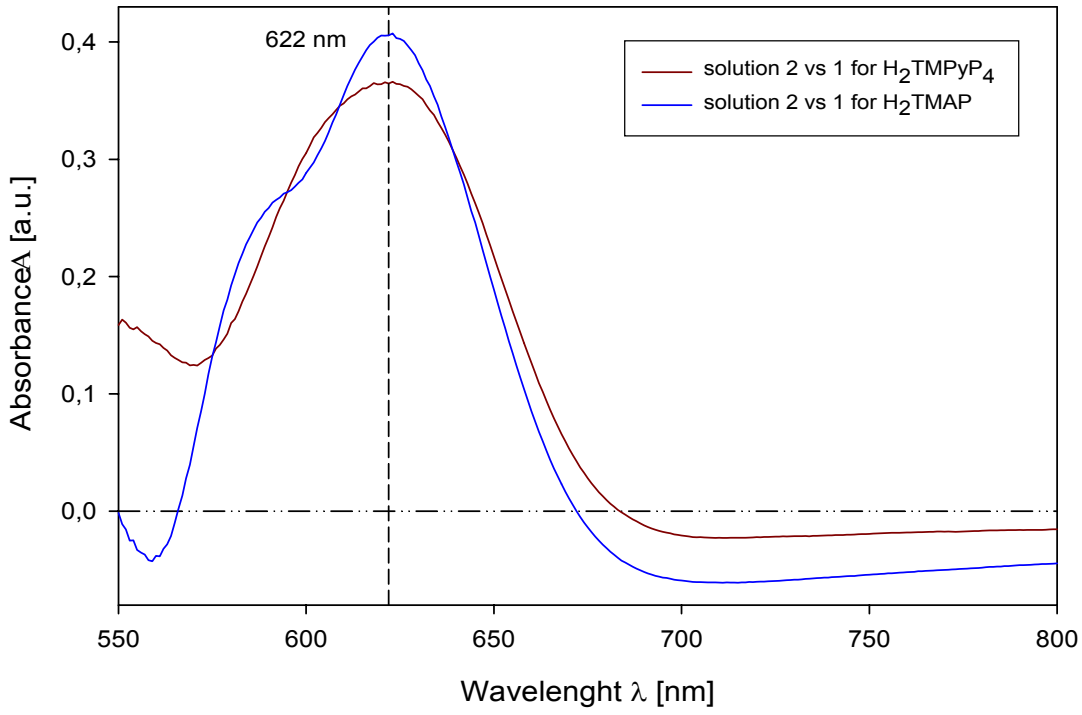

Figure 44. Differential spectra for H_2TMPyP_4 and H_2TMAP. Metallation by $ZnCl_2$.

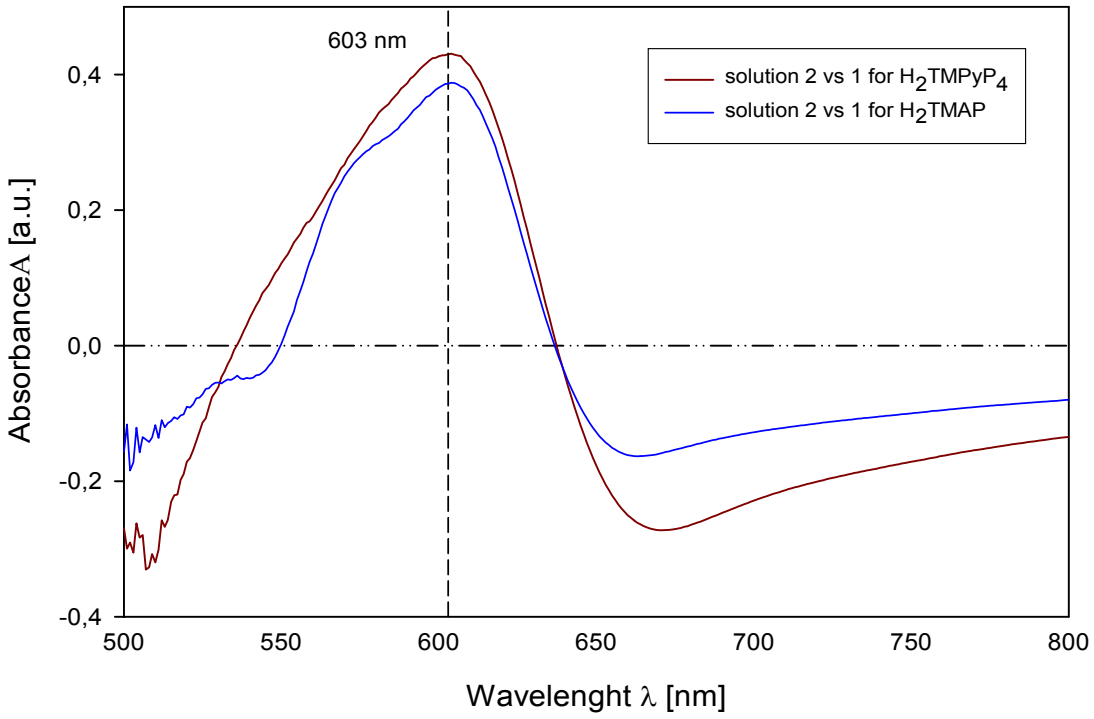

Figure 45. Differential spectra for H_2TMPyP_4 and H_2TMAP. Metallation by $CuCl_2$.

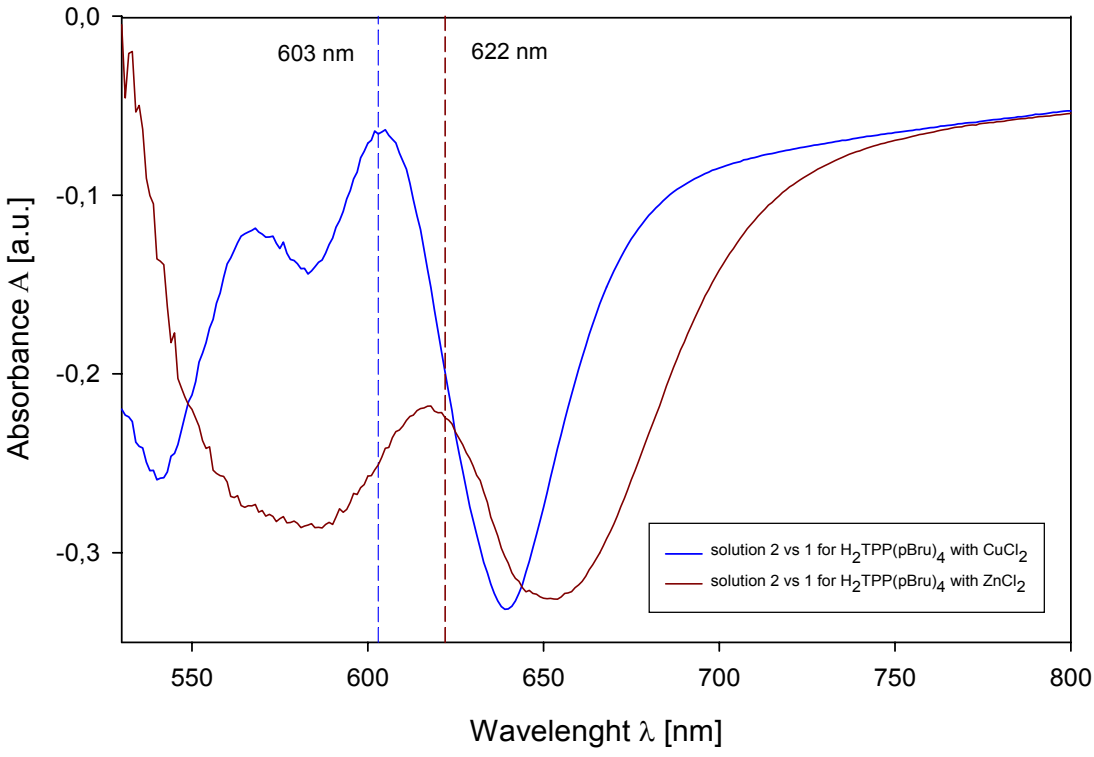

Figure 46. Differential spectra for H_2TPP-p-$(Bru)_4$. Metallation by $ZnCl_2$ and $CuCl_2$.

To find reasons of the procedure failure, we have started to study systematically complexes of zincon with cationic porphyrins in the presence and absence of metal cations. Firstly, the same procedure was repeated with $CuTMPyP_4$ instead of H_2TMPyP_4. Already fully metallated $CuTMPyP_4$ should not be metallated with the added Cu^{2+}, however, the procedure showed *(Figure 47)* considerable concentration of the free porphyrin, along with negative features in the longer wavelength region. This could be, hypothetically, due to traces of free-base porphyrin in the $CuTMPyP_4$ sample (which is highly improbable) or due to absorption of the complexes formed between the porphyrin and zincon. With more porphyrin added, the negative part of the spectrum decreases stronger *(Figure 47)*. Concentration dependence *(Figure 48)* shows that within some limits of the porphyrin concentration, the formation of the zincon-$CuTMPyP_4$ complex is linear. When greater amount of the porphyrin was added, linearity was lost and absorbance started to decrease. That means appearance of precipitates, probably due to aggregation of the complexes zincon-$CuTMPyP_4$. To find whether there exists direct interaction between zincon and $CuTMPyP_4$ without presence of Cu^{2+} ($CuCl_2$), the procedure was repeated replacing $CuCl_2$ solution by the same volume of water *(Figure 49)*.

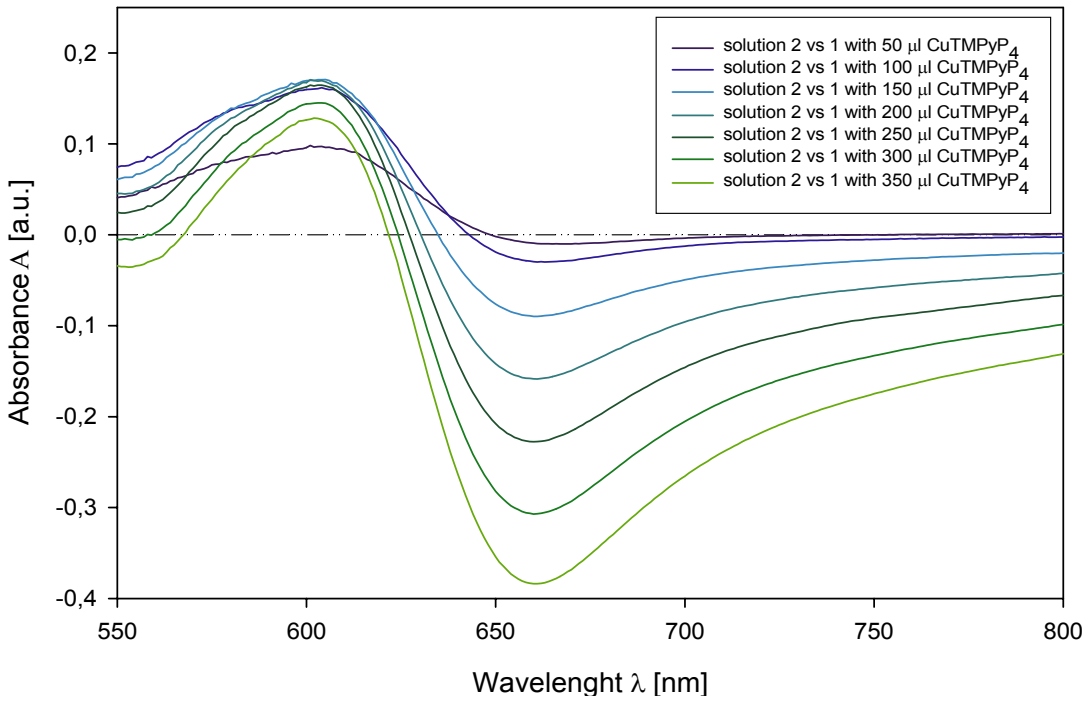

Figure 47. Differential spectra for $CuTMPyP_4$ using different total concentration of the porphyrin.

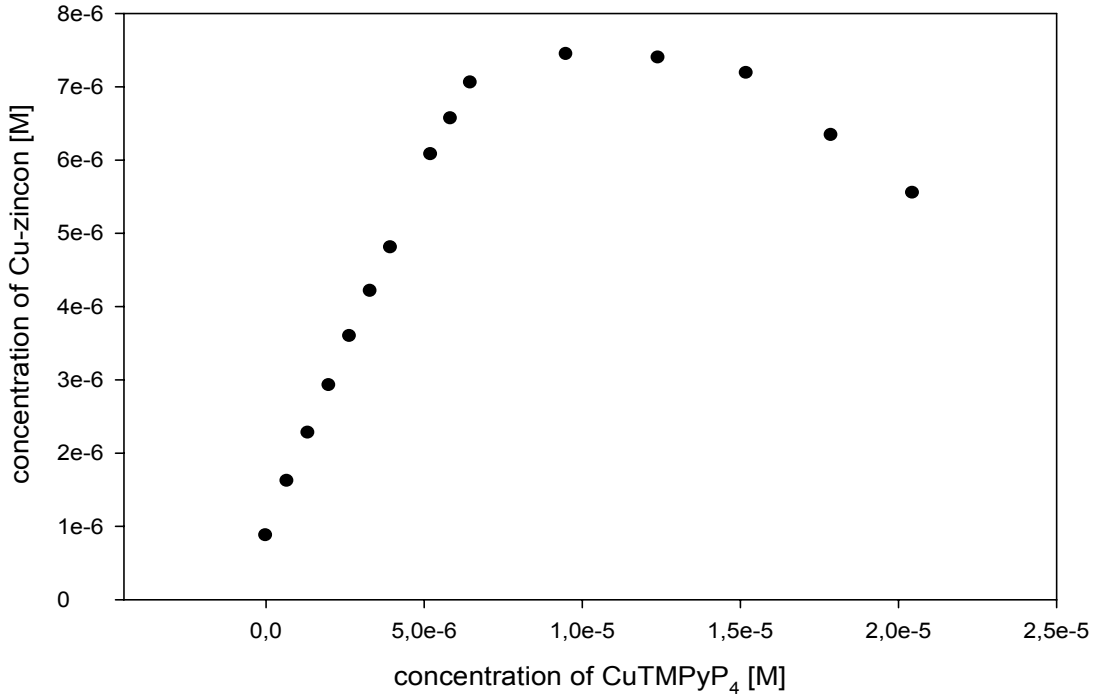

Figure 48. Concentration dependence of the Cu-zincon revealed by the procedure as a function of the total CuTMPyP$_4$ concentration.

Again, in the differential spectra two negative bands appeared at 603 and 570 nm, well to matching with the absorption of Cu-zincon complex and porphyrin-zincon complex, respectively Moreover, we have observed slow time-dependent interconversion from the band at 570 nm to band at 603 nm.

Since the zincon is in fact an acid having negative charge after dissociation, we have suspected cationic porphyrins of Coulombic interactions with zincon. Thus, we have tried to apply procedure of Pethö and Marzilli [34] for anionic H_2TPPS_4, and – as a control of the method – for metallated $CuTPPS_4$ *(Figure 50)*. In the case of H_2TPPS_4, differential spectra did not show any negative values around 660 nm, and the extinction coefficient calculated from (15) was $\varepsilon(H_2TPPS_4)_{412} = (4.2 \pm 0.3) \times 10^5\ M^{-1}cm^{-1}$, which is comparable with the published values. However, a small negative band at ~ 660 nm appeared for $CuTPPS_4$. It was much smaller then for cationic $CuTMPyP_4$, but it indicates some reaction between $CuTPPS_4$ and zincon. Both zincon and $CuTPPS_4$ have negative charge and there should be an electrostatic repulsion between them. Similar features found in the differential spectra of $CuTPPS_4$ and $CuTMPyP_4$ *(Figure 49, 50)* indicate similar kind of complex formation between zincon and the metalloporphyrins, despite theirs opposite charges. However, in the case of cationic metalloporphyrin, the effect is much more noticeable.

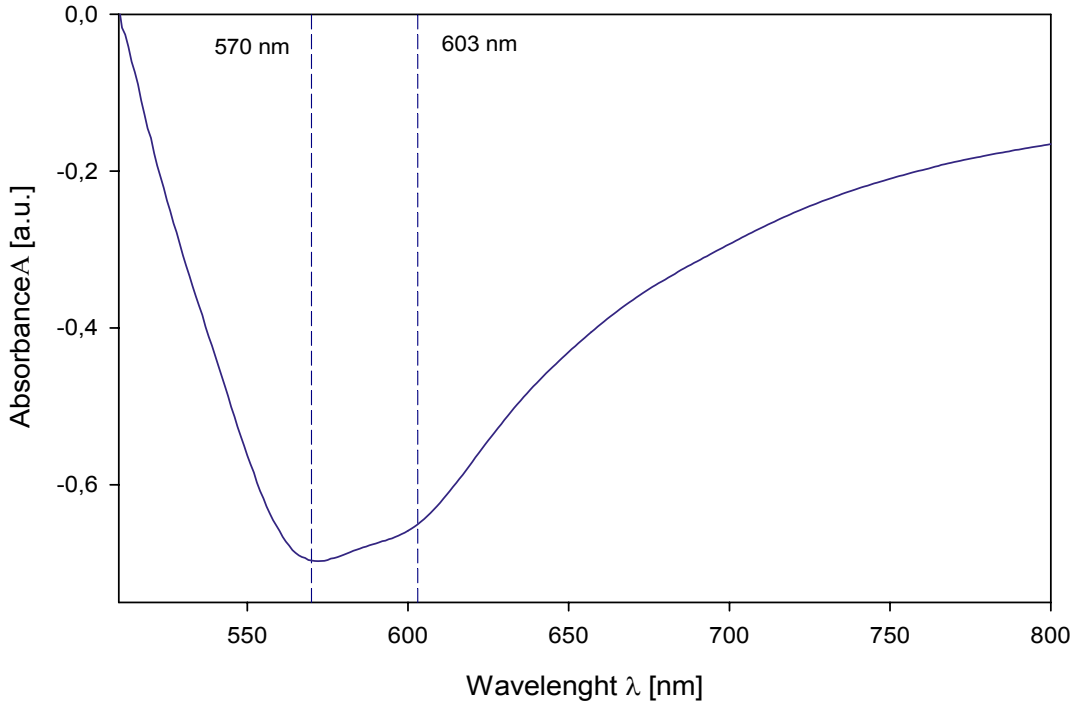

Figure 49. Differential spectrum for $CuTMPyP_4$ in the absence of $CuCl_2$.

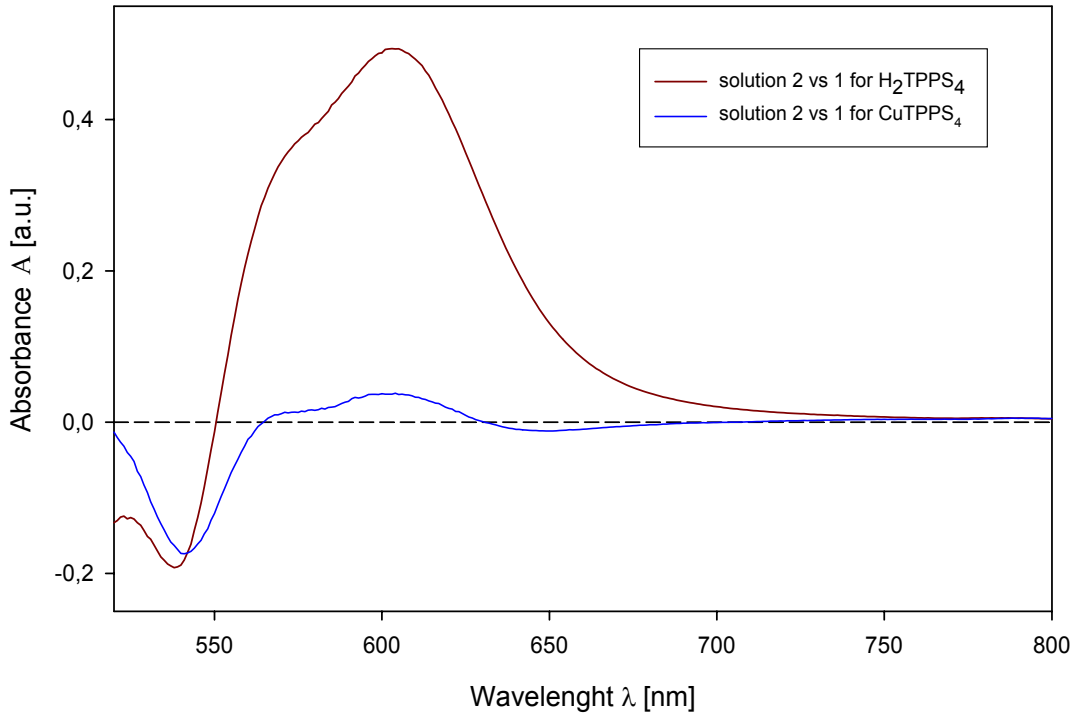

Figure 50. Differential spectra for H_2TPPS_4 and $CuTPPS_4$. Metallation by $CuCl_2$.

Our conclusion is, that the procedure of Pethö and Marzilli can be used, with some reservation, only for anionic porphyrins. In the case of cationic porphyrins it could provide misleading results. It would be worthwhile to publish our findings since several extinction

coefficients determined by this procedure and published [34], have been uncritically adopted by other authors [29].

Since we have found that zincon interacts well with cationic metalloporphyrins, we tried to use it as an indicator of the way the metalloporphyrins bind onto nucleic acids. Our working hypothesis was that the outside–bound metallopophyrins could be accessible for zincon and should show specific absorbance bands, while intercalated metalloporphyrin should be inaccessible for interaction. Firstly, it was necessary to test whether zincon itself does not interact with ST-DNA. Absorption spectra of zincon did not show any change on adding up to 350 μl of ST-DNA (c ~ 10^{-4} M) into 2 ml solution of zincon (c = 2.5 x 10^{-4} M), and no spectral changes were observed in time.

Then, solution of $CuTMPyP_4$ with ST-DNA was prepared in such a way that all the porphyrins should be bound to nucleic acid ([ST-DNA] ~ 10^{-4} M, [$CuTMPyP_4$] = 3 x 10^{-5} M). From the differential titration of the zincon solution by $CuTMPyP_4$-ST-DNA complex *(Figure 51)*, the formation of zincon–metalloporphyrin complex is well detectable. There was observed a slight red shift of the band at 560 nm, and this band converts to band at 603 nm in time, just like in the absence of ST-DNA *(Figure 49)*. This finding indicates ability of zincon to interact with some fraction of metalloporphyrin bound to double-stranded ST-DNA. To check the hypothesis more profoundly in the future, it would be necessary to use synthetic polynucleotides providing only one binding mode for $CuTMPyP_4$ (poly(dA-dT)$_2$ for outside groove-binding and poly(dG-dC)$_2$ for intercalation).

To find whether presence of the central atom Cu^{2+} plays important role in the zincon interaction with H_2TMPyP_4 because of its binding to Cu^{2+} in the porphyrin core, or whether zincon interacts with the porphyrin independently of the central atom, we have tested complex formation at various pH *(Figure 52)* where affinity of the zincon to Cu^{2+} should be different. Zincon-Cu^{2+} complex was shown [35] to be stable only in the pH range 5.0 – 9.5 At the pH 7, differential spectra exhibit two negative bands at 603 and 550 nm, and zincon-porphyrin aggregation seems to progress in time in a similar way as for $CuTMPyP_4$ *(Figure 49)*. However, time evolution for metalloporphyrin was less profound, and there was only a small red-shift of the band at 603 nm. This band is probably due to formation of Cu-zincon complex overlapped by a Q-band of the metallated porphyrin. The band at 570 nm is probably the second Q-band of the $CuTMPyP_4$. In the case of free-base porphyrins and in the absence of Cu^{2+} ions, all the peaks are due to own Q-bands of the free porphyrin and/or due to complex of zincon-porphyrin.

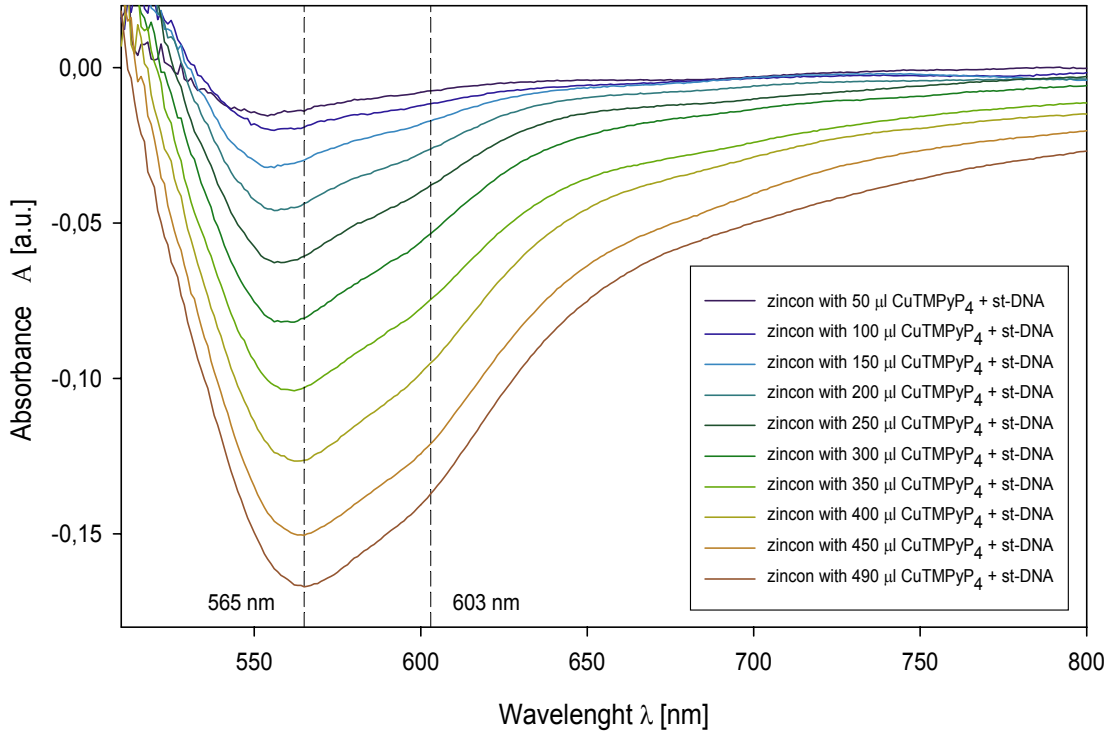

Figure 51. Differential spectra for $CuTMPyP_4$ in the complex with ST-DNA.

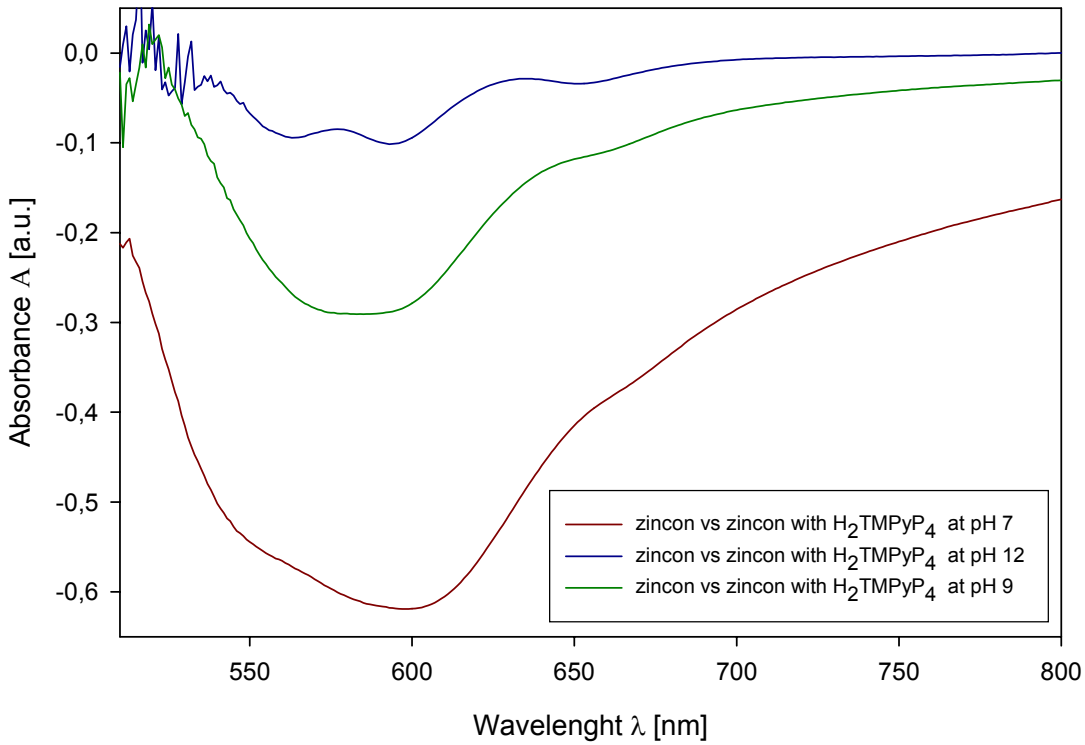

Figure 52. Differential spectra for H_2TMPyP_4 metallated by $CuCl_2$. The pH dependence.

As shown on *Figure 52*, by increasing the pH of the solution, the zincon–porphyrin complex really dissociates and characteristic bands corresponding to the Q-bands of the

free-base porphyrin appeared. With decreasing the pH, light-scattering background increases as well, indicating the formation of zincon–porphyrin aggregates. However, the pH effect can be explained also by other mechanisms, e.g. due to neutralization of the porphyrin charge or due to increased ionic strength on addition of NaOH.

Detail mechanism of interaction between zincon and cationic porphyrin cannot be fully understood on the basis of the present results, and other experiments have to be suggested. There is a possibility of pure electrostatic interaction between cationic substituents of the porphyrin and negatively charged zincon, not necessarily including the porphyrin macrocycle and its central atom. Such an attraction can be assumed for both free-base and metallated derivatives intercalated as well as outside-bound to nucleic acids, and our hypothesis about use of zincon as discriminator of the porphyrin binding mode have to be tested more rigorously.

5.5.2. Dimers formed from cationic and anionic porphyrins

After finding that the procedure of Pethö and Marzilli cannot be used for exact and reliable determination of the extinction coefficients of the cationic porphyrins, we have tried to test other procedure based on dimer formation between cationic and anionic porphyrins. Due to strong attraction between 4 charges, cationic and anionic porphyrins are expected to form 1:1 dimers of great stability. Very weak absorption maxima of such dimers are blue shifted from the Soret maxima of both cationic and anionic porphyrins. Thus, on addition of a small amount of cationic porphyrin of unknown concentration into the solution of anionic porphyrin of well-determined concentration, nonabsorbing dimers are formed, and from the changes of the Soret band, the concentration of the porphyrin added can be estimated.

For this method, we have used extinction coefficient of H_2TPPS_4 determined in this diploma thesis by using the procedure of Pethö and Marzilli, i.e. $\varepsilon_{412} = (4.2\pm0.3) \times 10^5\ M^{-1}\ cm^{-1}$, the value within the error interval of the previously published values. Exact volumes of the cationic porphyrin were added consecutively into the solution of H_2TPPS_4 with known concentration c_1, and from decrease of the concentration of H_2TPPS_4 Δc calculated from decrease of the Soret band (supposing formation of dimers and their negligible absorbance), concentration of the cationic porphyrin was determined (16):

$$c_2 = \Delta c\left(1 + \frac{V_1}{V_2}\right) - c_1 \qquad (16)$$

where V_1 is the volume of H_2TPPS_4 and V_2 is the volume of cationic porphyrin added. The unknown extinction coefficient was then evaluated from Equation (7).

To test applicability and reliability of this procedure, we have used firstly H_2TMPyP_4 with known extinction coefficient $\varepsilon_{423} = 2.63 \times 10^5\ M^{-1}cm^{-1}$. However, first problem appeared while measuring the spectrum of H_2TPPS_4 dissolved in pure water *(Figure 53)*. Besides the monomeric H_2TPPS_4 Soret band at 413 nm, strong band at 432 nm occurred, indicating formation of the J-aggregates. To suppress formation of the H_2TPPS J–aggregates, a borate buffer (pH = 9.0) was used *(Figure 53)*, since moderate basic pH was shown to reduce self-aggregation of anionic porphyrins. To the total volume of 2 ml of H_2TPPS_4 ($c_1 = 5.3 \times 10^{-7}\ M$), volumes of 10 µl of H_2TMPyP_4 ($c_2 = 3.4 \times 10^{-7}\ M$) were added *(Figure 54)*. Formation of dimers (and their aggregates) was detected by increasing absorbance at 430 nm, along with appearance of other red-shifted band at 420 nm, which indicate could indicate formation of J-aggregates from H_2TPPS_4 rather than aggregates with H_2TMPyP_4. In any case, we have concluded that free-base H_2TPPS_4 could not be used for determination of extinction coefficients of novel cationic porphyrins as well. However, their interactions with H_2TPPS_4 could be an interesting subject for further studies. Anyway, more profound investigation goes beyond aim and time capacity of this diploma thesis.

In the shortage of other possibilities and time, we have tried to use metalloderivative $CuTPPS_4$ instead of free-base H_2TPPS_4. Due to risk of transmetallation effects appearing on interaction between metallated CuTPPS4 and free-base cationic porphyrins, we have used this method only for Cu^{2+} derivatives. At first we have tested $CuTMPyP_4$ with published extinction coefficient ($\varepsilon = 2.31 \times 10^5\ M^{-1}cm^{-1}$) using the same titration procedure as used with H_2TMPyP_4 *(Figure 55)*. The concentration of $CuTMPyP_4$ was $c_2 = 8.2 \times 10^{-7}\ M$. Absorption spectra of the $CuTPPS_4$ titrated by the $CuTMPyP_4$ exhibit two isobestic points, indicating thus occurrence of two spectroscopic forms in solution *(Figure 55)*. One form is apparently the free $CuTPPS_4$, the other should be a 1:1 dimer $CuTPPS_4$-$CuTMPyP_4$. For small volumes of $CuTMPyP_4$ added, the concentration changes were also small, thus one can expect considerable experimental error in a single titration step. To obtain more reliable result, extinction coefficient was determined from several independent

experiments using factor analysis, fitting and statistical treatment. By this way, extinction coefficient of the $CuTPPS_4$ was estimated, $\varepsilon(CuTPPS_4)_{412} = (2.7 \pm 0.5) \times 10^5\ M^{-1}cm^{-1}$.

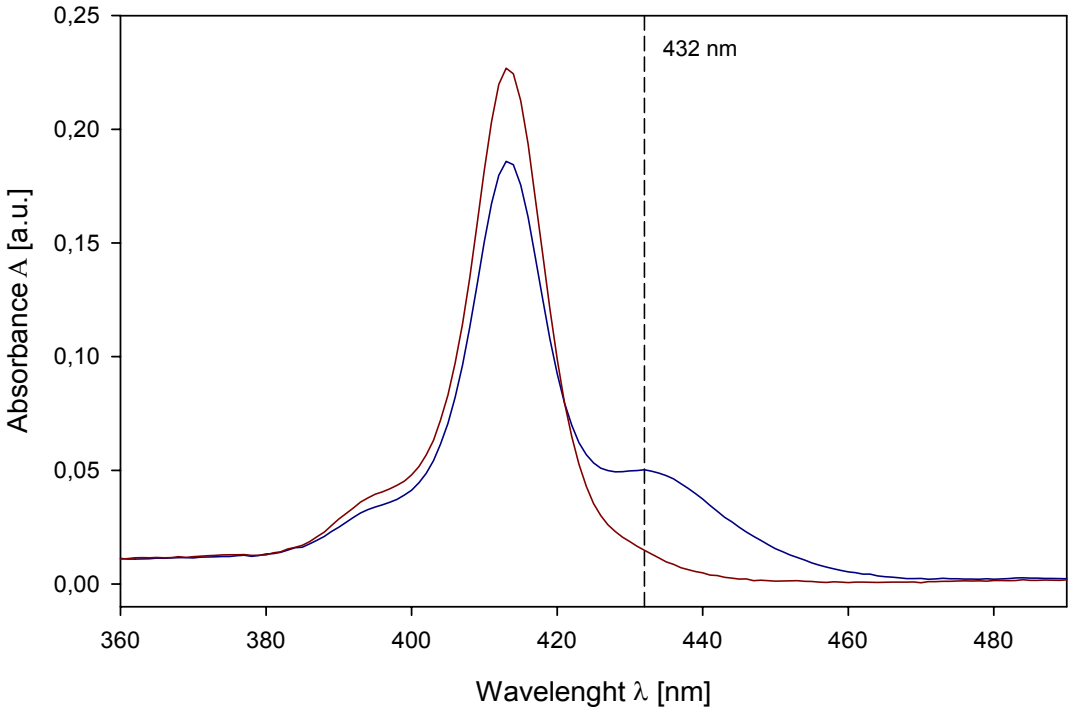

Figure 53. Absorption spectra of H_2TPPS_4 in water and in borate buffer ($c = 5.3 \times 10^{-7}$ M)

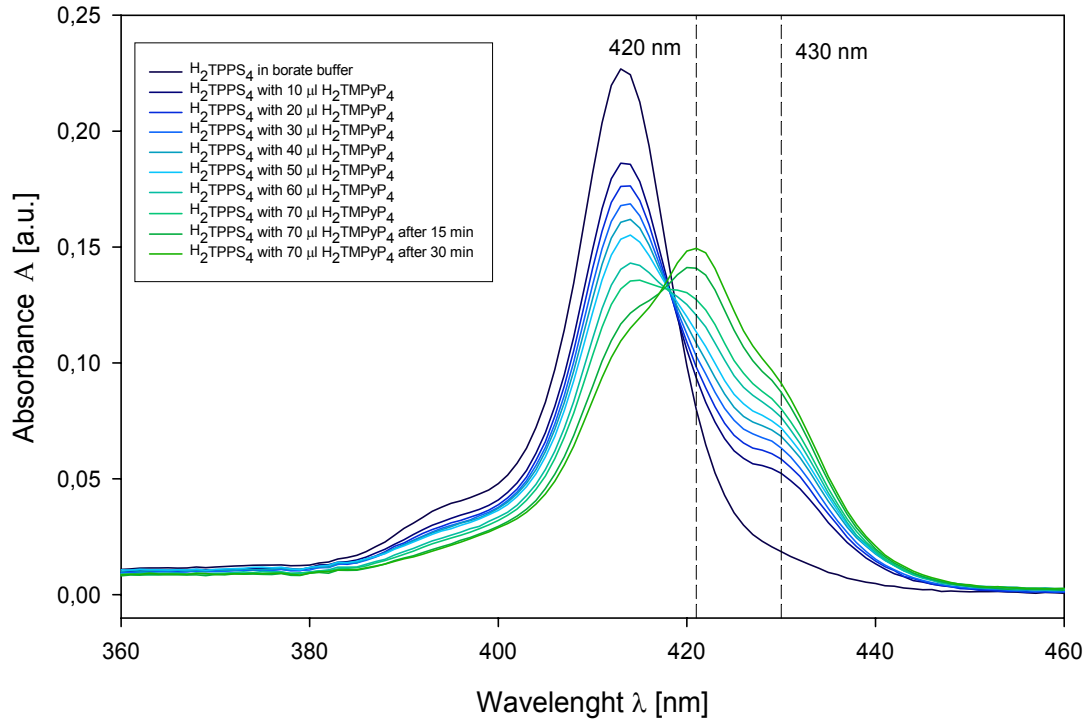

Figure 54. Titration of H_2TPPS_4 with H_2TMPyP_4 in borate buffer, pH 9,0

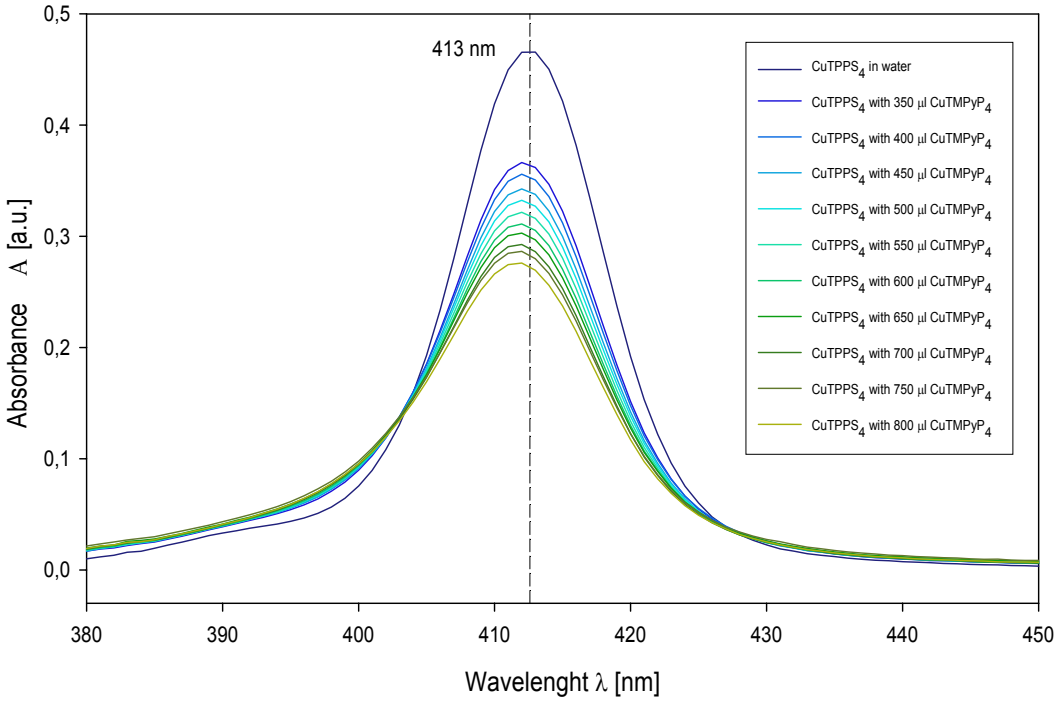

Figure 55. Titration of $CuTPPS_4$ by $CuTMPyP_4$ in aqueous solution

As this value seemed reasonable, and because there was no other extinction coefficient published or available at the time, we have used our estimate for further determination of extinction coefficients of Cu^{2+} derivatives of some cationic porphyrins studied in the diploma thesis. Solutions of CuTPP-$(NMe_3)_4$, CuTPP-p-$(Bru)_4$ and CuTPP-m-$(Bru)_4$ were titrated by solution of $CuTPPS_4$ in the same way, and Soret absorption spectra were measured. For a specific range of porphyrin additions, presence of clear isosbestic points was observed for all porphyrins tested. Finally, following extinction coefficients were estimated:

For CuTPP-$(NMe_3)_4$, $\varepsilon(CuTPP\text{-}(NMe_3)_4)_{412} = (2.5 \pm 0.5) \times 10^5\ M^{-1}cm^{-1}$

For CuTPP-p-$(Bru)_4$, $\varepsilon(CuTPP\text{-}p\text{-}(Bru)_4)_{421} = (4.1 \pm 0.7) \times 10^5\ M^{-1}cm^{-1}$

For CuTPP-m-$(Bru)_4$, $\varepsilon(CuTPP\text{-}m\text{-}(Bru)_4)_{416} = (3.0 \pm 0.6) \times 10^5\ M^{-1}cm^{-1}$

We are well aware of incertitude and deficits of the used procedure and vagueness of the extinction coefficients determined, however, their values correspond surprisingly well with usual values of other cationic porphyrins and metalloporphyrins, thus we believe that our approach is in principle correct and can be utilize. However, further experiments have to be done to verify it in details.

5.6 Porphyrins with single-stranded nucleic acids

To simulate processes taking part on the porphyrin-assisted delivery of short *antisense* single-stranded oligonucleotides into the cell nucleus, we have studied mutual complex formation between free-base H_2TMPyP_4, short ss-deoxyoligonucleotide and ss-polyribonucleotide. Antisense deoxyoligonucleotide in complex with cationic porphyrin is expected to interact, after its uptake to the cell, with the complementary sequence of the cell RNA by forming a mixed DNA/RNA double-helix. Therefore, interaction with the porphyrin should not preclude recognition and base-pairing between nucleic acids. Furthermore, because of high affinity for nucleic acids once attached to oligonucleotide, the porphyrin should arrange its binding mode according to newly formed DNA/RNA double-helix.

We have used an oligo$(dA)_{15}$ as a model of antisense ss-oligonucleotide, and poly(rU) as a simplest model of single-stranded mRNA. At first, H_2TMPyP_4 with oligo$(dA)_{15}$ was bound in ratio 1:5, thus 1 porphyrin for 5 residues (i.e. 3 porphyrins for each oligo$(dA)_{15}$). At this ratio, formal charge of oligo$(dA)_{15}$ (15-) is nearly compensated by a formal charge of 3 H_2TMPyP_4 molecules (12+) and the porphyrin should cover the entire oligonucleotide surface. The concentration of H_2TMPyP_4 in all these measurements (determined spectroscopically) was ~ 1 x 10^{-6} M, and absorption spectra were measured in 10 mm cells *(Figure 56)*. Absorption spectrum of the H_2TMPyP_4-oligo$(dA)_{15}$ complex consisted of two peaks located at ~ 424 and 446 nm, thus suggesting two binding modes, outside-binding and intercalation, respectively. It is also possible that 424 nm band contains some fraction of the uncomplexed porphyrin, and 446 nm covers also contribution from porphyrin self aggregates on the oligonucleotide pattern. To find effect of the porphyrin presence on the oligo$(dA)_{15}$ pairing with poly(rU), and - on the other hand - effect of DNA/RNA duplex formation on the porphyrin binding mode, solution of poly(rU) of various concentration was added (ratio expressed in nucleotide residues). As seen on *Figure 56*, dramatic spectral changes were observed on addition of poly(rU) to H_2TMPyP_4-oligo$(dA)_{15}$ complex, however there was no substantial difference when using various concentration ratio of oligo$(dA)_{15}$: poly(rU) (only slight absorbance decrease at 436 nm at lower poly(rU) concentrations). It seems that some kind of DNA/RNA duplex was formed between oligo$(dA)_{15}$ and poly(rU) at any oligonucleotide ratio, inducing change of the porphyrin binding mode, probably towards duplex intercalation. Differences between spectra for various poly(rU) concentrations can be explained by the presence of uncomplexed

porphyrin (or loosely bound porphyrin) coming into the mixture with oligo(dA)$_{15}$ that can bind to free poly(rU) or to DNA/RNA duplex by a slightly different binding mode.

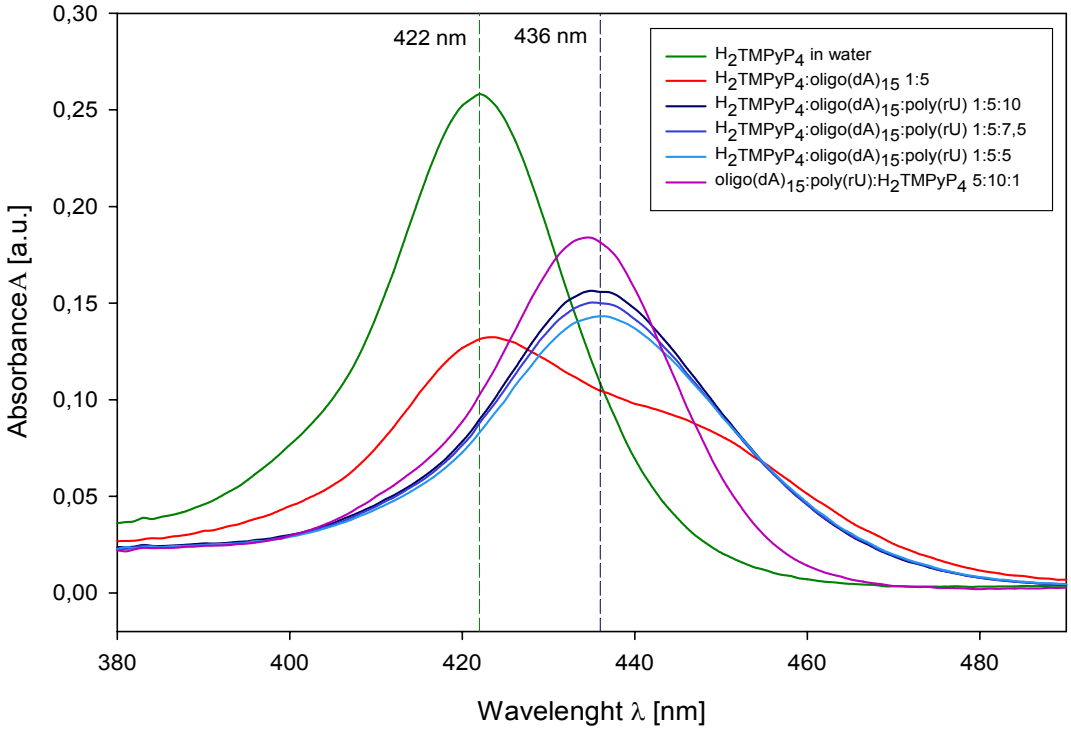

Figure 56. Absorption spectra of H_2TMPyP_4 in various complexes with oligo(dA)$_{15}$ and poly(rU).

To find whether the presence of H_2TMPyP_4 affects pairing of oligo(dA)$_{15}$ with poly(rU), we have measured absorption of the H_2TMPyP_4 complexes with DNA/RNA duplex prepared (by mixing of oligo(dA)$_{15}$ with poly(rU) 1:1) before addition of the porphyrin *(Figure 56)*. For such a system, the Soret maximum at 436 nm was shifted to lower wavelengths and its intensity increased. This shows an evidence of a different way of porphyrin binding to DNA/RNA duplex. It is possible that DNA/RNA duplex is paired in somewhat different way when the porphyrin is absent. One can suggest, that only oligonucleotides with a porphyrin fixed to oligo(dA)$_{15}$ in a proper way are able to form hybrid duplexes. The rest remains intact, or the porphyrin loosely bound to oligo(dA)$_{15}$ is moved to poly(rU) due to higher affinity. If the later explanation is correct, pophyrin should have greater affinity to poly(rU) than to DNA/RNA duplex. This finding is in accordance with [33], where it was suggested that some single-stranded propensity of the porphyrin macrocycle should exist due to higher flexibility and hydrophobicity of ss-polynucleotides.

As mention above, a strange absorption spectrum was observed in the 1:5 mixture of H_2TMPyP_4 and oligo$(dA)_{15}$. Two broad absorption bands were observed. The band at 424 nm seemed to be due to outside-bound or unbound porphyrin, the other one should belong to intercalative of self-stacked H_2TMPyP_4-oligo$(dA)_{15}$ complexes. To better understand this feature, we have titrated H_2TMPyP_4 with oligo$(dA)_{15}$, starting from the ratio 1 : 100 *(Figure 57)*. However, in the course of this titration, no two-band spectra similar to that of direct mixture of H_2TMPyP_4 with oligo$(dA)_{15}$ at ratio 1:5 were obtained. High hypochromism (> 30%) and remarkable red shift (16 nm) seems to indicate intercalation. We have tried to prepare complex H_2TMPyP_4-oligo$(dA)_{15}$ 1:5 having two-band features, but we did not get the same shape of spectrum as before. It is possible that the spectrum taken from direct mixing of porphyrin with oligo$(dA)_{15}$ has the two-bands shape only for some specific concentration ratio, which we were not able to reproduce. As reported previously [20, 46], H_2TMPyP_4 and $CuTMPyP_4$ form outside-binding complexes with poly(dA). However, in the case of oligo$(dA)_{15}$, binding mode can be different from polynucleotide. It was shown recently [9] that interaction of cationic porphyrins (reported for $CuTMPyP_4$) with short oligo$(dA)_n$ depends on the oligonucleotide length. The outside-binding, preferential for poly(dA), is gradually converting to intercalation as the length is decreasing. That is in agreement with our present results.

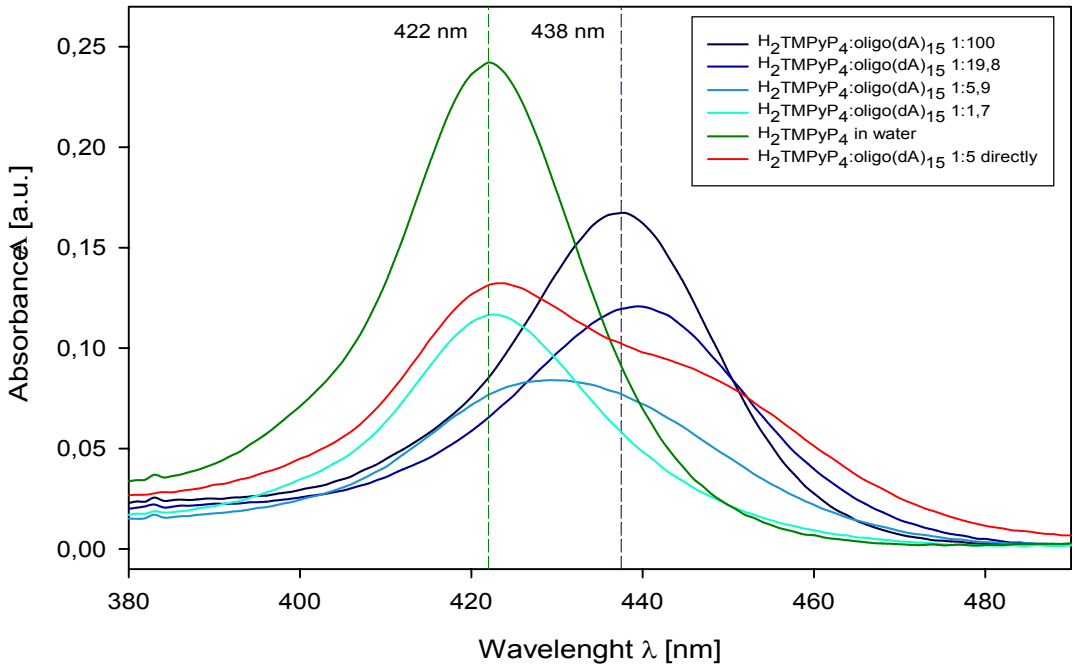

Figure 57. Spectrophotometric titration of H_2TMPyP_4 with oligo$(dA)_{15}$. Soret band region.

To see if some strange behavior appears also for poly(rU), we have measured titration of H_2TMPyP_4 with poly(rU), starting from ratio 1:100 *(Figure 58)*. Spectra showed remarkable red-shift of the Soret band (12 nm), but the hypochromism was quite low (< 10%) in comparison with oligo$(dA)_{15}$. Therefore, outside-binding is possible, probably some kind of interaction bearing features of partial intercalation and outside-binding. When comparing spectra of porphyrin-poly(rU) complexes 1:5 prepared by a mixing, there were no deviations from the titration spectra.

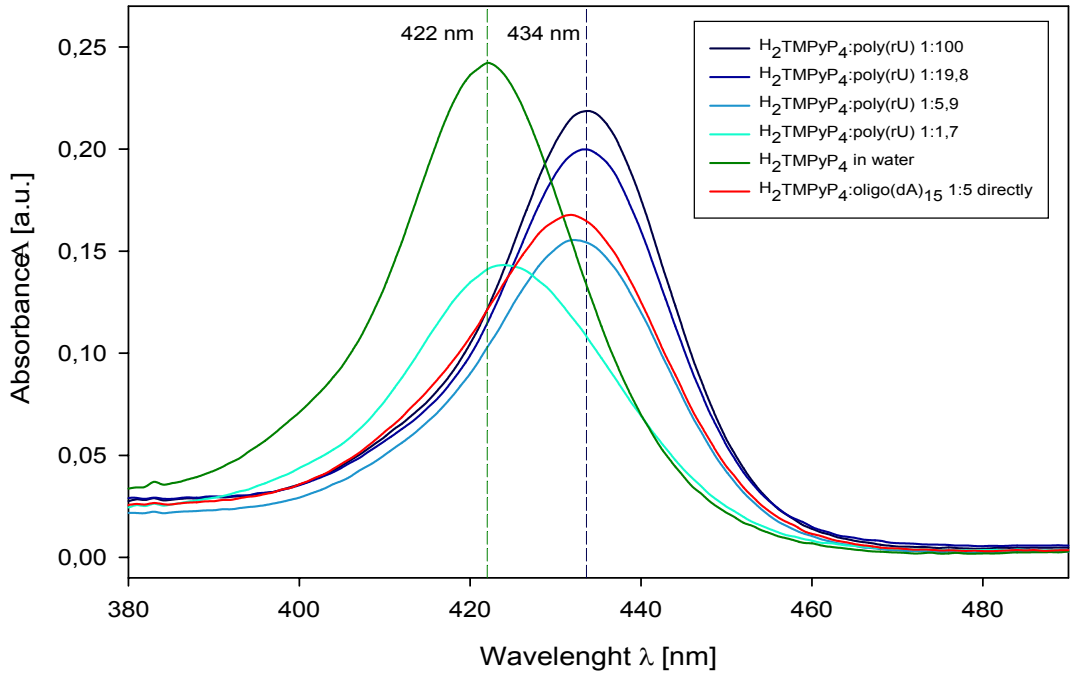

Figure 58. Spectrophotometric titration of H_2TMPyP_4 with poly(rU). Soret band region

To summarize the interactions between H_2TMPyP_4 and DNA/RNA duplexes, they are characteristic by a strong hypochromism of the Soret band, which is red-shifted by ~ 14 nm *(Figure 56)*. This features indicate predominantly intercalation [37, 38] as observed for H_2TMPyP_4 and $CuTMPyP_4$ in complexes with poly(rA).poly(dT), where it was assumed that for RNA-duplexes the outside-binding with a porphyrin self-stacking is preferred, and for RNA-DNA hybrids the intercalation is favored. These findings should not depend on the base composition but only on ribose/deoxyribose content. Therefore our dA-rU duplexes should also prefer intercalation, which is in agreement with our findings.

Interactions of single-stranded oligonucleotides with cationic porphyrins have not been studied as extensively as with double-strands. There are only few publications concerning this subject, dealing mainly with H_2TMPyP_4 and H_2TMAP. Even in that case it is difficult

to compare our data with relevant published results. In the case of other cationic porphyrins bearing bulky substituents, there are even less information, thus continuation of the present research with novel cationic porphyrins will be of great importance.

5.7 Porphyrins with double–stranded DNA

We have tried to characterized basic structural features of the novel cationic porphyrins with standard double-stranded nucleic acids, i.e. ST-DNA, poly(dA-dT) and poly(dG-dC), by use of absorption and resonance Raman (RRS) spectroscopies. Many works dealing with cationic porphyrins characterize their interactions with nucleic acids only by using natural DNA (CT-DNA, ST-DNA). Since some porphyrins have been found to exhibit sequential selectivity (H_2TMPyP_4: groove-binding for poly(dA-dT) and intercalation for poly(dG-dC) [17, 18]), it is worthwhile to use more defined polynucleotides instead of natural DNA.

For spectroscopic methods (e.g. RRS) that can induce photodecomposition of the free-base porphyrins due to singlet oxygen production, the Cu^{2+} metalloderivatives are frequently used as models, since they are more photostable and their binding modes are, to some extent, similar to free-base derivatives. E.g., $CuTMPyP_4$ with no axial ligands is very similar to free-base H_2TMPyP_4 when interacting with different sequences of DNA [17].

Outside binding is favored by electrostatic and H-bonding interactions. Intercalation needs planar region of DNA binder, relatively hydrophobic and polar. Therefore the lack of planarity close to the porphyrin core can inhibit intercalation and cause outside binding [18]. This is expected in the case of porphyrins with bulky, nonplanar and differently twisted substituents. For effective intercalation, bulky substituents have to become more coplanar to the porphyrin macrocycle to be able pass through interior of the double helix. The greater the meso-substituents are, the greater energy barrier is to be overcome. Intercalation of H_2TMPyP_4 requires rotation of the N-methylpyridyl group to coplanar configuration with porphyrin macrocycle on the cost of more than 15 kcal/mol in [17]. Consequently, novel cationic porphyrins with bulky substituents are expected, in general, to be outside binders to DNA regardless of the base sequence.

All the porphyrins and metalloporphyrins perform numerous in-plane and out-of-plane vibrational motions of the porphyrin macrocycle and of the peripheral substituents. Even the simplest molecular model of metalloporphyrins macrocycle having D_{4h} symmetry [39] consists of 37 atoms and exhibits thus 71 in-plane degrees of internal freedom *(Figure 59)*.

Other modes shoot up when considering vibrational motions of peripheral substituents. Thus, one could expect rich and rather complicated vibrational, e.g. Raman spectra. However, due to selectivity of the resonance enhancement (excitation in the electronic absorption band), symmetry properties of porphyrin macrocycle and selection rules, actual RRS spectra of the metalloporphyrins are reasonable plentiful. In the past two decades, RRS was proven to be excellent method for investigation porphyrin complexes with nucleic acids [41-46].

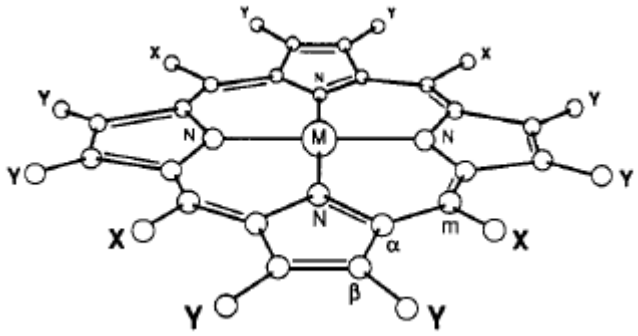

Figure 59. Structural diagram of metalloporphyrin macrocycle having symmetry D_{4h}, with meso-substituents X, pyrrole-substituents Y. and central atom M (taken from [39]).

As a first attempt, we have studied complexes of selected Cu^{2+} porphyrins ($CuTMPyP_4$, $CuTPP\text{-}(NMe_3)_4$, $CuTPP\text{-}p\text{-}(Bru)_4$, $CuTPP\text{-}m\text{-}(Bru)_4$ and $CuTPPS_4$) with natural ST-DNA by means of resonance Raman spectroscopy, using excitation 441.6 nm, thus in resonance with Soret-band electronic transition. Due to resonance enhancement, it was possible to obtain spectra of reasonable signal-to-noise ration at the porphyrin concentrations ~ 1 - 3 x 10^{-5} M. The ratio ([base pairs]/[porphyrin]) R ~ 50 was used to ensure high excess of binding sites.

As expected, no RRS signs of interaction were found for anionic $CuTPPS_4$ when mixed with ST-DNA (not shown). RRS spectra of other cationic porphyrins are represented on *Figures 61 – 64*. In the case of frequently studied $CuTMPyP_4$, there was a possibility to confront our result with published data. In the region 900 – 1700 cm^{-1}, 9 Raman bands can be distinguished [41, 42]. Bands at 1007 cm^{-1} and 1101 cm^{-1} have been assigned to vibrations of the porphyrin core, specifically to $\nu_S(C_\alpha\text{-}C_m)$ and $\delta_S(C_\beta\text{-}H)$, respectively. For the second band we have observed shift to higher wavenumbers (1107 $cm^{-}1$) when binding to ST-DNA. Vibrational motions of C_β hydrogens $\delta_S(C_\beta\text{-}H)$ were reported to be sensitive for intercalation, since they are strongly affected by obstructions with hydrogens from pyridinium (or phenyl) groups, which have to become coplanar with the macrocycle on

intercalation. The bands at 1193 cm^{-1} (*δ(prm)*, *ν(N^+-CH_3)*), 1223 cm^{-1} (*δ(prm)*) and 1257 cm^{-1} (*δ(C_m-prm)*) have been assigned mainly deformation vibrations of the N-methyl pyridinium rings with contributions from vibrational motions of methyl groups [42].

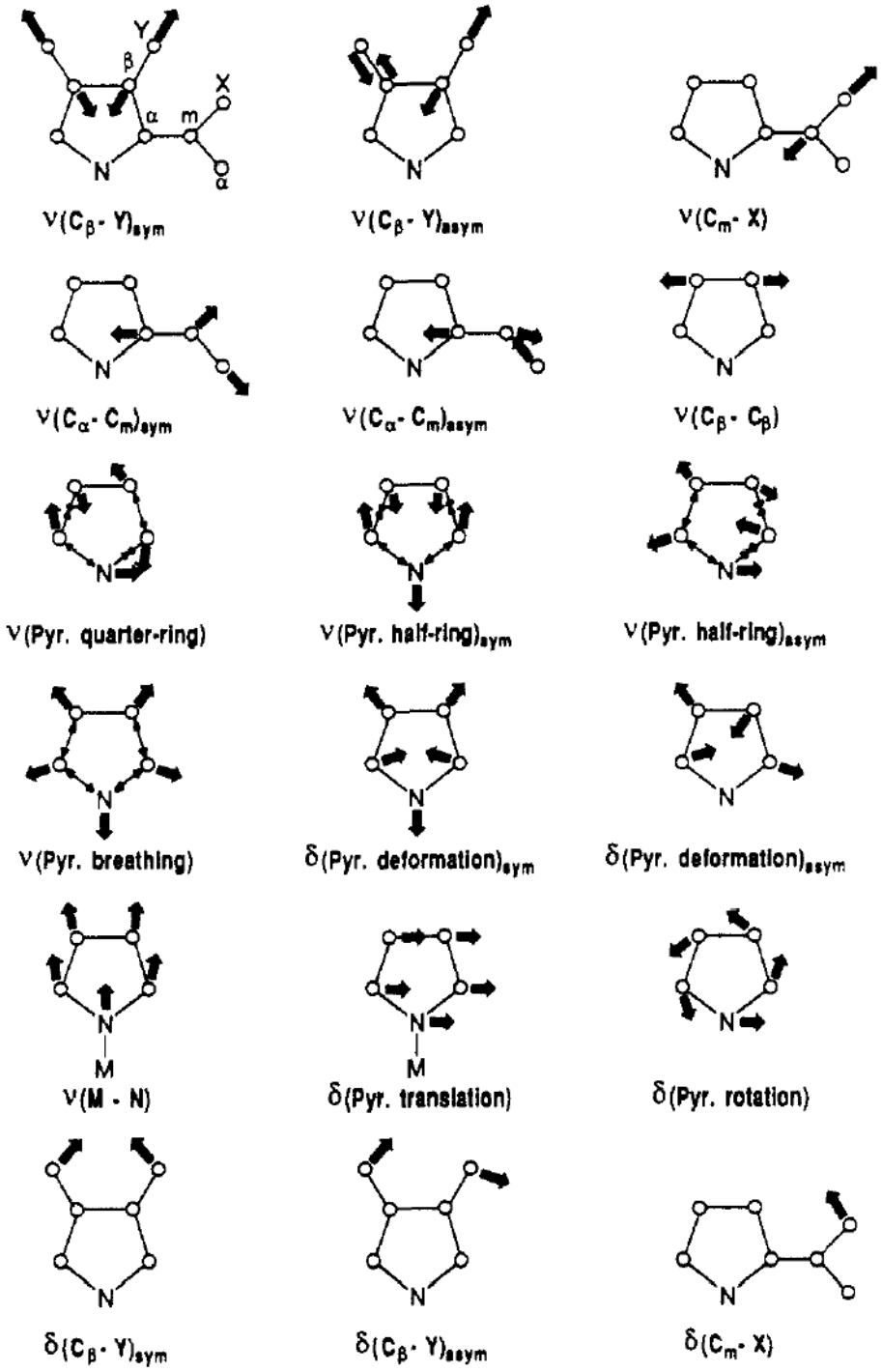

Figure 60. Illustration of the local in-plane porphyrin skeletal modes. Stretching motions of the $C_\alpha N$ and $C_\alpha C_\beta$ pyrrole bonds are considered collectively, ν means stretching and δ bending/deformational vibration, Pyr assigns the pyrrole ring in that case, not to be confused with prm assigned to N-methyl pyridinium group (taken from [39]).

Highly symmetrical collective vibrations (A_{1g}) of the porphyrin macrocycle giving rise to intense bands at 1367 (ν_4), 1466 (ν_3) and 1570 (ν_2) are localized mainly at $\nu_S(C_\alpha\text{-}N)$, $\nu_S(C_\alpha\text{-}C_\beta)$ and $\nu(C_\beta\text{-}C_\beta)$ vibrational modes, respectively [42].

When the $CuTMPyP_4$ is bound to ST-DNA, relative intensity of the ν_4 band at 1367 cm^{-1} decreases and intensity of the ν_2 1570 cm^{-1} increases [41]. The band at 1644 cm^{-1} was assigned to deformational mode of N-methyl pyridinium $\delta(prm)$ coupled with of the vibrations of macrocycle. However, since the spectra shown on *Figures 61 – 64* represent our first own attempt to measure RRS, their quality and reliability was negatively affected by lack of practice and skill. Evidently, in the spectra there are present several artefacts, e.g. incorrect calibration of the wavenumber scale which results in appearance of false spectral features in the difference spectra. Regardless of the quality of the RRS spectra, the changes observed for $CuTMPyP_4$ were consistent with coincident existence of intercalation and groove-binding, as reported previously [41, 42]. Similar coexistence can be proposed for CuTPP-$(NMe_3)_4$.

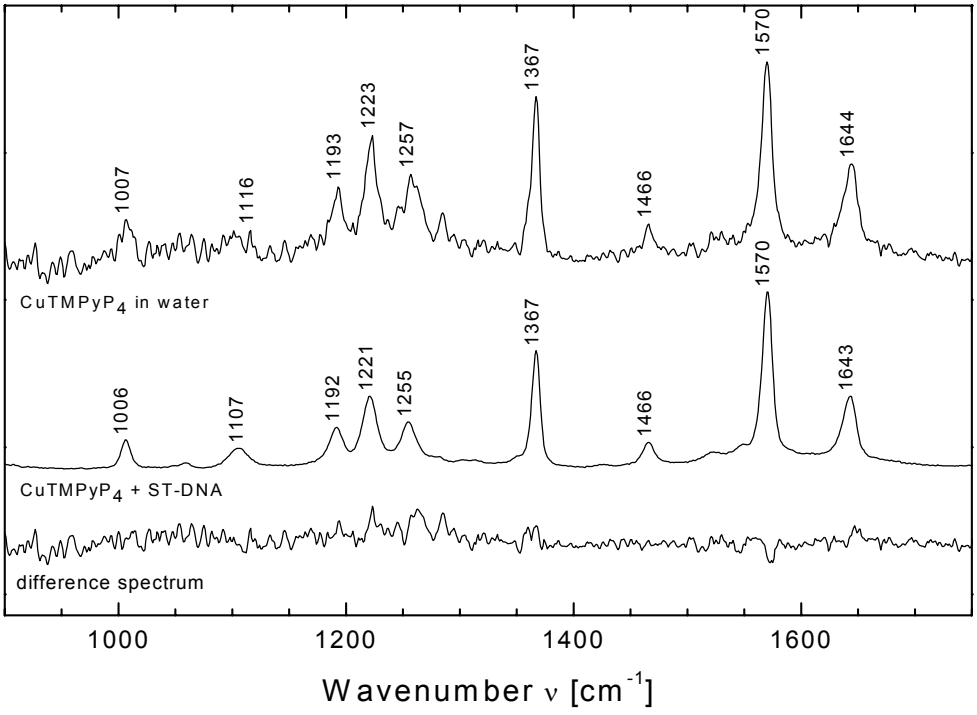

Figure 61. RRS spectra of $CuTMPyP_4$ with ST-DNA

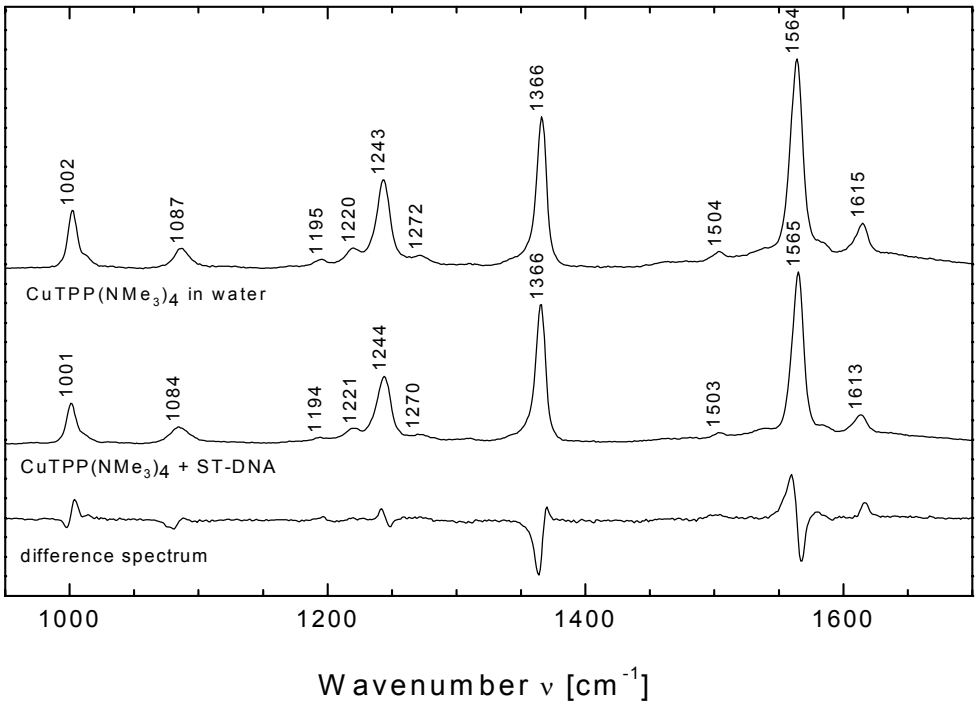

Figure 62. RRS spectra of CuTPP-$(NMe_3)_4$ with ST-DNA

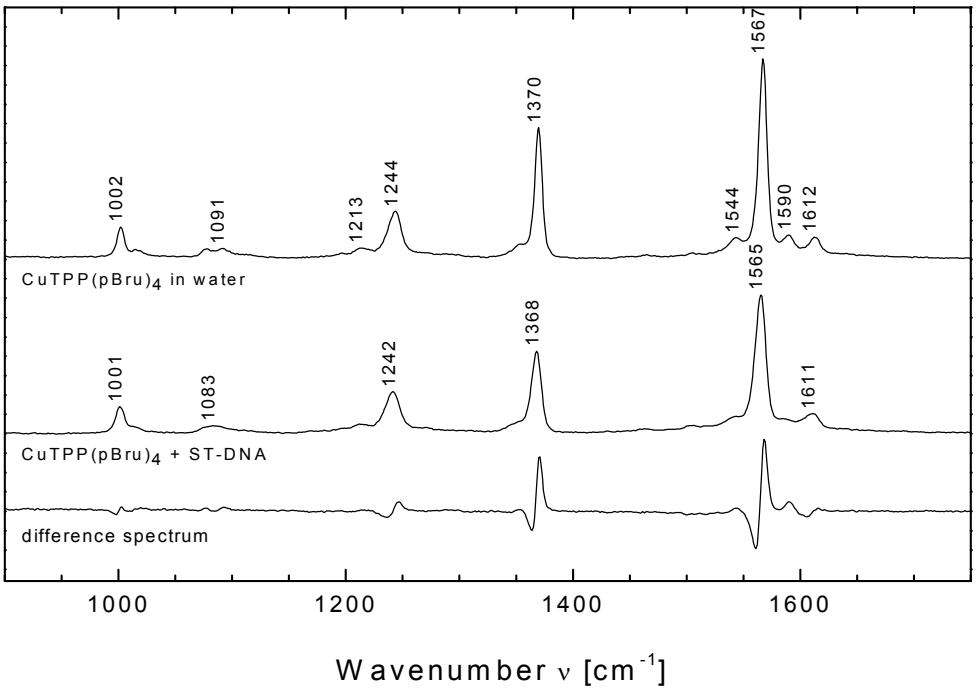

Figure 63. RRS spectra of CuTPP-$p(Bru)_4$ with ST-DNA

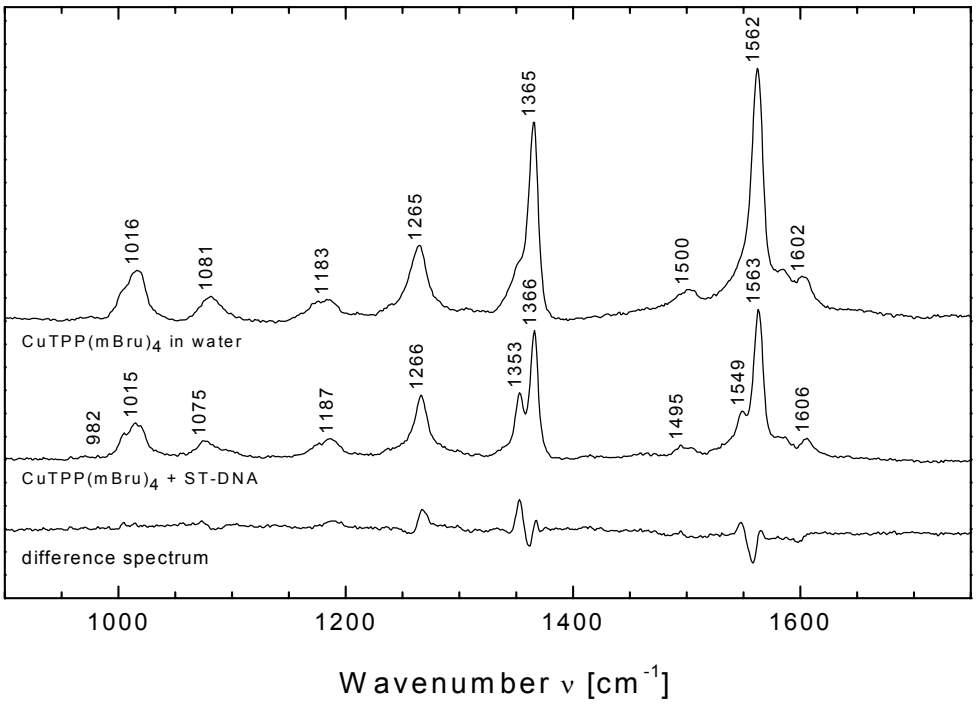

Figure 64. RRS spectra of CuTPP-m(Bru)$_4$ with ST-DNA

Very interesting results were observed for CuTPP-p-(Bru)$_4$ and CuTPP-m-(Bru)$_4$ (differing structurally only in position of the brucine substituent at the phenyl ring), where new down-shifted Raman bands at 1353 and 1549 cm^{-1} have appeared in pairs to ν_4 (1366 cm^{-1}) and ν_2 (1563 cm^{-1}) bands, respectively for ST-DNA-CuTPP-m-(Bru)$_4$ complex. Other spectral features for both brucine porphyrins were consistent rather with some kind outside-binding than for intercalation. However, further measurements have to be done to identify the spectral changes more reliably.

To obtain first insight into the binding dependency of the novel porphyrins on the double-stranded polynucleotides providing typical intercalative and external binding sites, complexes of CuTMPyP$_4$, CuTPP-(NMe$_3$)$_4$, CuTPP-p(Bru)$_4$ and CuTPP-m-(Bru)$_4$ with synthetic poly(dA-dT)$_2$, poly(dG-dC)$_2$ and poly(dA).poly(dT) were studied again by RRS and absorption spectroscopies *(Figures 65 – 68)*. In the case of polynucleotides consisting of uniform base-pairs pattern, binding selectivity is more visible than with ST-DNA, which consists of numerous combinations of base pairs.

For CuTMPyP$_4$ *(Figure 65)*, the RRS spectrum for poly(dG-dC)$_2$ complex exhibits typical intercalation marker (1107 cm^{-1} $\delta_S(C_\beta\text{-}H)$ band upshifted from the 1100 cm^{-1} for

uncomplexed porphyrin). In the case of poly(dA-dT)$_2$, this band is downshifted by 1 cm^{-1}, indicating typical outside groove-binding [41].

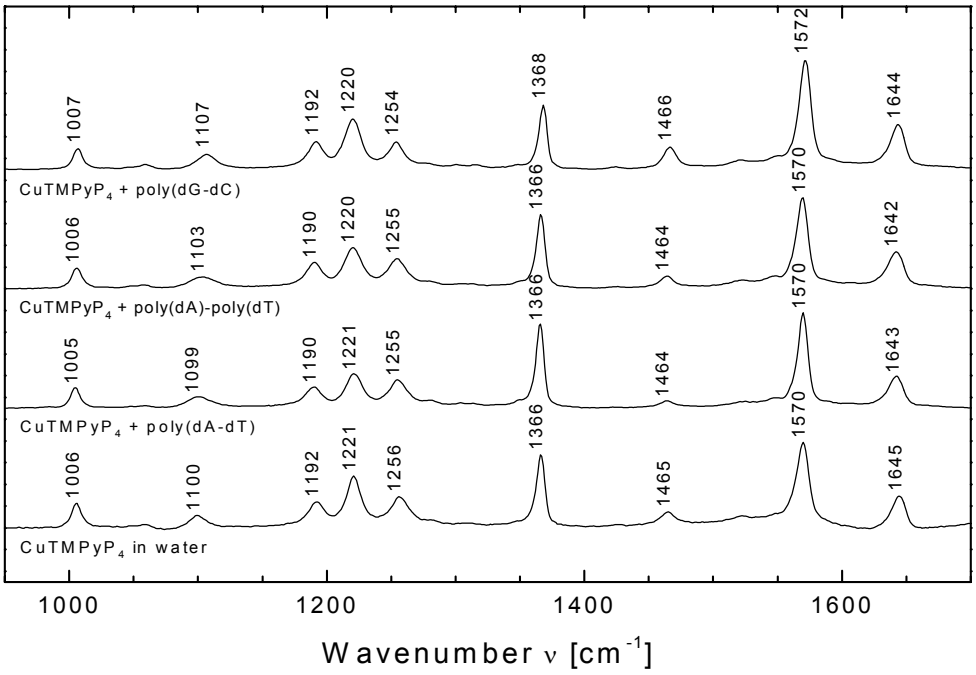

Figure 65. RRS spectra of CuTMPyP$_4$ with poly(dA-dT)$_2$, poly(dG-dC)$_2$, poly(dA).poly(dT)

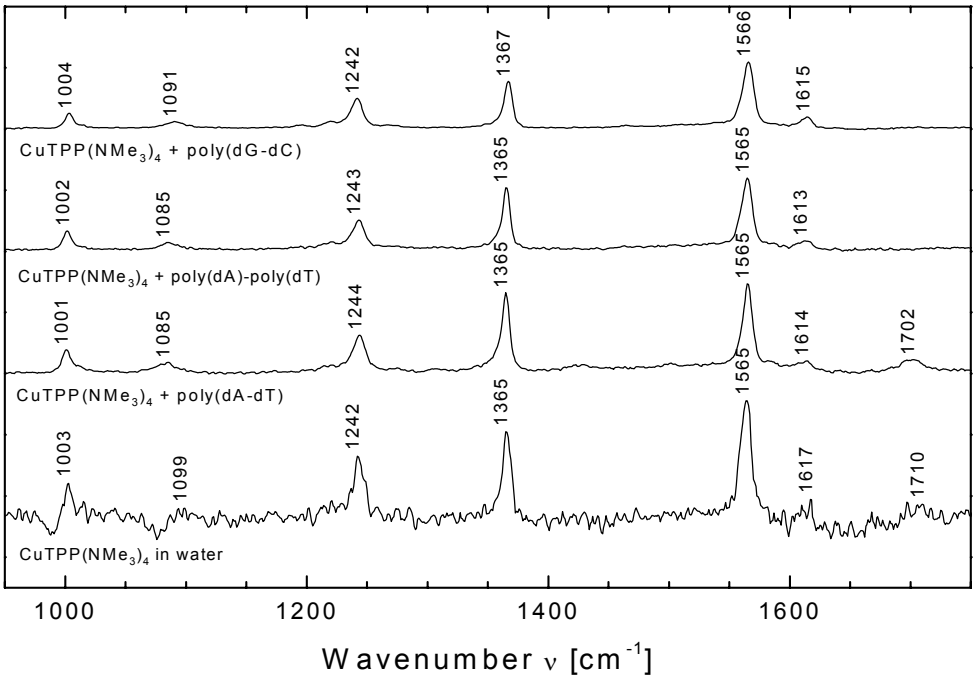

Figure 66. RRS spectra of CuTPP-(NMe$_3$)$_4$ with poly(dA-dT)$_2$, poly(dG-dC)$_2$, poly(dA).poly(dT)

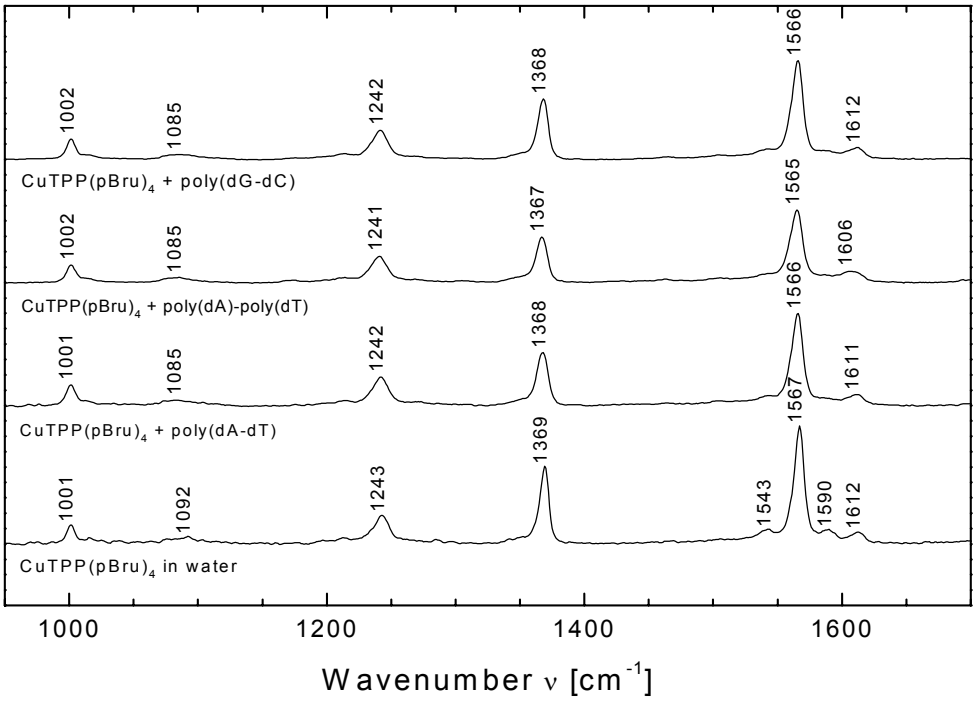

Figure 67. RRS spectra of CuTPP-p-(Bru)$_4$ with poly(dA-dT)$_2$, poly(dG-dC)$_2$, poly(dA).poly(dT)

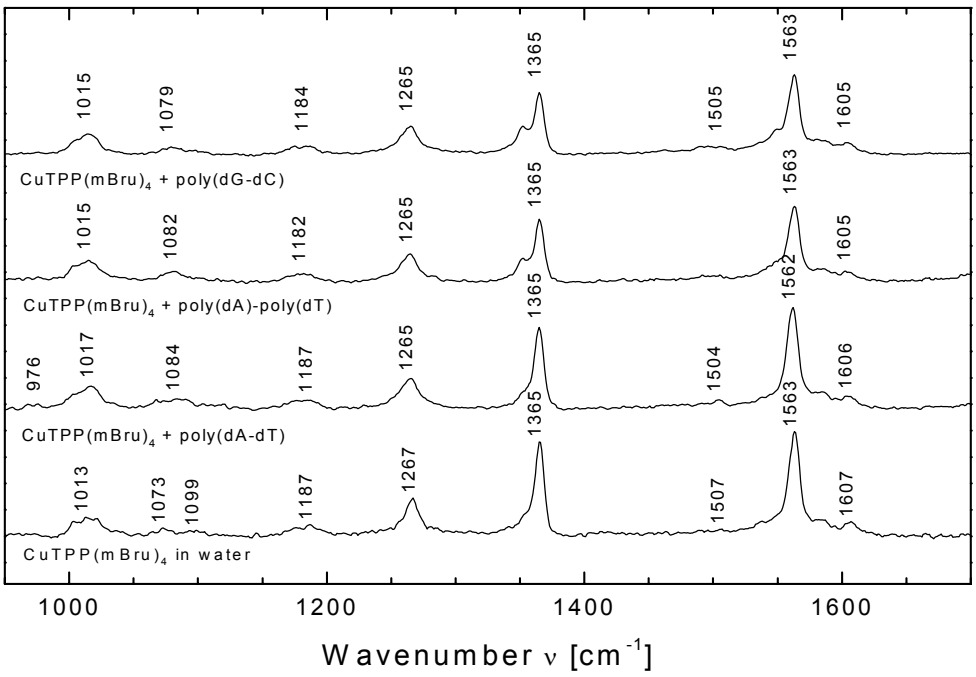

Figure 68. RRS spectra of CuTPP-m-(Bru)$_4$ with poly(dA-dT)$_2$, poly(dG-dC)$_2$, poly(dA).poly(dT)

For poly(dA).poly(dT), moderate upshift for 3 cm^{-1} was interpreted as other binding mode than typical groove-binding, however differing clearly also from typical G-C intercalation. Other changes concern three bands at 1192, 1221 and 1256 cm^{-1}. For poly(dA-dT)$_2$, intensity of the band at 1255 cm^{-1} increases. In poly(dG-dC)$_2$ spectrum the intensity of both outer bands is the same, while for free porphyrin 1192 cm^{-1} band is less intense than 1256 cm^{-1} band. For poly(dA).poly(dT) this change is somewhere in the middle of the changes observed for poly(dA-dT)$_2$ and poly(dG-dC)$_2$. Further changes concern the porphyrin core bands ν_4 $\nu_S(C_\alpha\text{-}N)$ at 1366 cm^{-1} and ν_2 $\nu(C_\beta\text{-}C_\beta)$ at 1570 cm^{-1}. Intensity ratio ν_4/ν_2 was 0.85, 0.9, 0.8 and 0.6 for uncomplexd porphyrin, poly(dA-dT)$_2$, poly(dA).poly(dT) and poly(dG-dC)$_2$, respectively. The decrease of the ratio down to 0.6 clearly indicates intercalation for poly(dG-dC)$_2$, and its increase to 0.9 is excellent marker for outside groove-binding for poly(dA-dT)$_2$, fully in agreement with [17, 41]. Changes for poly(dA).poly(dT) are somewhere between those for poly(dA-dT)$_2$ and poly(dG-dC)$_2$, indicating binding mode between intercalation and outside binding. Changes observed for $CuTMPyP_4$ with ST-DNA are similar but not identical to changes for poly(dG-dC)$_2$. This supports tendency of $CuTMPyP_4$ to intercalate into natural DNA. However, some part of $CuTMPyP_4$ seems to bind in a different way [43, 44].

For CuTPP-$(NMe_3)_4$ *(Figure 66)* there is a shift of $\delta_S(C_\beta\text{-}H)$ to 1085, 1085 and 1091 cm^{-1} for poly(dA-dT)$_2$, poly(dA).poly(dT) and poly(dG-dC)$_2$, respectively. We have attributed this band, in analogy with $CuTMPyP_4$ [42], to the $\delta_S(C_\beta\text{-}H)$ mode, which have to be hampered by hydrogens from phenyl groups after intercalation. The higher frequency (+ 6 cm^{-1}) observed for poly(dG-dC)$_2$ could indicate intercalation, similarly to ST-DNA. On the other hand, for poly(dA-dT)$_2$ and poly(dA).poly(dT), an outside-binding mode can be suggested. There are also visible intensity changes for ν_4 and ν_2 bands. The ratio ν_4/ν_2 was found to 0.75, 0.9 and 0.7 for free porphyrin, poly(dA-dT)$_2$ as well poly(dA).poly(dT), and for poly(dG-dC)$_2$, respectively. For poly(dG-dC)$_2$, both bands are shifted to higher wavenumbers. However, in the case of ST-DNA, the ratio was slightly greater than for unconplexed porphyrin. Thus, CuTPP$(NMe_3)_4$ seems to intercalate into poly(dG-dC)$_2$. For poly(dA-dT)$_2$ the changes indicate some kind of outside-binding, similarly as for poly(dA).poly(dT). For ST-DNA the binding mode is probably something between intercalation and outside binding, probably with greater affinity for intercalation.

For CuTPP-p-$(Bru)_4$ *(Figure 67)*, the band $\delta_S(C_\beta\text{-}H)$ seems to be splitted into two components located at 1083 and 1092 cm^{-1} for free porphyrin, while for ST-DNA,

poly(dA-dT)$_2$, poly(dG-dC)$_2$ and poly(dA).poly(dT) there is only one peak at ~ 1085 cm^{-1}. For $\nu_S(C_\alpha\text{-}N)$ and $\nu(C_\beta\text{-}C_\beta)$ bands, no intensity ratio was changed on interaction with any nucleic acid. However, there are some changes around $\nu(C_\beta\text{-}C_\beta)$ band at 1567 cm^{-1}. When interacting with any of the DNAs, intensities of the bands at 1543 cm^{-1} and 1590 cm^{-1} decrease, and at the same time, peak at 1612 cm^{-1} increases. Despite some slight differences, interactions of CuTPP-p-(Bru)$_4$ with poly(dA-dT)$_2$, poly(dG-dC)$_2$ and poly(dA).poly(dT) seem to be of the same type, most probably an outside binding mode that relates only peripheral substituens, without interfering strongly porphyrin macrocycle.

For CuTPP-m-(Bru)$_4$ *(Figure 68),* the band at 1013 cm^{-1} is upshifted when interacting with nucleic acids. In the case of poly(dA-dT)$_2$ the shift is ~ 4 cm^{-1}, for poly(dG-dC)$_2$ and poly(dA).poly(dT) only 2 cm^{-1}. In all the complexes, the binding-sensitive Raman band at 1073 cm^{-1} is also shifted to higher wavenumbers and its intensity increases. For poly(dA-dT)$_2$ the shift was ~ 11 cm^{-1}, ~ 10 cm^{-1} for poly(dG-dC)$_2$ and for poly(dA).poly(dT) it was ~ 9 cm^{-1}. For ST-DNA this shift was only ~ 6 cm^{-1}, indicating no unique binding mode. The most apparent spectral changes were found for $\nu_S(C_\alpha\text{-}N)$ and $\nu(C_\beta\text{-}C_\beta)$ bands at 1365 cm^{-1} and at 1563 cm^{-1}. In the case of poly(dA-dT)$_2$, there is no significant change. However, for poly(dA).poly(dT), poly(dG-dC)$_2$ and ST-DNA we have observed appearance of new down-shifted Raman bands in pairs to $\nu_S(C_\alpha\text{-}N)$ and $\nu(C_\beta\text{-}C_\beta)$. The effect was most noticeable for poly(dG-dC)$_2$. Both bands ν_4 and ν_2 are known to be very sensitive to the porphyrin core size [18, 41], usually decreasing their frequencies when the core size of the porphyrin increases. Typical situation of the core size enlargement is when the porphyrin gets some axial ligands. This was observed for NiTMPyP$_4$ [18, 41], when 4-coordinate porphyrin is changed to 6-coordinate by addition of two water molecules as axial ligands. Such an axial coordination results in appearance of new red-shifted bands in pairs to ν_4 and ν_2. Another core size effect was observed in pulse-excited RRS spectra of CuTMPyP$_4$ [43 - 46] where formation of a transient exciplex with fifth axial ligand was shown to cause appearance of similar doublets [43]. Nevertheless, mechanisms of the core size enlargement in the case of NiTMPyP$_4$ 6-coordinate form and CuTMPyP$_4$ exciplex can differ from that observed for CuTPP-m-(Bru)$_4$ complexes with poly(dA).poly(dT) and poly(dG-dC)$_2$. Moreover, it is not sure that the core size enlargement is a unique explanation of new bands. In any case, in the framework of this diploma thesis, an interesting difference in binding modes of structurally relating CuTPP-p-(Bru)$_4$ and CuTPP-m-(Bru)$_4$ was observed for the first time. This phenomenon have to be explained. For more detail analysis, there will be necessary to obtain additional experimental data.

To establish basic spectrophotometric characteristics for interactions of novel cationic porphyrins with nucleic acids, complexes of $CuTMPyP_4$, $CuTPP\text{-}(NMe_3)_4$, $CuTPP\text{-}p(Bru)_4$ and $CuTPP\text{-}m\text{-}(Bru)_4$ with $poly(dA\text{-}dT)_2$, $poly(dG\text{-}dC)_2$ and poly(dA).poly(dT) were studied also by absorption spectroscopy *(Figures 69 – 80)*. The basic changes induced by interactions are summarized in *Table 2*.

Because of strong hypochromism and considerable red-shift of the Soret band, intercalation can be clearly identified for $CuTMPyP_4$ with $poly(dG\text{-}dC)_2$ *(Figure 70)*. Complex formation with $poly(dA\text{-}dT)_2$ or poly(dA).poly(dT) induces changes of the same character *(Figure 69 and 71)*, nevertheless there are considerable differences between both AT polynucleotides, indicating their distinct outside binding modes Finally, different binding modes for $poly(dA\text{-}dT)_2$ and poly(dA).poly(dT) was confirmed also by RRS spectra. Our results are fully consistent with the published works [e.g. 17].

In the case of $CuTPP\text{-}(NMe_3)_4$ we can distinguish two binding modes. Complexes with $poly(dA\text{-}dT)_2$ and poly(dA)-poly(dT) seem to have typical outside binding character, contrary to $poly(dG\text{-}dC)_2$ where intercalation can be recognized due to red shift and broadening of the Soret band, hypochromism and marked Q-band red shift.

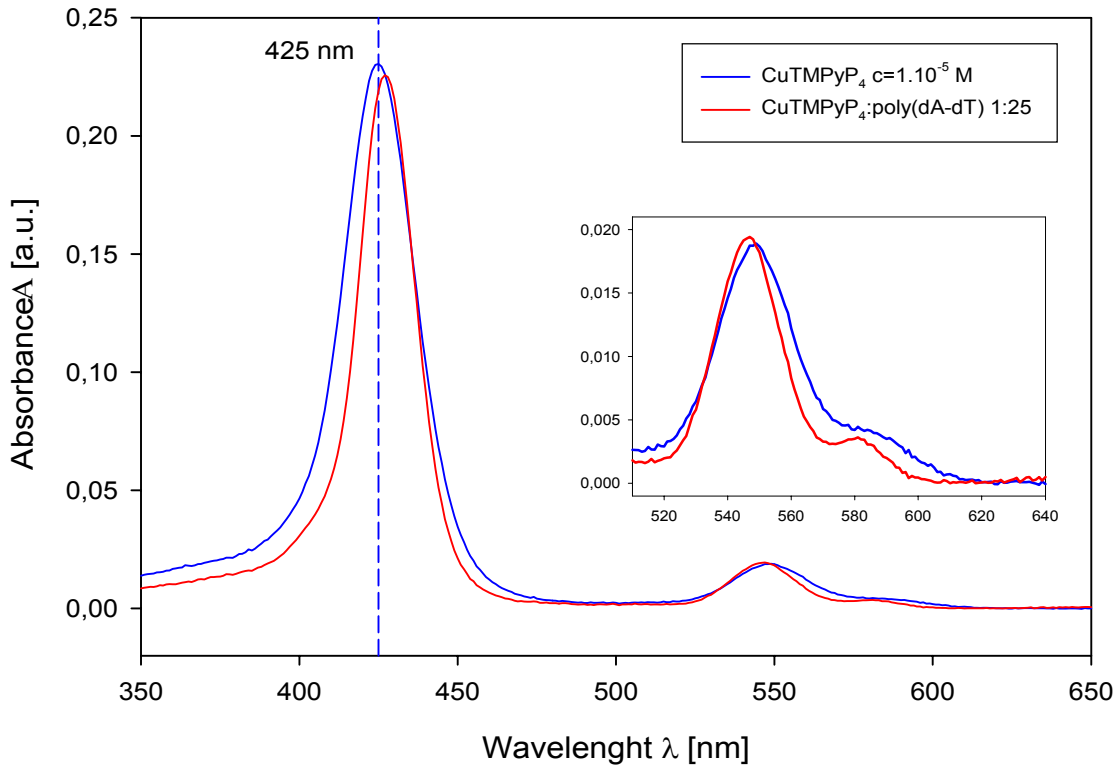

Figure 69. Absorption spectra of $CuTMPyP_4$ -$poly(dA\text{-}dT)_2$, R=[bp]/[porphyrin]~25

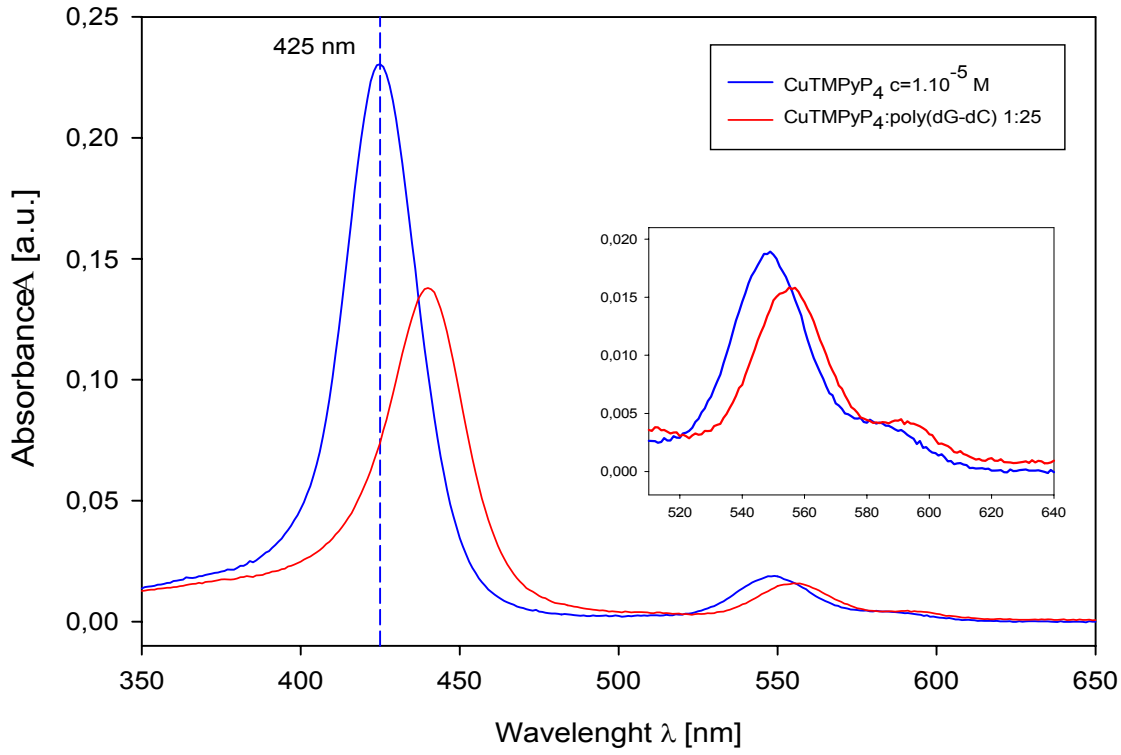

Figure 70. Absorption spectra of CuTMPyP$_4$- poly(dG-dC)$_2$, R~25

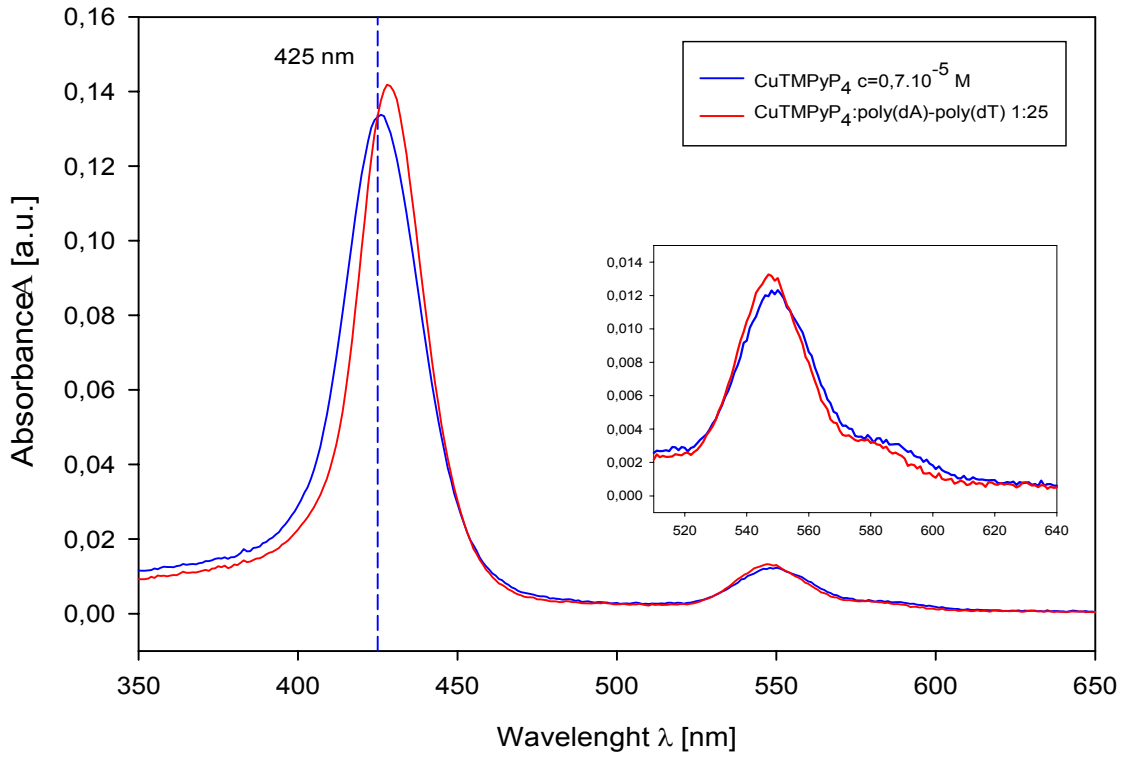

Figure 71. Absorption spectra of CuTMPyP$_4$-poly(dA).poly(dT), R~25

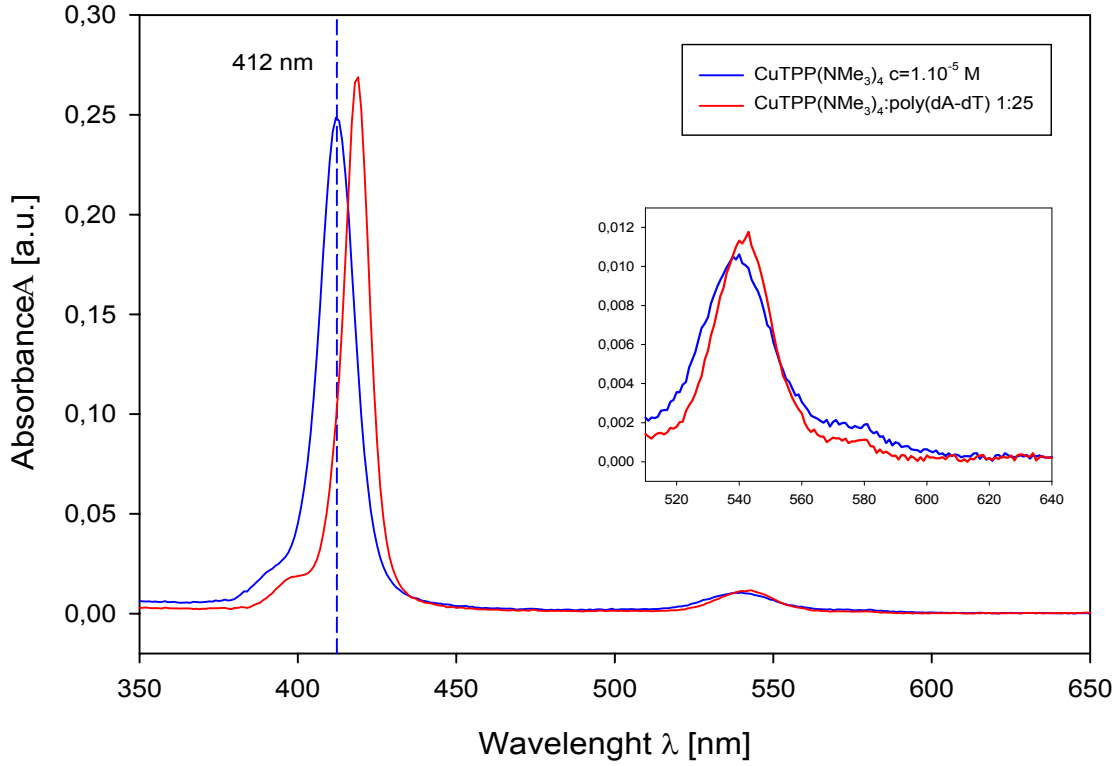

Figure 72. Absorption spectra of CuTPP-$(NMe_3)_4$-poly(dA-dT)$_2$, R~25

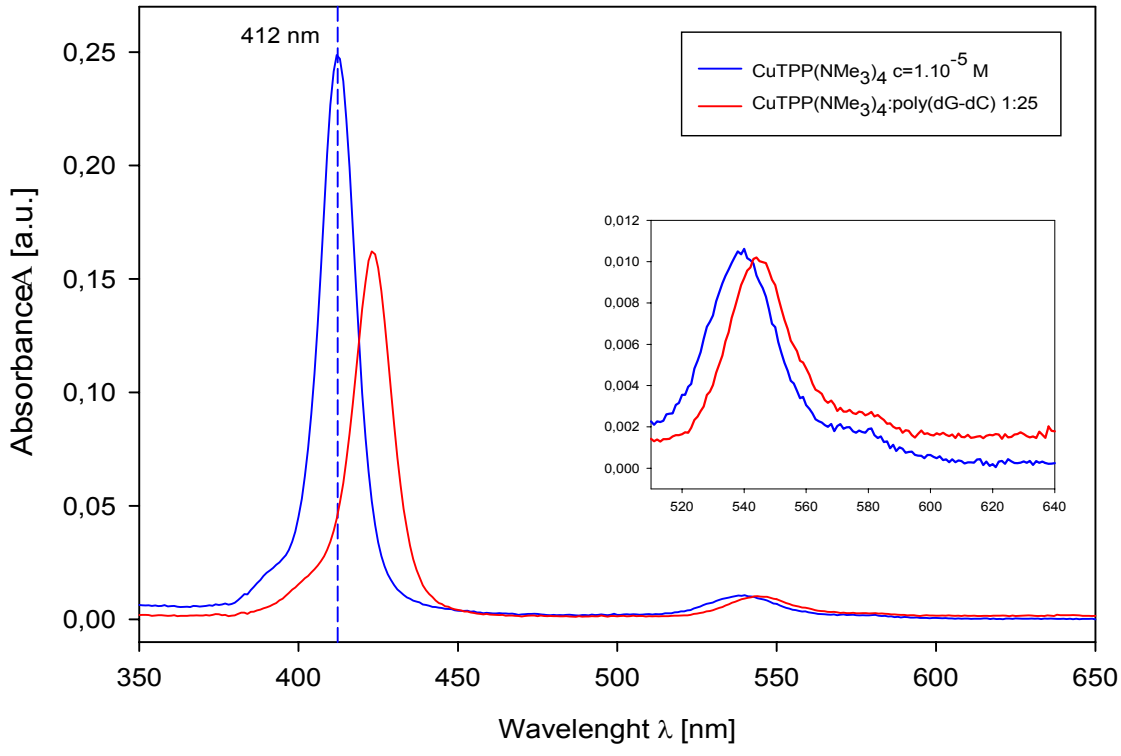

Figure 73. Absorption spectra of CuTPP$(NMe_3)_4$-poly(dG-dC)$_2$, R~25

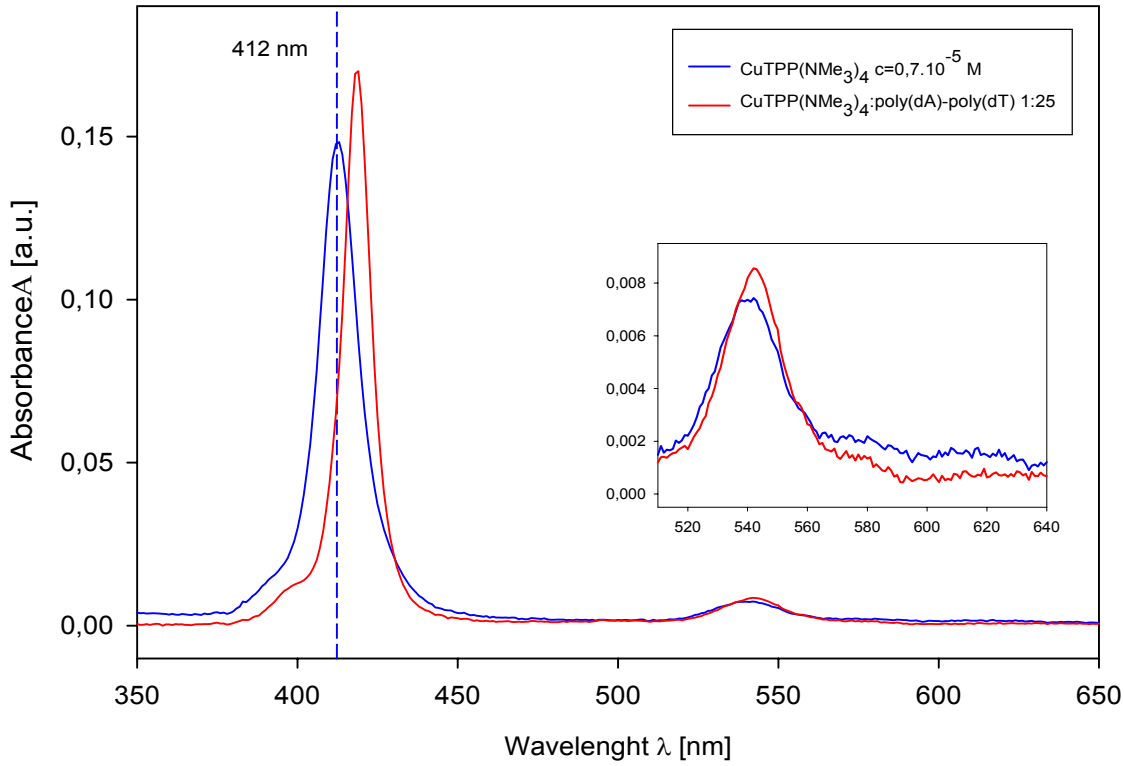

Figure 74. Absorption spectra of CuTPP-$(NMe_3)_4$ poly(dA).poly(dT), R~25

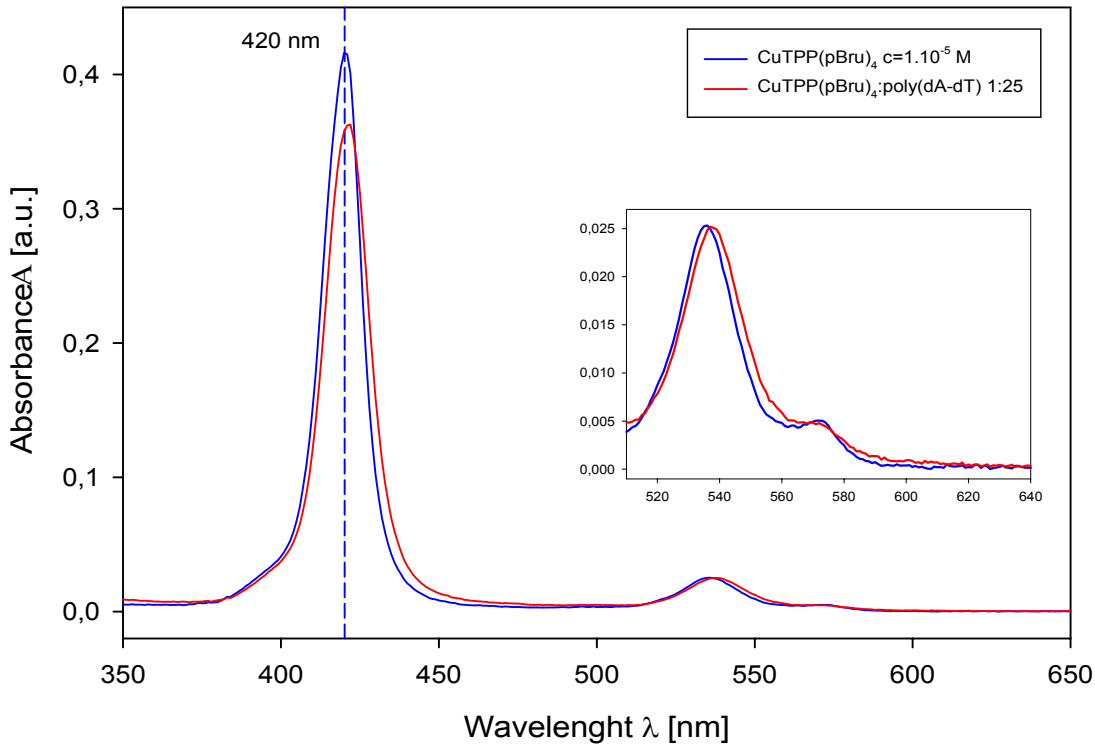

Figure 75. Absorption spectra of CuTPP-p-$(Bru)_4$-$poly(dA\text{-}dT)_2$, R~25

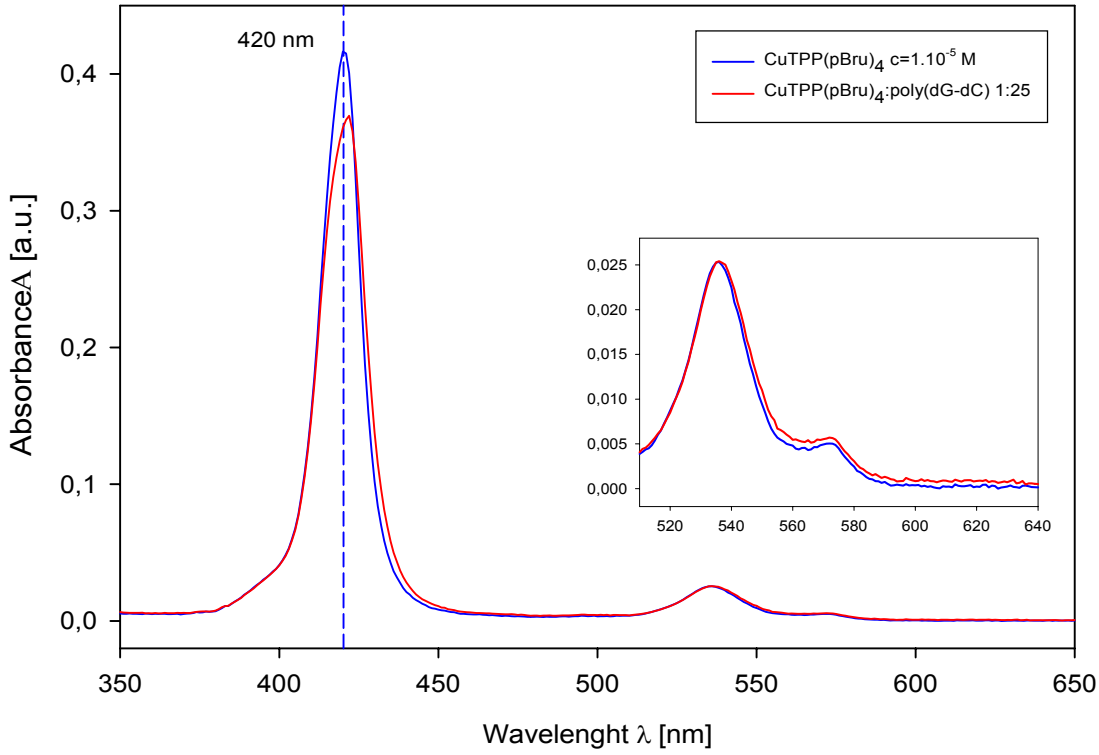

Figure 76. Absorption spectra of CuTPP-p-(Bru)$_4$- poly(dG-dC)$_2$, R~25

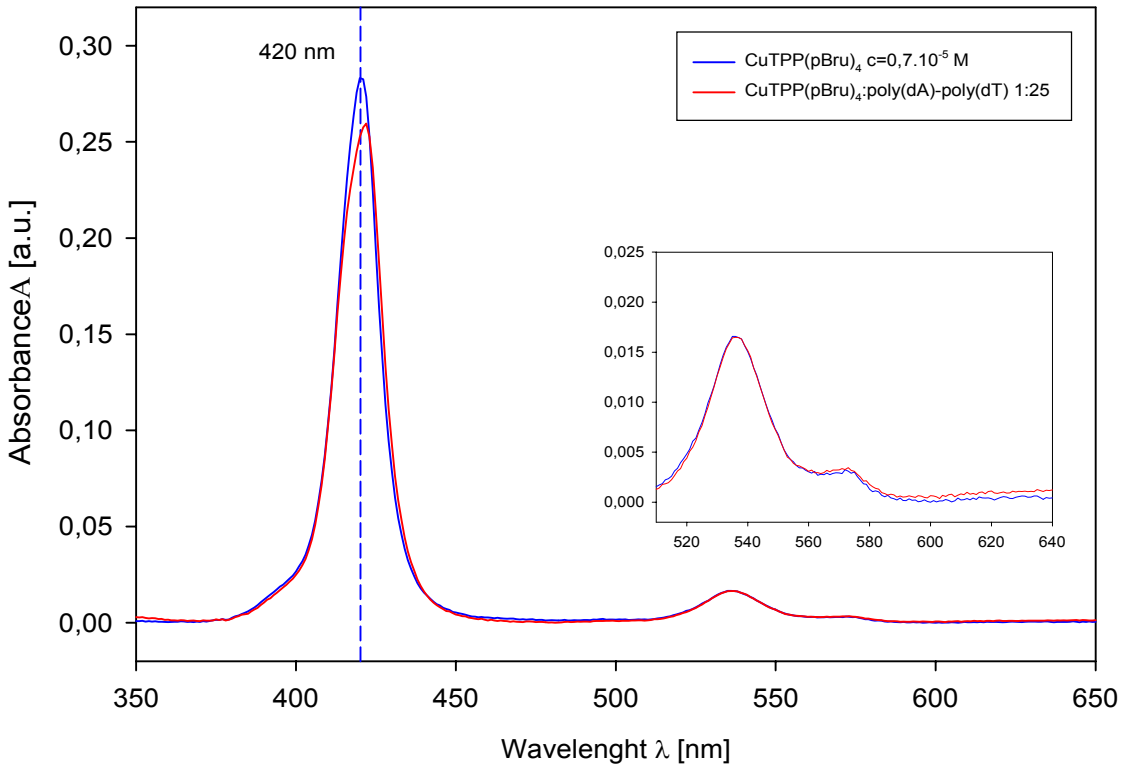

Figure 77. Absorption spectra of CuTPP-p(Bru)$_4$ -poly(dA).poly(dT), R~25

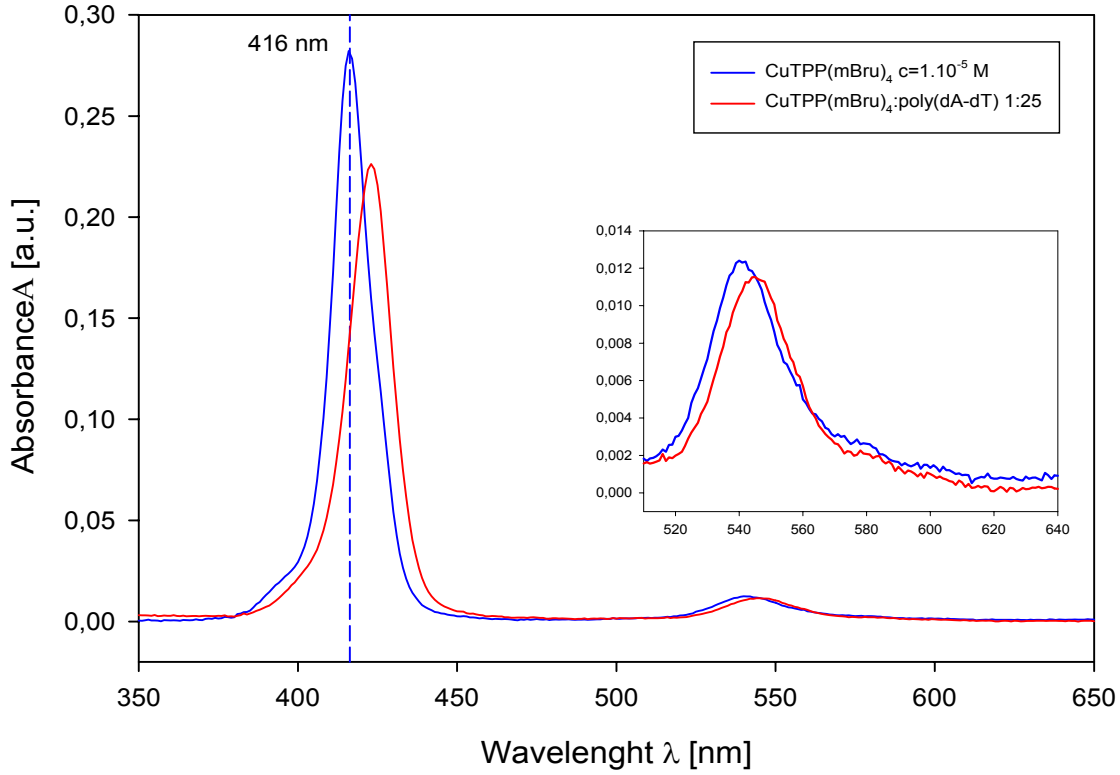

Figure 78. Absorption spectra of CuTPP-m-(Bru)$_4$-poly(dA-dT)$_2$, R~25

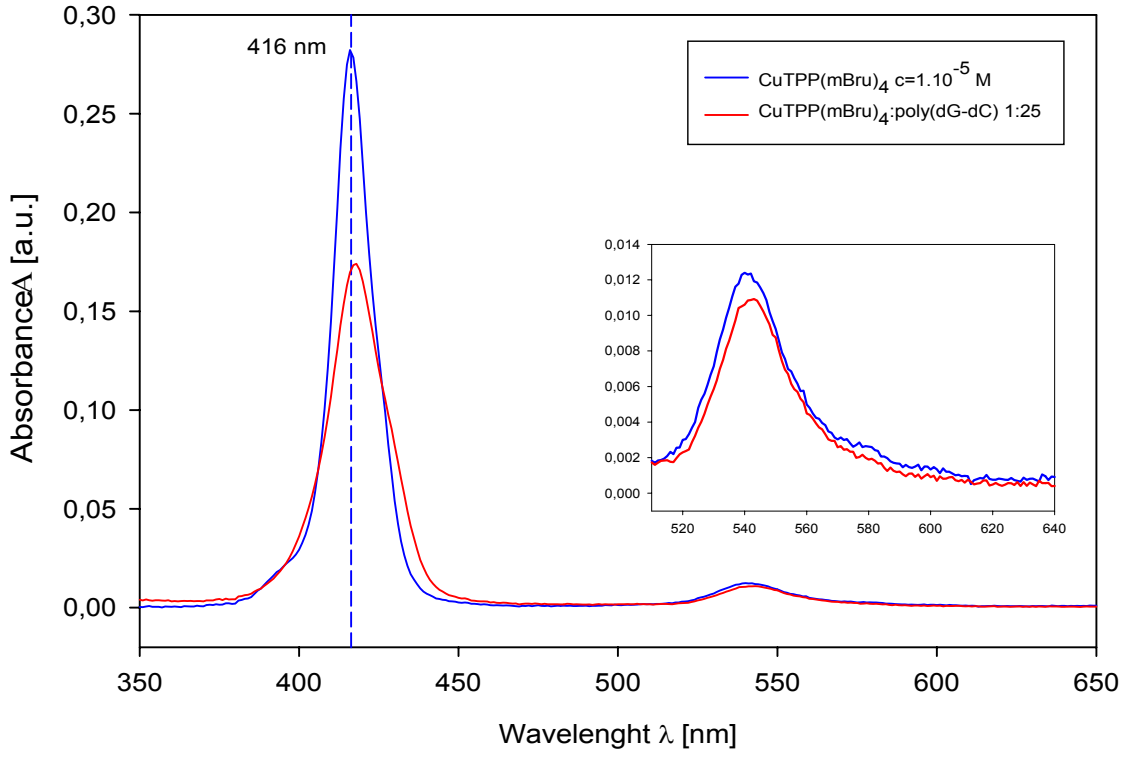

Figure 79. Absorption spectra of CuTPP-m-(Bru)$_4$-poly(dG-dC)$_2$, R~25

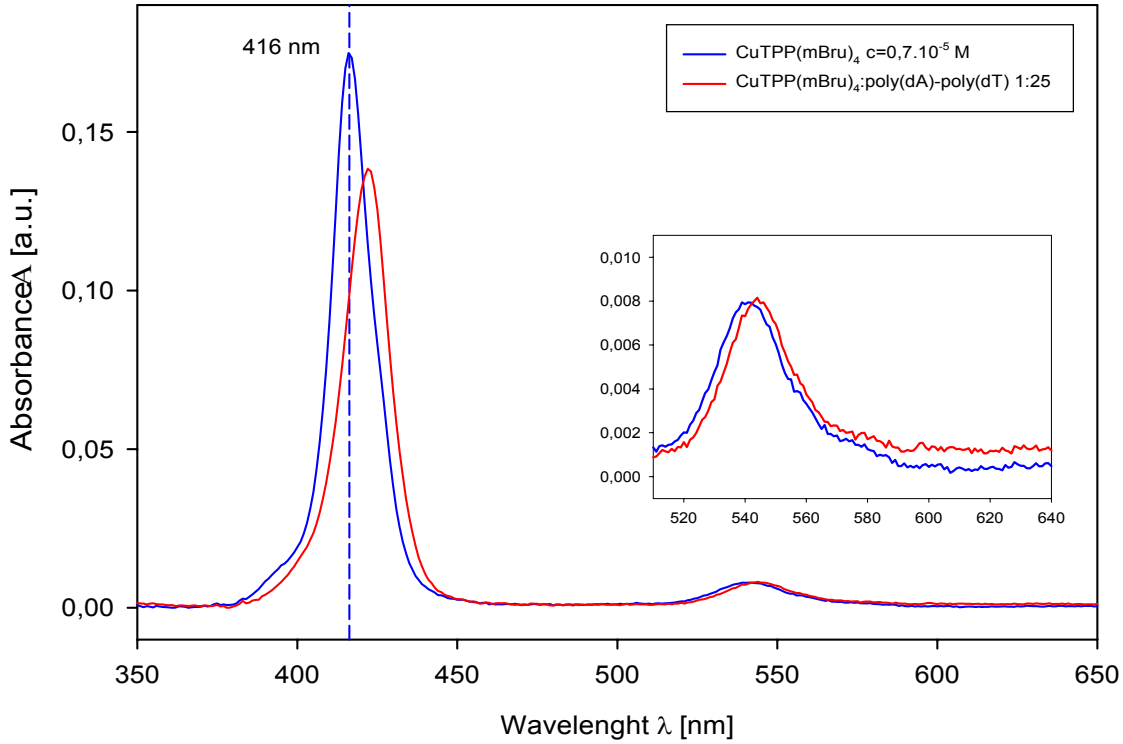

Figure 80. Absorption spectra of CuTPP-m-(Bru)$_4$-poly(dA).poly(dT), R~25

		Soret red shift [nm]	hypochromism	Soret fwhm change [nm]	Q-band red shift [nm]	hypochromism
CuTMPyP4	with poly(dA-dT)	2	2,0%	-4,5	-2	-2,6%
	with poly(dG-dC)	15	40,1%	3	6	16,4%
	with poly(dA).poly(dT	2	-6,0%	-2	-3	-8,1%
CuTPP-(NMe3)4	with poly(dA-dT)	7	-8,1%	-2	3	-11,3%
	with poly(dG-dC)	11	34,8%	3	4	3,8%
	with poly(dA).poly(dT	6	-14,6%	-2	2	24,3%
CuTPP-p-(Bru)4	with poly(dA-dT)	2	12,9%	4	1	0,4%
	with poly(dG-dC)	2	10,7%	4	0	-0,4%
	with poly(dA).poly(dT)	2	8,3%	4	0	0,6%
CuTPP-m-(Bru)4	with poly(dA-dT)	7	19,8%	0,5	3	8,7%
	with poly(dG-dC)	2	38,3%	5,5	1	13,5%
	with poly(dA).poly(dT	6	22,0%	1,5	2	6,8%

Table 2. Changes in absorption spectra of cationic porphyrins with various DNAs

Free-base form of H_2TPP-(NMe_3)$_4$ and its complexes with natural CT-DNA and mononucleotides (AMP, GMP) were recently studied by Kubát *et al.* [26] along with

relative *meso*-tetraphenylporphyrins bearing different bulky cationic substituents. They observed considerable hypochoromism (~ 30%), moderate red-shift (7 nm) and presence of a single isobestic point, however they assumed that this porphyrin is too large to intercalate into DNA, and that it rather binds to the surface of DNA. The reason for such an assumption was mainly the high number of DNA base pairs *n* covered by porphyrin, *n = 6.2* for H_2TPP-$(NMe_3)_4$ while *n = 2.7* for H_2TMPyP$_4$, estimated from spectral titrations with CT-DNA. However, our present results obtained for CuTPP-$(NMe_3)_4$ and poly(dG-dC) indicate, that trimethylammonio-p-tolyl substituens cannot block intercalation, at least for Cu^{2+} derivative. Clear difference between spectral changes caused by external binding to poly(dA-dT)$_2$ and poly(dA).poly(dT), on the other hand by intercalation to poly(dG-dC)$_2$ suggest, that also data on natural DNA can be interpreted in different way.

In the case of CuTPP-p-(Bru)$_4$ (*Figures 75-77*), absorption spectra of the mixtures with poly(dA-dT)$_2$, poly(dG-dC)$_2$ and poly(dA)-poly(dT) showed the same changes: weak hypochromism and slight red-shift. Thus, CuTPP-p-(Bru)$_4$ cannot discriminate between polynucleotides of various base composition. It seems that porphyrin macrocycle is not perturbed significantly by interactions with DNA. From the RRS we have assigned the changes to interaction of bulky peripheral cationic substituents with negative phosphate groups of DNA, leaving porphyrin ring isolated from the contact with polynucleotide surface. When the porphyrin interacts via peripheral substituents (moreover insulated from the macrocycle by methylene groups), and there are no other changes in the microenvironment of the porphyrin core caused by neighbors (R ~ 25), we can barely observe any changes in absorption spectra. It would be necessary to find, whether decrease of the ratio R (R = [bp]/[porphyrin] would induce self-aggregation of the CuTPP-p-(Bru)$_4$ at the DNA matrix.

However, absorption spectra of the CuTPP-m-(Bru)$_4$ complexes seems to suggest that this structural form of the brucine porphyrin can discriminate between different duplexes, since at least two binding modes have been detected (*Figure 78 - 80*). Spectral changes for the complexes with poly(dG-dC)$_2$, i.e. strong hypochromism but small red-shift, and broadening of the Soret band, seem to indicate strong perturbation of their π-electrons, probably because of the self-stacking interactions between porphyrins, or due to strong attachment of the porphyrin macrocycle to the DNA hydrophobic surface. On the other hand, spectra of the complexes with poly(dA-dT)$_2$ and poly(dA).poly(dT) exhibit some ambiguous indications of intercalation (Soret red-shift) as well as of outside binding (relatively small hypochromism). Considering the size of the porphyrin substituents and

structural properties of poly(dA-dT)$_2$ and poly(dA).poly(dT), it is improbable for this molecule to intercalate into DNA. Some kind of outside-binding, probably with attachment to DNA surface of selfstacking of the porphyrins sems to be more reasonable. The changes in absorption spectra do not allow to determine the binding mode more exactly. As shown above, new bands observed in the RRS spectra indicate increase of the porphyrin core size for the complexes with poly(dA).poly(dT) and poly(dG-dC)$_2$. We can even speculate about axial coordination of the ligand from the brucine moiety, since there are several potential donor atoms. Brucine substituents attached at *meta*-position can be turned towards the central atom due to interaction with DNA, and support such an axial bond. However, correct and sound explanation of this effect need more experimental results.

Very interesting is the difference between binding modes of CuTPP-p-(Bru)$_4$ and CuTPP-m-(Bru)$_4$ to various DNA. The only structural difference between both molecules is a position where the substituents are attached to phenyl group. However, such a structural difference could have profound consequences for physico-chemical and conformational properties, as well as for interactions with other molecules. Our finding is not a single case when a difference between these two molecules was reported. Recently, Král *et al.* [47] discovered that H_2TPP-p-(Bru)$_4$ can serve as gelator of methanol and acetonitrile at extremely low level of concentration. Surprisingly, the change of the position of the brucine substituent from *para*- to *meta*- led to complete loss of the gelating properties.

6 Conclusion

In the present work, physico-chemical properties of three novel cationic porphyrins having therapeutic importance have been studied by use of electronic absorption and resonance Raman spectroscopies. Complexes of their free-base and Cu^{2+} derivatives with single- and double-stranded nucleic acids were studied along with properties of standard model cationic porphyrins H_2TMPyP_4, H_2TMAP and $H_2TPP\text{-}(NMe_3)_4$.

Low-scale metallation procedure was proposed and successfully applied to obtain Cu^{2+} derivative of the $H_2TPP\text{-}(Dist)_4$. Methodology for comprehensive study of porphyrin aggregation was tested on the H_2TMAP aqueous solutions of various concentrations and ionic strengths. Solubility of $H_2TPP\text{-}(Dist)_4$ in aqueous solutions and formation of aggregates were studied by use of absorption spectroscopy. Employing factor analysis and global fits, formation of $H_2TPP\text{-}(Dist)_4$ dimers and higher order H-aggregates was studied.

Interactions of free-base $H_2TPP\text{-}(Dist)_4$ and $H_2TPP\text{-}p\text{-}(Bru)_4$ with single- and double-stranded nucleic acids were studied by absorption spectroscopy. External binding mode and formation of self-associated porphyrin assemblies on the polynucleotide matrices were identified for both porphyrins.

Several spectrophotometric procedures for determination of extinction coefficients of cationic porphyrins were tested. Differential spectroscopic method of Pethö and Marzilli [34] based on zincon was shown to fail systematically for cationic porphyrins because of their previously unnoticed interactions with zincon. Original procedure based on dimer formation between anionic and cationic porphyrins was proposed, tested and used for determination of extinction coefficients of $CuTPP\text{-}(NMe_3)_4$ (ε_{412} = (2.5 ± 0.5) x 10^5 M^{-1} cm^{-1}), $CuTPP\text{-}p\text{-}(Bru)_4$ (ε_{421} = (4.1 ± 0.7) x 10^5 M^{-1} cm^{-1}) and $CuTPP\text{-}m\text{-}(Bru)_4$ (ε_{416} = (3.0 ± 0.6) x 10^5 M^{-1} cm^{-1}). Furthermore, extinction coefficients of H_2TPPS_4 (ε_{412} = (4.2 ± 0.3) x 10^5 $M^{-1}cm^{-1}$) and $CuTPPS_4$ (ε_{412} = (2.7 ± 0.5) x 10^5 $M^{-1}cm^{-1}$) were determined as well.

To simulate interactions taking part in the porphyrin-assisted delivery of antisense oligonucleotides, complexes of H_2TMPyP_4 with $oligo(dA)_{15}$ and poly(rU) have been studied by absorption spectroscopy. Noncovalent attachment of the porphyrin to antisense oligonucleotide was proven to cause no serious obstructions for recognition of the complementary sequence. Formation of the DNA/RNA double helices on uptake was shown to be identifiable spectroscopically due to various binding-mode sensitive spectral features of the porphyrins employed for oligonucleotide delivery.

Complexes of CuTPP-p-$(Bru)_4$ and CuTPP-m-$(Bru)_4$ with natural ST-DNA and synthetic poly(dA-dT)$_2$, poly(dA). poly(dT) and poly(dG-dC)$_2$ were studied and characterized for the first time by absorption and resonance Raman spectroscopies, and their base and sequence specificities of the binding modes established were confronted with $CuTMPyP_4$ and CuTPP-$(NMe_3)_4$. Contrary to CuTPP-p-$(Bru)_4$ exhibiting no base specificity, CuTPP-m-$(Bru)_4$ was shown to discriminate between divers polynucleotide structures. Structural difference between CuTPP-p-$(Bru)_4$ and CuTPP-m-$(Bru)_4$ seems to have profound consequences for physico-chemical and conformational properties, as well as for interactions with nucleic acids.

Experimental results presented in the diploma thesis should serve as a starting point for further more systematic investigation of interactions between novel cationic porphyrins and nucleic acids. Better understanding of the porphyrin-oligonucleotide complex formation and porphyrin binding modes can contribute to design and synthesis of tailored porphyrins applicable as transport agents in oligonucleotide strategies.

Literature

[1] Alberts et al., *Molecular biology of the cell, 4th edition.,* Garland science, New York, ISBN 0-8153-4072-9, 2002, 537-538.

[2] Lebedeva I.; Benimetskaya L.; Stein C. A.; Vilechnik M., *European Journal of Pharmaceutics and Biopharmaceutics,* 2000, **50**, 101-119.

[3] Dass C. R., *Journal of Pharmacy and Pharmacology,* 2002, **54**, 3-27.

[4] Weyerman J.; Lochmann D.; Zimmer A., *Journal of Controlled Release,* 2004, **100**, 411-423.

[5] Flynn S. M.; George S. T.; White L.; Devonish W.; Takle G. B., *BioTechniques,* 1999, **26**, 736-746.

[6] Benimetskaya L.; Takle G. B.; Vilenchik M.; Lebedeva I.; Miller P.; Stein C. A., *Nucleic Acids Research,*1998, **26**, 5310-5317.

[7] Králová J.; Dvořák M.; Král V., *Journal of Medicinal Chemistry,* 2003, **46**, 2049-2056.

[8] Sarkar T.; Conwell C. C.; Harvey L. C.; Santai C. T.; Hud N. V., *Nucleic Acids Research,* 2005, **33**, 143-151.

[9] Vít M., *Diplomová práce,* OFB MFF UK Praha, 2004.

[10] Fleischer E. B., *Accounts of Chemical Research,* 1970, **3**, 105-112.

[11] Fiel R. J.; Dattagupta N, Mark E. H.; Howard J. C., *Cancer Research,* 1981, **41**, 3543-3545.

[12] Sessler J. L.; Cyr M. J.; Lynch V.; McGhee E.; Ibers J. A., *Journal of the American Chemical Society,* 1990, **112**, 2810-2813.

[13] Ding L.; Etemad-Moghadam G.; Meunier B., *Biochemistry,* 1990, **29**, 7868-7875.

[14] Dabrowiak J. C.; Ward B.; Goodisman J., *Biochemistry,* 1989, **28**, 3314-3322.

[15] Keating L. R.; Szalai V. A., *Bichemistry,* 2004, **43**, 15891-15900.

[16] Procházková K.; Zelinger Z.; Lang K.; Kubát P., *Journal of Physical Organic Chemistry,* 2004, **17**, 890-897.

[17] Pasternack R. F.; Gibbs E. J.; Villafranca J. J., *Biochemistry,* 1983, **22**, 2406-2414.

[18] Yue K. T.; Lin M.; Gray T. A.; Marzilli L. G., *Inorganic Chemistry,* 1991, **30**, 3214-3222.

[19] Chaires J. B., *Biophysical Approaches,* 2001, 3-22.

[20] Pasternack R. F.; Brigandi F. A.; Abrams M. J., *Inorganic Chemistry,* 1990, **29**, 4483-4486.

[21] Pasternack R. F.; Gurrieri S.; Lauceri R.; Purello R., *Inorganica Chimica Acta,* 1996, **246**, 7-12.

[22] Prosser V. et al., *Experimentální metody biofyziky,* Academia, Praha, ISBN 80-200-0059-3, 1989, 337-365.

[23] Akins D. L., *Journal of Physical Chemistry,* 1986, **90**, 1530-1534.

[24] Kano K.; Minamizono H.; Kitae T.; Negi S., *Journal of Physical Chemistry A,* 1997, **101**, 6118-6124.

[25] Chen D.-M.; Zhang Y.-H.; He T.-J.; Liu F.-C., *Spectrochimica Acta Part A,* 2002, **58**, 2291-2297.

[26] Kubát P.; Lang K.; Anzenbacher P. Jr.; Jursíková K.; Král V.; Ehrenberg J., *Journal of the Chemical Society*, *Perkin Transactions 1*, 2000, 933-941.

[27] Malinowski E. R., *Factor Analysis in Chemistry, 3rd edition,* John Wiley and Sons, Inc., New York, ISBN 0-471-13479-1, 2002, 1-54.

[28] Pasternack R. F.; Huber P. J.; Boyd P.; Engasser G.; Francesconi L.; Gibbs E.; Fasella P.; Venturo G. C.; Hinds L. deC., *Journal of the American Chemical Society,* 1972, **94**, 4511-4517.

[29] Dixon D.W., Steullet V., *Journal of Inorganic Biochemistry,* 1998, **69**, 25-32.

[30] Kubát P.; Lang K.; Procházková K.; Anzenbacher P. Jr., *Langmuir*, 2003, **19**,422-428.

[31] Sehlstedt U.; Kim S. K.; Carter P.; Goodisman J.; Vollano J. F.; Nordén B.; Dabrowiak J. C., *Biochemistry*, 1994, **33**, 417-426.

[32] Schneider H. S.; Wang M., *Journal of Organic Chemistry,* 1994, **59**, 7473-7478.

[33] Malinovski V.; Tumir L.; Piantanida I., *European Journal of Organic Chemistry,* 2002, **22**, 3785-3795.

[34] Pethö G.; Marzilli L.G., *Microchemical Journal*, 1994, **50**, 178-183.

[35] Rush R.M.; Yoe J.H., *Analytical Chemistry*, 1954, **26**, 1345-1347.

[36] Hofstra U.; Koehorst R. B. M.; Schaafsma T. J., *Chemical Physics Letters,* 1986, **130**, 555-559.

[37] Uno T.; Aoki K.; Shikimi T.; Hiranuma Y.; Yoshikazu T.; Ishikawa Y., *Biochemistry*, 2002, **41**, 13059-13066.

[38] Uno T; Hamasaki K.; Tanigawa M.; Shimbayashi S., *Inorganic Chemistry,* 1997, **36**, 1676-1683.

[39] Li X.-Y.; Czernuszewicz R. S.; Kincaid J. R.; Su Y. O.; Spiro T. G., *Journal of the Physical Chemistry,* 1990, **94**, 31-47.

[40] Stein P.; Ulman A.; Spiro T. G., *Journal of the Physical Chemistry,* 1984, **88**, 369-374.

[41] Schneider J. H.; Odo J.; Nakamoto K., *Nucleic Acids Research,* 1988, **16**, 10323-10338.

[42] Blom N.; Odo J.; Nakamoto K.; Strommen P., *Journal of the Physical Chemistry,* 1986, **90**, 2847-2852.

[43] Chinsky L.; Turpin P.-Y.; Al-Obaidi A. H. R.; Bell S. E. J.; Hester R. E., *Journal of the Physical Chemistry,* 1991, **95**, 5754-5756.

[44] Kruglik S. G.; Mojzeš P.; Mizutani Y.; Kitagawa T.; Turpin P.-Y., *Journal of the Physical Chemistry B,* 2001, **105**, 5018-5031.

[45] Mojzeš P.; Praus P.; Baumruk V.; Turpin P.-Y.; Matoušek P; Towrie M., *Biopolymers,* 2002, **67**, 278-281.

[46] Mojzeš P.; Kruglik S. P.; Baumruk V.; Turpin P.-Y., *Journal of the Physical Chemistry B,* 2003, **107**, 7532-7535.

[47] Král V.; Pataridis S.; Setnička V.; Záruba K.; Urbanová M.; Volka K., *Tetrahedron,* 2005, **61**, 5499-5506.

[48] Saenger W., *Principles of Nucleic Acids Struc*ture, Springer-Verlag, New York, 1984, ISBN 0-387-90762-9.

[49] Fiel R. J.; Howard J. C.; Mark E. H., Datta-Gupta N., *Nucleic Acids Res.*, 1979, **6**, 3093 - 3118.

[50] Friedman R. A. G., Manning G. S., Shahin M. A., *Chemistry and Physics of DNA-Ligand Interactions*, Adenine Press 1988, 37-64, ISBN 0-940030-25-X

[51] Pasternack R. F., Gianetto A., Pagano P., Gibbs E. J., *J. Am. Chem. Soc.*, 1991, **113**, 7799 – 7800.

[52] Bustamante C., Gurrieri S., Pasternack R. F., Purrello R., Rizzarelli E., *Biopolymers*, 1994, **34**, 1099 –1104.

[53] Yamashita T., Uno T., Ishikawa Y., *Bioorganic Medical Chemistry*, 2005, **13**, 2423 – 2430.

[54] Kubát P., Lang K., Král V., Anzenbacher P., jr., *J. Phys. Chem. B*, 2002, **106**, 6784 – 6792.

[55] Mojzeš P., Chinsky L., Turpin P.-Y., *J. Phys. Chem.*, 1993, **97**, 4841 – 4847.

[56] Schrader B., *Infrared and Raman Spectroscopy*, VCH, Weinheim 1995, ISBN 3-527-26446-9